Institut für Kernenergetik
und Energiesysteme

Development and Validation of Models for Simulation of Supercritical Carbon Dioxide Brayton Cycles and Application to Self-Propelling Heat Removal Systems in Boiling Water Reactors

Jeanne Venker

Universität Stuttgart IKE 2 – 156 2015

Institut für Kernenergetik
und Energiesysteme

Development and Validation of Models for Simulation of Supercritical Carbon Dioxide Brayton Cycles and Application to Self-Propelling Heat Removal Systems in Boiling Water Reactors

von der Fakultät Energie-, Verfahrens- und
Biotechnik der Universität Stuttgart
zur Erlangung der Würde eines
Doktor-Ingenieurs (Dr.-Ing.) genehmigte Abhandlung

vorgelegt von

Jeanne Venker

aus Rheda-Wiedenbrück

Hauptberichter: Prof. Dr.-Ing. Jörg Starflinger

Mitberichter: Prof. Dr.-Ing. Thomas Schulenberg

Tag der mündlichen Prüfung: 31.03.2015

ISSN – 0173 – 6892

Universität Stuttgart IKE 2 – 156 2015

Vorwort

Die vorliegende Forschungsarbeit wurde von mir am Institut für Kernenergetik und Energiesystem (IKE) an der Universität Stuttgart erarbeitet und von der RWE Technology GmbH gefördert. Bei beiden Institutionen möchte ich mich zuallererst für die erfolgreiche Zusammenarbeit und die guten Rahmenbedingungen bedanken!

Besonderer Dank gilt meinem Betreuer Prof. Dr.-Ing. Jörg Starflinger, dem Leiter des Instituts für Kernenergetik und Energiesysteme, für seine vielen Anregungen und seine fachliche Unterstützung. Er stand jederzeit für produktive Gespräche zur Verfügung, was maßgeblich zum Gelingen dieser Arbeit beigetragen hat.

Des Weiteren danke ich meinem Mitberichter Prof. Dr.-Ing. Thomas Schulenberg, dem Leiter des Instituts für Kern- und Energietechnik am Karlsruher Institut für Technologie, für das Interesse an meiner Arbeit und seinen konstruktiven Anmerkungen.

Auch Dr.-Ing. Michael Buck, Leiter der Abteilung Reaktorsicherheit, Reaktorsysteme und Umwelt am IKE, möchte ich an dieser Stelle erwähnen, der mich zu Beginn meiner Arbeit bei der Einarbeitung in den Thermohydraulik-Code ATHLET unterstützt hat und mir während der gesamten Projektzeit bei Fragen zur Seite stand. Vielen Dank dafür!

Bei der RWE AG bin ich insbesondere meinem Betreuer Detlef Gitzel zu Dank verpflichtet, ohne dessen persönlichen Einsatz dieses Projekt nicht zustande gekommen wäre. Der kontinuierliche Austausch und seine bereichernden Hinweise haben meinen Blickwinkel erweitert. Vielen Dank!

Ebenso möchte ich mich bei Herrn Dr.-Ing. Dominik von Lavante, dem Entwickler des Turbo-Kompressor-Systems, für das entgegengebrachte Vertrauen und seine tatkräftige Mitarbeit bei der Dimensionierung des Joule-Kreislaufes und der Turbomaschinen bedanken.

Meinen Promotionskollegen, sowie allen anderen Mitarbeitern am IKE danke ich für die positive Arbeitsatmosphäre und die vielen wissenschaftlichen Diskussionen, die meinen Horizont auf verschiedensten Forschungsgebieten erweitert haben.

Ganz besonders danke ich meinem Lebensgefährten Richard Bargsten und meiner Familie. Ohne ihre unermüdliche Unterstützung wäre diese Arbeit nicht zu dem geworden, was sie heute ist.

I Abstract

The objective of the current work was to develop a model that is able to describe the transient behavior of supercritical carbon dioxide (sCO_2) Brayton cycles, to be applied to self-propelling residual heat removal systems in boiling water reactors. The developed model has been implemented into the thermohydraulic system code ATHLET. By means of this improved ATHLET version, novel residual heat removal systems, which are based on closed sCO_2 Brayton cycles, can be assessed as a retrofit measure for present light water reactors. Transient simulations are hereby of great importance. The heat removal system has to be modeled explicitly to account for the interaction between the system and the behavior of the plant during different accident conditions.

As a first step, transport and thermodynamic fluid properties of supercritical carbon dioxide have been implemented in ATHLET to allow for the simulation of the new working fluid. Additionally, a heat transfer correlation has been selected to represent the specific heat transfer of supercritical carbon dioxide. For the calculation of pressure losses due to wall friction, an approach for turbulent single phase flow has been adopted that is already implemented in ATHLET.

In a second step, a component model for radial compressors has been implemented in the system code. Furthermore, the available model for axial turbines has been adapted to simulate the transient behavior of radial turbines. All extensions have been validated against experimental data.

In order to simulate the interaction between the self-propelling heat removal system and a generic boiling water reactor, the components of the sCO_2 Brayton cycle have been dimensioned with first principles. An available input deck of a generic BWR has then been extended by the residual heat removal system. The modeled application has shown that the extended version of ATHLET is suitable to simulate sCO_2 Brayton cycles and to evaluate the introduced heat removal system. A first analysis of the system revealed the ability to remove the decay heat over more than 72 hours, even for combined station blackout and loss of ultimate heat sink scenarios. In addition, the simulations exposed an interaction between the retrofitted and already existing systems. Parameters, which influence the operation of the self-propelling heat removal system, have been identified and summarized in set of prerequisites. The simulations indicate the potential of the system to serve as a diverse heat removal system for existing boiling water reactors.

II Kurzfassung

Das Ziel der vorliegenden Arbeit war die Entwicklung eines Modells zur Simulation von Joule-Kreisläufen mit dem Arbeitsmedium überkritisches Kohlenstoffdioxid (sCO_2), für die Anwendung in Siedewasserreaktoren. Dieses Modell wurde in das Systemrechenprogramm ATHLET integriert. Mit dieser modifizierten Version können neuartige Nachwärmeabfuhrsysteme, die auf einem geschlossenen Joule-Kreisprozess aufbauen und eine potentielle Nachrüstmaßnahme für bestehende Leichtwasserreaktoren darstellen, modelliert und thermohydraulisch untersucht werden. Besonders wichtig sind hierbei Erkenntnisse über das instationäre Verhalten des Nachwärmeabfuhrsystems und dessen Reaktion auf die sich im Laufe eines Störfallszenarios verändernden Randbedingungen.

Zur Simulation des neuen Arbeitsmediums wurden zunächst die Stoffdaten von überkritischem Kohlenstoffdioxid in den Systemcode eingebaut. Des Weiteren wurde eine Korrelation zur Bestimmung des Wärmeübergangskoeffizienten ausgewählt, mit der sich das Aufheizen und Abkühlen von sCO_2 berechnen lässt. Druckverluste durch Wandreibung werden mit einem bereits in ATHLET vorhandenen Ansatz für einphasige, turbulente Rohrströmungen bestimmt.

Zusätzlich wurde ein Komponentenmodel zur Darstellung radialer Kompressoren implementiert, sowie das in ATHLET vorhandene Modell für axiale Turbinen für die Simulation von Radialturbinen angepasst. Alle durchgeführten Erweiterungen wurden anhand experimenteller Daten validiert.

Das neuartige System wurde exemplarisch als potentielle Nachrüstmaßnahme für einen generischen Siedewasserreaktor untersucht, wofür zunächst eine erste Dimensionierung der Hauptkomponenten erfolgte. Der Datensatz eines generischen Siedewasserreaktors wurde anschließend mit dem Nachwärmeabfuhrsystem erweitert und erste Simulationen wurden durchgeführt. Die Ergebnisse haben gezeigt, dass das System die Nachzerfallswärme auch in bestimmten auslegungsüberschreitenden Störfällen wie dem Verlust der Hauptwärmesenke bei gleichzeitigem Station Blackout, für mehr als 72 Stunden abführen kann. Die Auswertung hat weiter ergeben, dass es zu Interaktionen mit bereits existierenden Systemen kommt. Parameter, die den Betrieb des Nachwärmeabfuhrsystems beeinflussen, wurden herausgearbeitet und in einem Anforderungsprofil zusammengefasst. Die Simulationen deuten auf das Potential des Systems hin, in bestehenden Siedewasserreaktoren als diversitäres Nachwärmeabfuhrsystem zu fungieren.

III Table of Contents

I Abstract .... **I**

II Kurzfassung .... **III**

III Table of Contents .... **V**

IV Nomenclature .... **IX**

1 Introduction **1**

1.1 Motivation 1

1.2 State of the Art 3

1.2.1 Residual Heat Removal Systems of Boiling Water Reactors 3

1.2.2 Requirements for Retrofit Options for Residual Heat Removal 6

1.2.3 Evaluation of Residual Heat Removal Systems 6

1.3 Aim of the Present Work 7

2 Description of the Thermohydraulic Code **9**

2.1 Thermo-Fluiddynamics 10

2.1.1 Conservation Equations 11

2.1.2 Constitutive Equations 14

2.2 Time Integration 17

2.3 General Control Simulation Module 18

2.4 Neutron Kinetics 19

2.5 Component Models 19

3 Adaptation of ATHLET to Simulate the Turbo Compressor System **21**

3.1 Implementation of Supercritical Carbon Dioxide as Working Fluid 21

3.1.1 Fluid Properties 23

3.1.2 Heat Transfer Coefficients 26

3.1.3 Pressure Drop 28

3.2 Extension of the Model for the Turbomachinery 28

3.2.1 Adaption to Model Radial Turbines 28

3.2.2 The Implementation of a Compressor Model 31

4 Validation 33
4.1 Heat Transfer 33
4.1.1 Uncertainties of the Experimental Data of Walisch 34
4.1.2 Uncertainties of the Simulation 35
4.1.3 Comparison of the Experimental Data with the Simulations 36
4.2 Wall Friction 38
4.3 Experiments with Turbomachinery 40
4.3.1 Comparison of the Experimental and Simulated Behavior of the Turbomachinery 43
4.3.2 Performance 46
4.4 Discussion of the Model Validation 48

5 A BWR Retrofitted with a Self-Propelling Heat Removal System 51
5.1 Concept 51
5.2 Design 53
5.2.1 Turbomachinery 56
5.2.2 Compact Heat Exchanger 56
5.2.3 Air-Cooled Heat Exchanger 60
5.2.4 Starting Procedure 61
5.3 Modeling of a Supercritical Carbon Dioxide Brayton Cycle with ATHLET 62
5.3.1 Compact Heat Exchanger 62
5.3.2 Air-Cooled Heat Exchanger 64
5.3.3 Turbomachinery 64

6 Simulation of Station Blackout and Loss of Ultimate Heat Sink Scenarios 67
6.1 Modeling of the Generic Boiling Water Reactor 67
6.1.1 The Thermohydraulics 67
6.1.2 The Instrumentation and Control System 68
6.2 Reference Case 70
6.3 Retrofitted BWR 74
6.4 Retrofitted BWR with Adapted Depressurization System 78
6.5 Retrofitted and Adapted BWR with Control Strategy 84
6.6 Turbo Compressor System Combined with a Reactor Core Isolation Cooling System 87
6.6.1 Description and Modeling of the Reactor Core Isolation Cooling System 88
6.6.2 Thermohydraulic Analysis 90

7 Summary and Conclusion **97**

8 References **101**

Appendix A – B-Spline Coefficients **106**

Appendix B – Process Signal **110**

Appendix C – Uncertainty Analysis **111**

Appendix D – ATHLET Input **115**

IV Nomenclature

Latin Symbols

a_i		coefficient for the calculation of the thermal conductivity
A	m²	(flow) area
b_i		coefficient for the representation of the zero-density viscosity
C_ϕ		two phase multiplier
c_p	J/(kgK)	specific heat capacity at constant pressure
C	m/s	spouting velocity
d	m	channel width
d_i		coefficient for the representation of the excess viscosity
D	m	diameter
Ec		Eckert-Number
f_{fr}	N/m³	friction force per unit volume
g	m/s²	gravity constant
g_i		coefficient for the calculation of the thermal conductivity
h	J/kg	specific enthalpy
h_i		coefficient for the calculation of the thermal conductivity
htc	W/(m²K)	heat transfer coefficient
k		weighting coefficient
l	m	length
m	kg/s	mass flow
n	1/s	number of revolutions
$n_{channel}$		number of channels per plate
n_i		coefficient for the calculation of the thermal conductivity
n_f	1/m	number of fins
n_p		number of pair of plates
Nu		Nusselt number
p	Pa	pressure
P	W	power
Pr		Prandtl number
q	W/m²	heat flux

q_{mf}	Ws/kg	heat input per mass flow
$\dot{q}_{str}$	W/m³	heat flow through structures
$\dot{q}_i$	W/m³	heat flow at the phase interface
Q	W	thermal heat flow
r	m	radius
r_{in}	m	inner radius
r_{out}	m	outer radius
R	m	wall roughness
Re		Reynolds number
s	m	distance
S	N/m³	momentum source
$S_{e,l}$	W/m³	external source term
t	s	time
t_p	m	plate thickness
t_w	m	wall thickness
T	K	temperature
U	m/s	rotor tip speed
u		velocity ratio
v	m³/kg	specific volume
V	m³	volume
w	m/s	velocity
w_p	m	plate width
w_0		weighting coefficient
W	W/m³	specific heat generation rate
x	m	length

Greek Symbols

α		steam void fraction
η		efficiency
κ	W/(mK)	thermal conductivity of sCO_2
ϑ	°C	temperature
λ	W/(mK)	thermal conductivity of structures
λ_{DW}		Darcy-Weisbach friction factor
μ	Pa s	(dynamic) viscosity
ξ_{form}	m^{-4}	friction loss coefficient per unit of squared area
ρ	kg/m^3	density
σ	MPa	stress
τ_i	N/m^3	interfacial shear per unit volume
ψ	$kg/(sm^3)$	interphase mass transfer rate

Subscripts and Superscripts

0	design point
$aero$	aerodynamic
ATH	calculated with ATHLET
b	bulk
c	compressor
e	external source
exp	experimentally determined
h	hydraulic
HT	heat transfer
HX	heat exchanger
i	interphase
iv	initial value
in	inlet
ins	inside
is	isentropic
l	liquid
m	mixture
out	outlet
$outs$	outside
pc	pseudo critical
r	reduced
rad	radial
rel	relative
s	surface
sh	shear
$stat$	statistic
str	structure
sys	systematic
t	turbine
$t$an	tangential
v	vapor

Abbreviations

AC	alternating current
ATHLET	Analysis of THermal-hydraulics of LEaks and Transients
BWR	boiling water reactor
CO_2	carbon dioxide
CV	control volume
DBC	design basis conditions
DEC	design extension conditions
DC	direct current
DDV	diversified depressurization valve
DEC	design extension conditions
EDG	emergency diesel generator
ENSREG	European Nuclear Safety Regulators Group
EOS	equation of state
EUR	European Utility Requirements
FEBE	time integration module within ATHLET
FWL	feedwater line
GCSM	general control simulation module within ATHLET
GRS	Gesellschaft für Anlagen- und Reaktorsicherheit
HCO	heat conduction object
HCV	heat conduction volumes
HECU	heat conduction module within ATHLET
I&C	instrumentation and control
LUHS	loss of ultimate heat sink
MSL	main steam line
NEUKIN	neutron kinetics module within ATHLET
NIST	National Institute of Standards and Technology
ODE	ordinary differential equation
PDE	partial differential equation
PWR	pressurized water reactor
RCIC	reactor core isolation cooling system
RPV	reactor pressure vessel
SBO	station blackout
sCO_2	supercritical carbon dioxide
TAC	turbine-alternator-compressor
TCS	Turbo Compressor System
TFD	thermo-fluiddynamics
TFO	thermo-fluiddynamic objects

1 Introduction

1.1 Motivation

Worldwide, around 12 % of the overall electricity [57] is produced by nuclear power plants. Nuclear fission is thereby utilized to generate heat that is converted into AC power, for instance via a Rankine steam cycle. This way of electricity production is extremely advantageous: It provides environmental benefits, due to a CO_2 neutral electricity production, while being continuously available, in contrast to most renewable energy sources. Moreover, the operation of a nuclear power plant is relatively cheap, due to its low fuel consumption.

The normal power operation can be interrupted, either due to a scheduled shut-down or due to an unexpected event, for example a component failure or an emergency situation that causes an automatic reactor scram. Even though the nuclear chain reaction is stopped with the reactor shut-down, residual heat is still produced within the core due to the decay of the fission products. At the moment of reactor shut-down, the decay heat is around 7% of the nominal thermal power [14] and decreases with an exponential function to around 1% after 1 hour. It is essential to remove the decay heat, to avoid heating-up of the fuel elements and therefore, to prevent core melting. This is important because molten corium can damage the plant and may become a threat to the safety barriers, which normally hinder the release of radioactive material into the environment. Highly reliable safety systems are implemented in nuclear power plants, to ensure the *cooling of radioactive material* [26], one of the main safety functions, during operational states as well as in design basis conditions (DBC). These design basis conditions haven been taken into account for the design of the plant, *such that the facility can withstand them [...] by the planned operation of safety systems* [26]. However, certain, very unlikely accidents may exceed this design basis, which can result in a failure of safety systems.

Such a beyond design basis accidents occurred in 2011 in Fukushima Daiichi Unit 1-3 [58], after the Tōhoku earthquake struck Japan. The shock caused a loss of offsite power, but the emergency diesel generators were started and the safety systems worked as anticipated. However, the generators stopped permanently, when they were flooded with seawater, by the subsequent tsunami. This resulted in a station blackout (SBO), i.e. the loss of all AC power sources, which lasted for an unexpectedly long period of time. The steam-driven Reactor Core Isolation Cooling (RCIC) system took over in the units 2 and 3. It was able to inject water and to provide core cooling for a certain time, until the batteries were empty, which were needed for the control of the system. This severely limited the options to actively remove decay heat. Moreover, the tsunami destroyed the water intake structures and pumping stations, which resulted in the loss of the ultimate heat sink (LUHS) in addition to the SBO and withdrew the option to transfer decay heat into the pacific. Units 1-3 lost the ability to independently control the accident and became dependent on external measures. However, due to the profoundly destroyed infrastructure, the necessary support arrived delayed and the emergency injection of coolant through fire engines could not be implemented as required. The intended safety measures have not been successful. Eventually, the cores were partly uncovered and the fuel claddings were damaged. Hydrogen was produced by the chemical reaction of the zirconium of the fuel cladding with the steam, which later caused explosions in unit 1 & 3. Radioactive material has been released to the environment.

The majority of nowadays operating nuclear power plants are generation II reactor concepts, such as the units in Fukushima Daiichi. These light water reactors *use traditional active safety features involving electrical or mechanical operations* [21] and depend heavily on electricity, in order to remove the residual heat. At this point in time, there are only minimal requirements for these nuclear power plants to cope with long-term station blackouts or design basis exceeding events, comparable to those in Fukushima. However, it is clear that the ongoing discussion on safety requirements is strongly influenced by the information gained from the continuing evaluations of the Fukushima events [54]. The Reaktor-Sicherheitskommission even expects that a diversified heat sink will be demanded in the future [46]. Furthermore, the European Nuclear Safety Regulators Group (ENSREG) has recently published a compilation of recommendations and suggestions [15] regarding their peer review of the European stress tests conducted after the Fukushima accidents. ENSREG thereby recommends that national regulators should consider the *implementation of measures allowing prevention of accidents and limitation of their consequences in case of extreme natural hazards*, because *such situations can result in devastation and isolation of the site, an event of long duration* and *the unavailability of numerous safety systems* [15]. Such measures may strengthen the defense in depth of existing plants and may enable them to deal with certain design basis exceeding events independently.

Generally, the scenarios SBO and / or LUHS have become a center of attention in nuclear safety research, long before the accidents of Fukushima underlined the significance of these events. That is why state of the art safety systems of most of the presently build plants rely on *the use of passive rather than active systems* [21]. The probability of a core melt accident for these advanced reactor designs of generation III+, which are based on the concepts of generation II plants, has significantly been reduced, due to the conducted safety enhancements. In addition to the passive safety systems, these reactors are equipped with a diverse heat sink to counter the named design extension conditions (DEC) independently. This is in accordance with the regulatory demands that apply for newly build nuclear power plants, like the European Utility Requirements (EUR) [16]. In fact, the EUR are not legally binding, but its design targets are taken as a basis for advanced European reactor concepts. For these designs, *provisions shall ensure that, also in the long term, an adequate heat sink is available under DBC and DEC* [16]. Most commonly, passive safety systems utilize big water reservoirs as ultimate heat sinks [25], which provide an interim period until further emergency procedures have to be implemented. These systems make use of huge heat exchangers to transfer the residual heat to the corresponding heat sinks. Due to the size of their components, these systems cannot be retrofitted into existing plants. Therefore, new approaches have to be developed.

One option is the self-propelling Turbo Compressor System (TCS) [33]; [35], which is based on the concept of a Brayton cycle and utilizes decay heat to power itself. This system removes decay heat and transfers it to the ambient air, which serves as an alternative and unlimited heat sink. Air-fans are intended to enhance the heat transfer between an air-cooled heat exchanger and the air, which are powered by electricity produced with the Brayton cycle. The working fluid within the system is supercritical carbon dioxide and its specific fluid properties enable its components to be extremely compact, which makes the system retrofittable. Unfortunately, the impact of the system on the power plant could not be analyzed sufficiently. Up to now, no thermohydraulic system code was available to simulate such a sCO_2 system and the interaction with existing safety systems.

1.2 State of the Art

Engineered safety features, i.e. systems, structures or components, are implemented in all nuclear power plants to perform safety functions, in order to ensure achievement of the three fundamental safety objectives [16]:

- Reactivity control
- Core heat removal
- Limitation of release

The control of the reactivity, i.e. for example *the sustainable termination of the chain reaction within the core* [28], is ensured even in SBO and / or LUHS scenarios, either through the insertion of the control rods or by the implementation of the neutron poison boron.
The limitation of the release and the activity retention is fulfilled by the safety barriers, for example the pressure retaining boundary or the containment. However, *the preservation of the barrier integrity is ensured by the compliance with the other two safety goals* [28]. Therefore, it is extremely important to ensure the cooling of the fuel elements and the residual heat removal during design basis and even design basis exceeding events.

1.2.1 Residual Heat Removal Systems of Boiling Water Reactors

The general approach to residual heat removal in BWRs of generation II is systematically shown in Figure 1-1 [42], visualized with the black lines.
Steam is generated by the decay heat that is still produced, even after the reactor is shut-down. If the isolation valves of the main steam lines are closed, vapor is released via the depressurization system (1) into the pressure suppression chamber, in order to limit the primary circuit pressure. The temperature of the water inventory within the pressure suppression chamber increases subsequently, due the condensing primary steam. Therefore, the residual heat removal system (2) is intended to cool the water. Additionally, it injects water into the isolated primary circuit, to make up for the losses due to the blow-down of steam and to ensure core covering. High-pressure pumps are therefore installed, powered either by electricity from the grid, or by the emergency diesel generators (EDG). Heat is

transferred from the pressure suppression chamber via the residual heat removal system (2) to a closed cooling water system (3). This cycle simply ensures that potentially contaminated water cannot come into contact with the environment, e.g. the river water. Water is therefore circulated in a closed loop, driven by pumps dependent on AC power and the heat is further transferred to the service water (4). This water generally originates from the main heat sink, for instance a river or the ocean and is again, electrically propelled.
In the very unlikely event of a loss of the ultimate heat sink, the general approach to residual heat removal fails. The decay heat could not be removed from the containment. Furthermore, a station blackout would also result in the inability to remove heat, as the approach relies heavily on electrically driven pumps. Additionally, the option to inject coolant into the primary circuit by implemented measures would be lost. In order to deal with such a scenario, generation II BWRs depend on external support and mobile equipment.

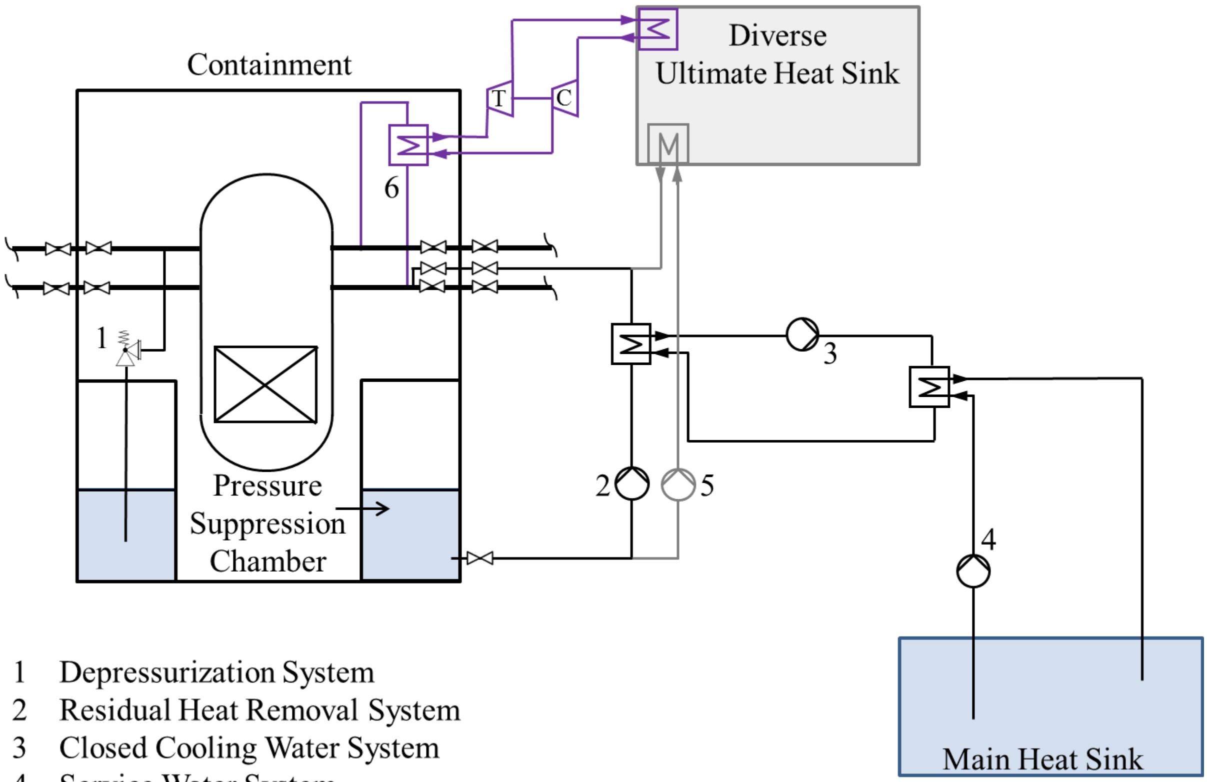

1 Depressurization System
2 Residual Heat Removal System
3 Closed Cooling Water System
4 Service Water System
5 Additional Heat Removal System
6 Turbo-Compressor-System

Figure 1-1: Residual Heat Removal for BWRs

Different approaches, as seen in Figure 1-2, have been conducted to enhance the safety of nuclear power plants of generation II and to provide an alternative path of residual heat removal, if the main heat sink is lost or the corresponding components are destroyed. One example is the Additional Heat Removal System (5) that has been retrofitted in Gundremmingen [32]. It is independent from the residual heat removal system and provides an option to cool the pressure suppression chamber and to inject water into the isolated primary circuit. The electricity that is necessary to power the corresponding pumps can be provided by a diversified, air-cooled emergency diesel generator. This is very important, as the regular EDGs are generally cooled with the service water system, which is assumed to be unavailable in case the main heat sink is lost. Furthermore, the ambient air is utilized as the alternative ultimate heat sink via a wet cell-type cooling tower. The ability to remove heat to the air is thereby dependent on a water reservoir that decreases continually due to evaporation losses. It has to be replenished within 10 hours from the system startup, in order to continue the heat removal. Therefore, the Additional Heat Removal System can extend the grace period by 10 hours [32].

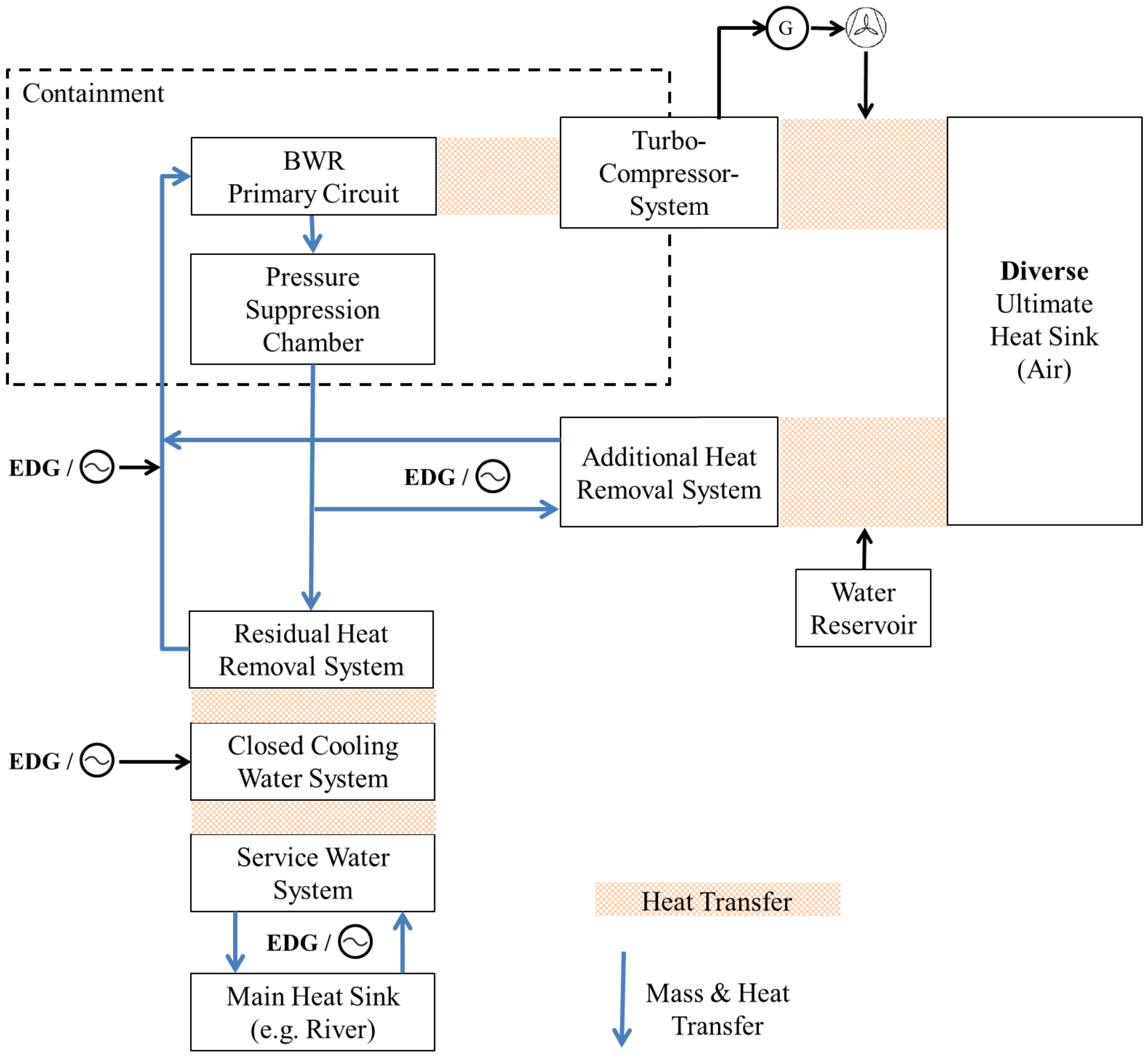

Figure 1-2: Retrofit Options for the Residual Heat Removal – Mass & Heat Flows

The Turbo Compressor System (6) [60]; [61], operates differently, because it removes the residual heat directly from the isolated primary circuit, due to the condensing of primary steam. The heat exchanger, in which the vapor condenses, has to be placed within the containment to ensure the confinement of radioactive material. So-called minichannels, with small hydraulic diameters are utilized in this compact heat exchanger, in order to establish a large heat transfer area regardless of the stringent space limitations. The decay heat is transferred to the cooling circuit, which is a Brayton cycle. It is self-propellant, since the expansion work gained in the turbine exceeds the necessary compression work. An attached generator even provides the electricity that is needed to power the air-fans. Since the system operates independent from any external supply, such as water or electricity, the implementation of this system has the potential to extend the grace period significantly. The reactor pressure vessel pressure stays within acceptable limits and the steam is not blown into the pressure suppression chamber. Thereby, it becomes unnecessary to inject coolant into the primary circuit.

1.2.2 Requirements for Retrofit Options for Residual Heat Removal

The European Utility Requirements summarize requirements, which apply to residual heat removal systems of newly build nuclear power plants. If feasible, these specifications should also be applied for retrofittable heat removal system to ensure highest safety standards and to achieve a state-of-the-art technology improvement of the existing plants. Generally, it is required that *the core heat removal function shall ensure transfer of the heat from the fuel to […] heat sink in all DBC and DEC* [16]. To be able to counter design extension conditions, occurring for example during a combined station blackout and loss of ultimate heat sink scenario, a retrofittable residual heat removal system has to be independent from external resources like water or electricity. Therefore, it has to be passive or self-propelling and has to transfer the decay heat to an alternative ultimate heat sink. Internally provided resources, for example a *water inventory, shall allow system operation for at least 72 hours without replenishment* [16]. This means that any retrofitted system should be able to operate independently for a minimum of three days. The corresponding components have to be integrated into existing buildings, which asks for a compact design, especially regarding the components that are placed in the containment, since stringent space limitations apply. In addition to the spatial integration, the approach of a retrofitted residual heat removal system has to be in accordance with the established safety concept, negative interferences between retrofitted and existing systems shall be avoided. The design has to be robust to ensure a low failure probability. This can be achieved through the usage of reliable components and by refraining from manual interventions, since these are prone to errors, especially during emergency situations. Therefore, any retrofittable residual heat removal system should be self-controlling, or passive mechanisms should be integrated, to adapt the amount of removed heat in line with the amount of decay heat. Because the system has to be available even under design extension conditions, it should not be vulnerable to external hazards. Potential retrofit options have to be capable to start and operate under all possible boundary conditions that may occur in the primary circuit or the utilized alternative heat sink.

1.2.3 Evaluation of Residual Heat Removal Systems

The impact of a residual heat removal system on the behavior of a plant has to be known precisely. It plays an important role during the design process as well as for the operation of a nuclear power plant. To account for complex interactions between different systems, advanced system codes are utilized to simulate the thermal-hydraulic behavior of a reactor during transient scenarios. The insight that is gained with these simulations helps to evaluate the plant and particular safety systems and reveals if the requirements for such a system can be fulfilled.

Different thermal-hydraulic codes are available, such as RELAP or ATHLET. These can be utilized to simulate heat removal systems composed of known components, such as heat exchangers, pumps or valves, which can be directly integrated into existing input decks that describe a plant. However, no system code exists at this point in time that is able to simulate the Turbo Compressor System and its interaction with the power plant adequately. In the past, RELAP5 has been extended by the fluid properties of supercritical carbon dioxide and an appropriate heat transfer correlation [6]. Additionally, efforts have recently been made to adapt RELAP5-3D for the *modelling of a supercritical CO2 power cycle for nuclear fusion reactors* [4] and therefore to simulate a Brayton cycle. However, the models utilized for the simulation of the turbomachinery are not able to simulate the behavior during off design conditions and assume for example a constant efficiency [4]. To improve these models, comprehensive modifications of the source code would be necessary. But, the source code of this modified RELAP version is not at hand. An alternative system code is ATHLET, which is developed by the Gesellschaft für Anlagen- und Reaktorsicherheit (GRS) in Germany. The code is widely used throughout numerous institutions and its development is done in close cooperation with the Institute of Nuclear Technology and Energy Systems at the University of Stuttgart. The availability of the source code, as well as the network with the GRS provides the perfect basis for the extension of ATHLET. Therefore, ATHLET has been selected as the simulation tool to model the self-propelling heat removal system.
However, several code extensions are necessary, because the novel self-propelling heat removal system includes components that have so far not been used in the nuclear industry. In addition, the working fluid, supercritical carbon dioxide, is unusual and therefore also not implemented in ATHLET. Consequently, the Turbo Compressor System cannot be simulated with the currently available ATHLET version 3.0 A [37].

Until now, the simulation of the novel system has been simplified. A constant heat sink was therefore attached to existing thermal-hydraulic objects of the applied input deck [48]. However, this approach does not account for the transient behavior of the self-propelling system itself and the influence of changing boundary conditions on the system's performance. The method seems only eligible for a first feasibility study to estimate the amount of decay heat that has to be removed, in order to control the scenario.
To simulate such a self-propelling system properly and to enable the code user to evaluate the system and its interaction with other systems on a more profound basis, a model has to be developed and integrated into ATHLET.

1.3 Aim of the Present Work

The aim of the present work is to develop and to provide a validated tool for complex thermal-hydraulic calculations of supercritical carbon dioxide Brayton cycles. The code development allows for the simulation and evaluation of the Turbo Compressor System. This is demonstrated for a typical application, i.e. a generic boiling water reactor of generation II, retrofitted with this novel heat removal system.

Main emphases of the present work are:

- The development of a model that is able to describe the thermal-hydraulic processes of a sCO_2 Brayton cycle and the integration of this model in the system code ATHLET. Therefore, the fluid properties of supercritical carbon dioxide shall be implemented to account for the additional working fluid. Furthermore, a correlation for the heat transfer has to be introduced, as well as component models for the radial turbomachinery.

- The validation of the implemented correlations and models against experimental data, to show that the developed model is able to simulate the behavior of a sCO_2 Brayton cycle within an acceptable range of accuracy. Therefore, single effect experiments, regarding the heat transfer and the pressure drop for sCO_2, shall be recalculated and compared to the available information. Furthermore, a closed Brayton cycle shall be modeled and the simulation results examined in contrast to experimental data, in order to gain confidence about the ability of the code to simulate the entire process.

- A typical application of the self-propelling system, as a potential retrofit measure for a boiling water reactor, to demonstrate the feasibility of the extended ATHLET version to simulate the novel heat removal system. Therefore, a rough dimensioning of the main components has to be conducted. The process shall include a feasibility study to determine the amount of heat that has to be removed, as well as first thermodynamic cycle calculations. The input deck of a generic BWR shall be extended by the Turbo Compressor System. Combined SBO & LUHS scenarios will have to be simulated and the impact of the self-propelling system on the overall behavior of the BWR has to be analyzed. Interferences with existing safety systems will be revealed and it shall be determined, which parameters have an effect on the operation of the Turbo Compressors System. A set of prerequisites shall be developed, which are necessary for the system to deal with such a scenario independently.

2 Description of the Thermohydraulic Code

A one-dimensional system code has been selected to analyze the influence of the self-propelling heat removal system on a generic boiling water reactor. This allows the simulation of the investigated transient over three days within an acceptable simulation time. In contrast, three-dimensional simulation tools, which are actually capable to model multi-dimensional flow behaviors [27], would require much higher computational costs. In addition, a comprehensive three dimensional model of a generation II reactor would be necessary, which is not available. Therefore, the one-dimensional system code ATHLET has been chosen for the conducted analysis.

The thermohydraulic system code ATHLET [37] (Analysis of THermal-hydraulics of LEaks and Transients) is developed by the GRS (Gesellschaft für Anlagen und Reaktorsicherheit) and describes two-phase flow in one-dimensional models. The computer code is able to reproduce design basis, as well as beyond design basis accidents of light water reactors without core degradation. It is suitable to analyze the response of existing plants to anticipated transients. Furthermore, as in the present work, it can be used to evaluate the influence of newly developed systems on the overall behavior of a plant and is able to reveal potential interactions between new and existing systems.

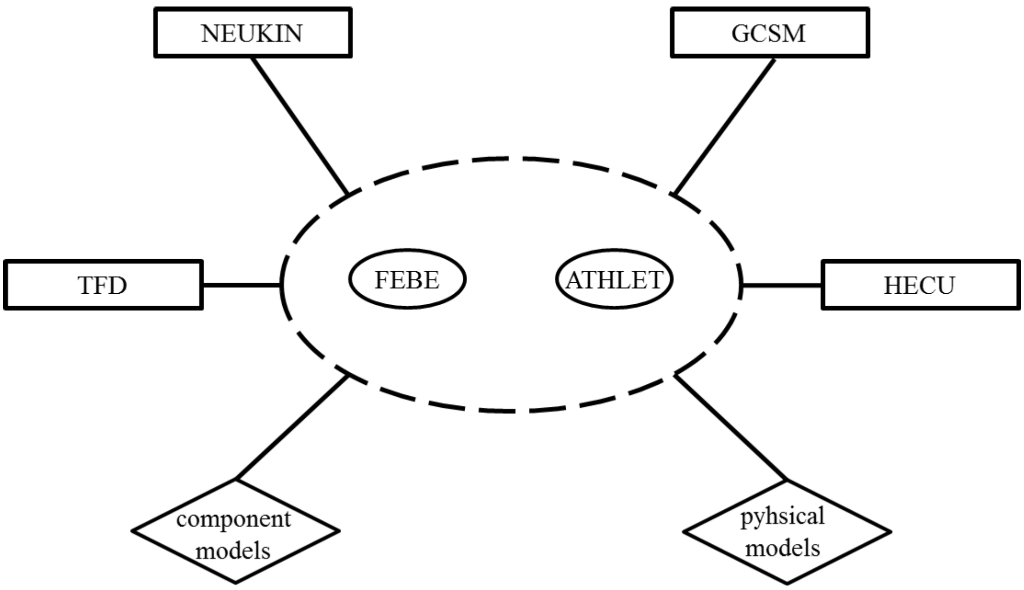

Figure 2-1: The Modular Structure of ATHLET

The computer code ATHLET has a modular structure and is organized on three levels. The four basic modules, which simulate the physical processes are: Thermo-fluiddynamics (TFD), Heat Transfer and Heat Conduction (HECU), General Control Simulation Module (GCSM) and Neutron Kinetics (NEUKIN). The general control and organization module ATHLET, as well as FEBE, which solves the ordinary differential equations (ODEs) belong to the second subdivision. The third level consists of a cluster of physical models, as well as component models.

2.1 Thermo-Fluiddynamics

The thermo-fluiddynamic (TFD) module determines the initial thermo-fluiddynamic state of a system through the steady state calculation and computes further the response of a system during transient boundary conditions. It receives and interchanges data with other modules and is the leading module of ATHLET.

A one-dimensional system code approximates the relevant flow variables of a two-phase flow over the corresponding flow cross section and averages the values over a short time interval. The thermo-fluiddynamics can be expressed with two different approaches. Firstly, by 5 partial differential equations (PDEs), which are explained in chapter 2.1.1 and describe the conservation equations for mass, momentum and energy. This 5-equation model determines the mass and energy conservation equation separately for the liquid and vapor phase and computes one homogenous mixture momentum conservation equation. Secondly, a two-fluid model with 6 partial differential equations can be selected by the user, which applies also the momentum conservation equation separately for the liquid and vapor phase.
However, the conservation equations are not a closed mathematical system. Therefore, constitutive equations are necessary, described in chapter 2.1.2. Sets of empirical correlations are available in ATHLET to account for instance for friction losses or the heat transfer regarding to the flow characteristics. Flow regimes that can occur in a vertical pipe are exemplarily shown in Figure 2-2. Additionally, the thermodynamic properties of the working fluids have to be available in form of an equation of state.

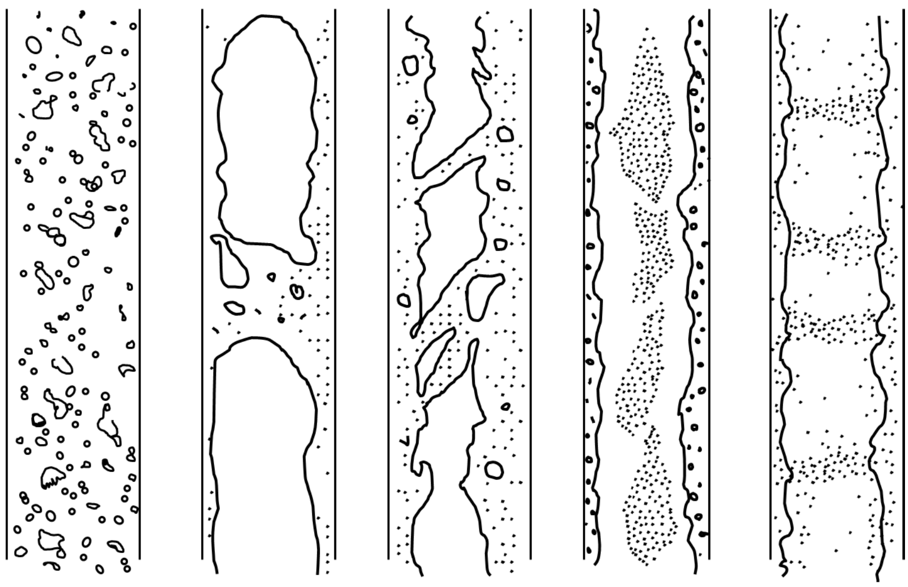

Figure 2-2: Flow Regimes in a Vertical Pipe, According to [5]

The flow regimes are differentiated based on the orientation of the pipe and the average vapor and liquid velocity, by means of appropriate flow pattern maps, as seen in Figure 2-3.

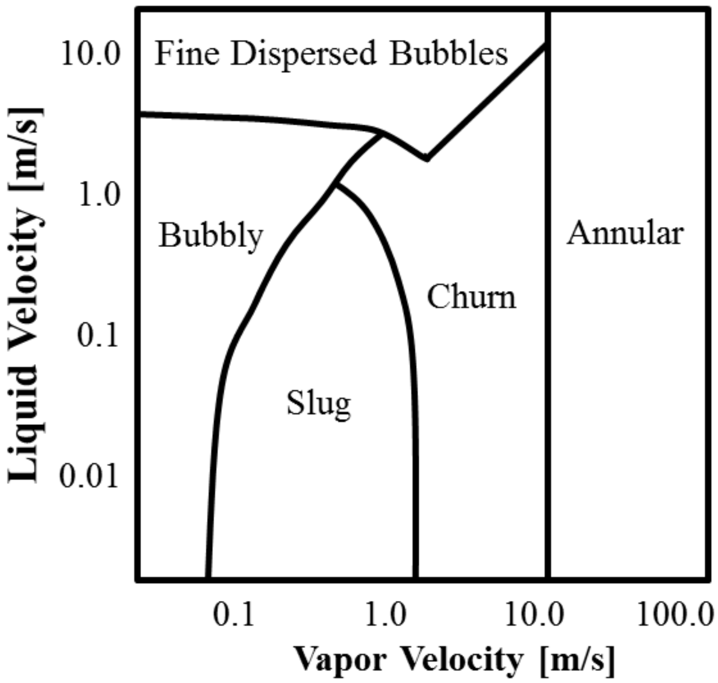

Figure 2-3: Flow Pattern Map for Upward Flow in Vertical Pipes, According to [55]

2.1.1 Conservation Equations

For the current analysis, the 5-equation model has been selected, since the supercritical carbon dioxide, which is the focus of attention, is considered as single-phase fluid. Separated momentum conservation equations are therefore not necessary. The 5-equation model is described in more detail in the following.

Thermo-fluiddynamic systems are represented by chains of connected thermo-fluiddynamic objects (TFOs), which form a network. These TFOs are discretized in cells, in order to obtain a staggered grid. The cells are in the following referred to as control volumes (CVs) and their connections are called junctions. This is illustrated in Figure 2-4.

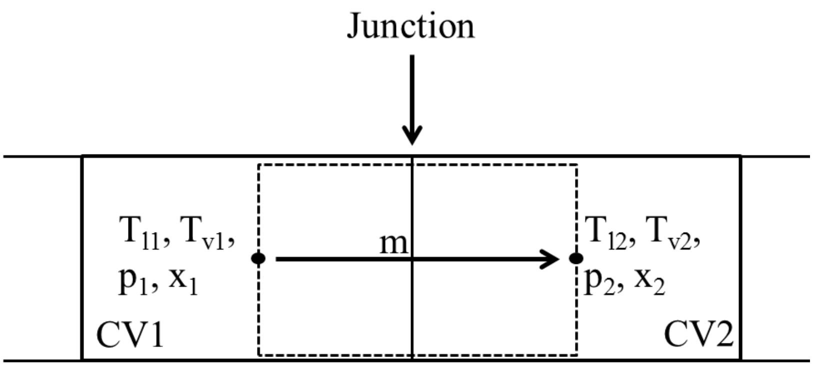

Figure 2-4: Control Volumes and Junction

The partial differential equations are set up over the control volumes, whereby the conservation equations for mass and energy are solved within these control volumes and the momentum equation is solved over the flow paths, i.e. the junctions. The solution variables of ATHLET are the pressure, the vapor and liquid temperature, the mass quality, as well as the mass flow rate.
The pressure and temperature, and accordingly the enthalpy and density of the working fluid are defined within the control volume. However, the mass flow is defined over the junction.

The general **mass conservation** equations for liquid and vapor are

$$\frac{\partial((1-\alpha)\rho_l)}{\partial t} + \frac{\partial}{\partial x}\left((1-\alpha)\rho_l \vec{w}_l\right) = -\psi \tag{2.1}$$

$$\frac{\partial(\alpha\rho_v)}{\partial t} + \frac{\partial}{\partial x}(\alpha\rho_v \vec{w}_v) = \psi \tag{2.2}$$

Where α is the void and correspondingly $1-\alpha$ the liquid fraction; ρ_v and ρ_l are the vapor and liquid densities; and $\vec{w}_v$ and $\vec{w}_l$ are the velocities of the vapor and the liquid. Changes either over time t and / or the flow path x will result in an interphase mass exchange ψ.
The partial differential equations 2.1 and 2.2 are spatially integrated over the flow path, i.e. the length of the control volume, in order to obtain ordinary differential equations (ODEs).

The **energy conservation** for the liquid phase is given by equation 2.3, whereas the energy conservation of the vapor phase is described by equation 2.4.

$$\frac{\partial\left[(1-\alpha)\rho_l\left(h_l + \frac{1}{2}\vec{w}_l\vec{w}_l - \frac{p}{\rho_l}\right)\right]}{\partial t} + \frac{\partial}{\partial x}\left[(1-\alpha)\rho_l\vec{w}_l\left(h_l + \frac{1}{2}\vec{w}_l\vec{w}_l\right)\right] = \tag{2.3}$$

$$-p\,\frac{\partial(1-\alpha)}{\partial t}$$

$+\,\psi(h_{\psi,l} + \frac{1}{2}\,\vec{w}_\psi\vec{w}_\psi)$	energy flow due to phase change
$+\,\vec{\tau}_i\vec{w}_l$	shear work at the phase interface
$+\,(1-\alpha)\vec{\tau}_i(\vec{w}_v - \vec{w}_l)$	dissipation due to interfacial shear
$+\,(1-\alpha)\rho_l\vec{g}\vec{w}_l$	gravitational work
$+\,\dot{q}_{str}$	heat flow through structures
$+\,\dot{q}_i$	heat flow at the phase interface
$+S_{e,l}$	external source terms

$$\frac{\partial\left[\alpha\rho_v\left(h_v+\frac{1}{2}\vec{w}_v\vec{w}_v-\frac{p}{\rho_v}\right)\right]}{\partial t}+\frac{\partial}{\partial x}\left[\alpha\rho_v\vec{w}_v\left(h_v+\frac{1}{2}\vec{w}_v\vec{w}_v\right)\right]= \tag{2.4}$$

$-p\,\frac{\partial\alpha}{\partial t}$

$+\,\psi(h_{\psi,v}+\frac{1}{2}\,\vec{w}_\psi\vec{w}_\psi)$	energy flow due to phase change
$-\,\vec{\tau}_i\vec{w}_v$	shear work at the phase interface
$+\,\alpha\,\vec{\tau}_i(\vec{w}_v-\vec{w}_l)$	dissipation due to interfacial shear
$+\,\alpha\rho_v\vec{g}\vec{w}_v$	gravitational work
$+\,\dot{q}_{str}$	heat flow through structures
$+\,\dot{q}_i$	heat flow at the phase interface
$+S_{e,v}$	external source terms

Where h_l are the liquid and h_v correspondingly the vapor enthalpy; p is the pressure; and $\vec{w}_\psi$ is either the velocity of the liquid, in case of evaporation or the velocity of the vapor, in case of condensation.

Again, the PDEs 2.3 and 2.4 are spatially integrated over the control volume, leading to ordinary differential equations that can be solved by means of the FEBE module, which includes a time advancement procedure.

The last term of the 5-equation model is the **momentum conservation** equation for a two-phase mixture

$$\frac{\partial(\rho_m\vec{w}_m)}{\partial t}-\vec{w}_m\frac{\partial\rho_m}{\partial t}+\rho_m\vec{w}_m\frac{\partial}{\partial x}\vec{w}_m+\frac{\partial}{\partial x}\left(\alpha(1-\alpha)\frac{\rho_v\rho_l}{\rho_m}\vec{w}_r\frac{\partial}{\partial x}\vec{w}_r\right)+\frac{\partial}{\partial x}p= \tag{2.5}$$

$\vec{f}_{fr}$	wall friction and form losses
$+\,\rho_m\vec{g}$	gravitation
$+\,S_{e,m}$	external momentum source terms

Where the two-phase mixture density is determined with

$$\rho_m=\alpha\,\rho_v+(1-\alpha)\rho_l \tag{2.6}$$

The mixture velocity with

$$\vec{w}_m = \frac{1}{\rho_m}\,(\alpha\rho_v\vec{w}_v + (1-\alpha)\rho_l\vec{w}_l) \tag{2.7}$$

And the relative velocity

$$\vec{w}_{rel} = \vec{w}_v - \vec{w}_l \tag{2.8}$$

2.1.2 Constitutive Equations

Since the conservation equations are not a closed mathematical system, the thermohydraulic model is completed by empirical correlations and physical models, the constitutive equations.

Physical models are called upon by the modules and comprise for instance the heat transfer package, which is needed by the Heat Conduction and Heat Transfer module HECU, for the determination of the heat transfer coefficient. Furthermore, a working fluid property package is included that supplies the thermodynamic and transport properties of different fluids, for example light, heavy and supercritical water, helium or liquid lead. They can be computed as a function of the state variables temperature and pressure.

During thermodynamic non-equilibrium conditions, i.e. during condensation or evaporation, the equations of mass conservation (2.1 & 2.2) are determined by the total mass transfer rate over the phase boundary interface within a control volume. The total mass transfer rate is composed of ψ_s, i.e. the evaporation or condensation directly at heated or cooled surfaces, as well as ψ_b, which accounts for mass transfer rate within the bulk

$$\psi = \psi_b + \psi_s \tag{2.9}$$

The calculation of the mass transfer due to evaporation within the bulk is thereby based on heat transfer correlations, whereas the condensation within the bulk is calculated with a model based on the energy balance at the phase boundary interface. The condensation or evaporation rate immediately at the wall surface ψ_s is directly accounted for in the heat transfer models called by HECU.

The relative velocity $\vec{w}_r$ between the fluid and the vapor phase is determined by means of the constitutive drift-flux model. It provides a one-dimensional description of the velocity differences, such that the liquid and vapor phase velocities can be calculated by

$$\vec{w}_l = \frac{m}{A\,\rho_m} - \frac{\alpha\rho_v\vec{w}_r}{\rho_m} \tag{2.10}$$

$$\vec{w}_v = \frac{m}{A\,\rho_m} + \frac{(1-\alpha)\rho_l\vec{w}_r}{\rho_m} \tag{2.11}$$

Where m is the total mass flow and A is the total cross section.

The **Heat Conduction and Heat Transfer module HECU** can simulate one-dimensional temperature profiles and heat conduction in the components.
A heat conduction object (HCO) can link two thermo-fluiddynamic objects, to model the heat transfer between them. Alternatively, a HCO can be coupled to one TFO and a time-dependent temperature as the second boundary conditions, provided via GCSM.
The nodalization of the HCOs in heat conduction volumes (HCVs) occurs automatically, according to the control volumes of the attached TFOs.

An appropriate heat transfer coefficient (HTC) has to be determined beforehand, in order to calculate a realistic heat flow into and out of the HCOs. The user can choose between four different options to determine the heat transfer coefficient:

- a constant HTC can be input via the data deck,
- a constant heat flow can be applied, i.e. the HTC adapts to meet the heat flow,
- the HTC can be a function of the temperature and inserted via a GCSM signal and
- the HTC can be determined by means of empirical correlations.

Besides the heat transfer coefficient, also the geometry of the component has a strong influence on the heat flow. Therefore, the heat conduction objects can be represented as plates, as well as full and hollow cylinders and spheres. In accordance with the geometry, ATHLET selects an appropriate equation.

The time-dependent behavior of the temperature profile in a HCV can be determined, by applying the law of energy conservation

$$\int_V W\, dV \qquad = \qquad c_p\, \rho \int_V \frac{\partial T}{\partial t}\, dV \qquad + \qquad \int_x \vec{q}\, d\vec{A} \tag{2.12}$$

heat generation W that takes place within the volume V of the HCV	change of internal energy, due to enthalpy changes, with respect to the specific heat capacity c_p of the solid structure	heat flow crossing the boundary, i.e. the surface $\vec{A}$ over the length x of the HCV

Eventually, this leads to equation 2.13, which can be solved with a time integration package

$$\frac{dT}{dt} = \frac{1}{\rho\, c_p\, V}\,(Q_{in} + WV - Q_{out}) \tag{2.13}$$

The module HECU is able to model heat losses through structures and contains a special model to simulate for instance the nuclear heat input through the rods. It can describe heat exchangers either in co- or counter-current flow, but is not able to represent a cross-flow heat exchanger without a significant increase of computational time.

The pressure losses due to **form losses and wall friction**, as in equation 2.5, are determined with a constitutive model, based on the assumption of homogenous flow

$$\Delta p_{friction} = -\int f_{fr}\, dx = \Delta p_{form} + \Delta p_{wall} \tag{2.14}$$

Form losses are caused through bends and branches or cross section changes of the flow path

$$\Delta p_{form} = -\xi_{form} \frac{1}{2\,\rho_m} m\,|m| \tag{2.15}$$

The form loss coefficient ξ_{form} can be specified by the user. However, ATHLET calculates a minimum form loss coefficient, according to the cross section changes and selects the maximum value of both alternatives.
The pressure loss due to the wall friction is calculated according to

$$\Delta p_{wall} = -\lambda_{DW} \frac{1}{2\,\rho_l} \frac{l}{A^2 D_h} C_\phi\ m\,|m| \tag{2.16}$$

The Darcy-Weissbach friction factor λ_{DW} can be determined by the user via the input data deck, or can be calculated, depending on the flow regime, i.e. laminar or turbulent. For turbulent flows, ATHLET applies the Colebrook equation 2.17

$$\frac{1}{\sqrt{\lambda_{DW}}} = -2\,lg\left(\frac{2.51}{Re\,\sqrt{\lambda_{DW}}} + 0.27\,\frac{R}{D_H}\right) \tag{2.17}$$

To account for higher pressure losses for two-phase flows, a two-phase multiplier C_ϕ is included, which can be determined with different methods. Figure 2-5 shows exemplarily the Martinelli-Nelson two-phase friction multiplier, depending on the steam void fraction and the fluids pressure. One can see that the factor becomes one for a purely liquid fluid.

Due to the one-dimensional approach, ATHLET is not able to account for differences between the wall and bulk temperature of the fluid. However, in the vicinity of the critical or pseudo-critical temperature, this effect becomes dominant as the fluid properties change drastically. Therefore, a correction factor for the determination of the pressure losses due to the wall friction and form losses has been implemented in ATHLET for the working fluid supercritical water. The factor accounts for density and viscosity differences at the surface temperature.

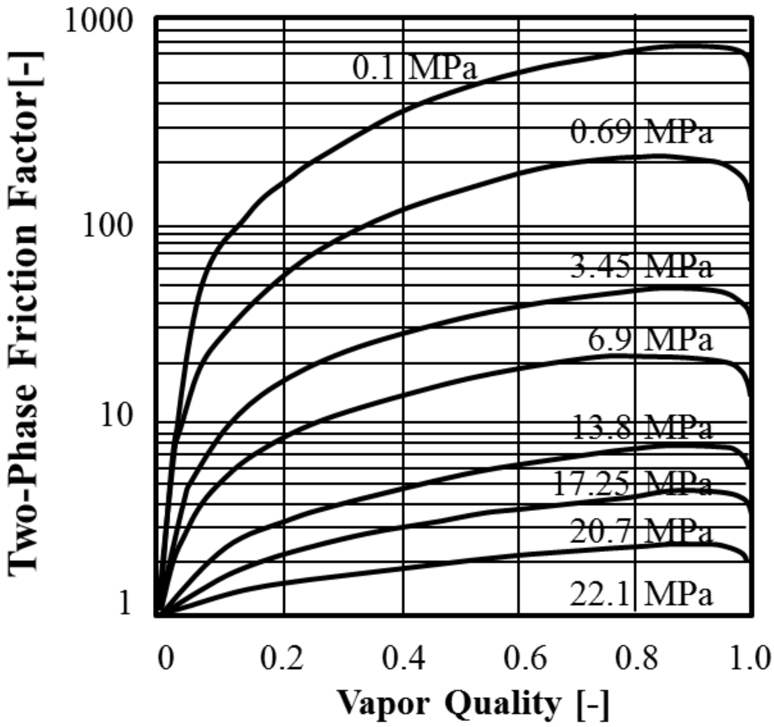

Figure 2-5: Two Phase Multiplier, According to [39]

2.2 Time Integration

Originally, the conservation equations for mass, momentum and energy are time and space dependent and formulated as partial differential equations (PDE). However, the thermo-fluiddynamic objects are discretized in space, as the pipe objects are subdivided in adjacent spatial entities, the control volumes (CVs). Therefore, the PDEs can be integrated over the flow path. The physical quantities in each basic element, i.e. CVs and junctions, are therefore time-dependent only. Their temporal evolution can be described by a system of ordinary differential equations (ODE)

$$\frac{d\vec{u}}{dt} = f(\vec{u}(t), t) \tag{2.18}$$

This leads to an initial value problem, which cannot be solved analytically and the solution variables have to be approximated numerically

$$\vec{u}(t_{iv}) = \overrightarrow{u_{iv}} \tag{2.19}$$

Therefore, the time advancement procedure, i.e. the module FEBE, short for Forward-Euler, Backward-Euler, discretizes the system of ODEs in time and performs the numerical time integration of the thermo-fluiddynamics.

The time advancement procedure is twofold. Firstly, the linear implicit Euler method is applied and solutions of the ODE system can be calculated. Unfortunately, only small time steps would be allowed, in order to fulfill satisfactory accuracy requirements. However, to increase the time step and therefore to reduce the computational cost of the integration, secondly, an extrapolation algorithm is applied.
Two Euler solutions are calculated, at the determined time step Δt and at half the time step Δt/2. A third solution is extrapolated with these values, as shown in Figure 2-6. Subsequently the solution at Δt is compared with the extrapolated value. If the difference is below the preset error bound, the extrapolation is taken as the solution. Otherwise an additional Euler solution at Δt/3 is determined and also extrapolated. The new extrapolation is again compared with the solution at Δt. If the difference is still larger than the error bound, a reduced time step Δt_r is introduced and the procedure is repeated.

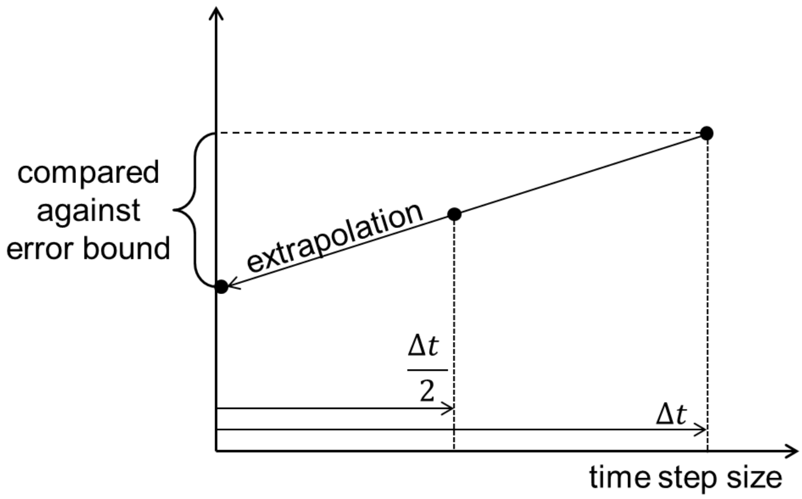

Figure 2-6: FEBE Extrapolation Pattern

2.3 General Control Simulation Module

General Control Simulation Module (GCSM) can be used for the simulation of control systems and can provide for example time-dependent information. In the current analysis, it is for example used to simulate the power balance of the Turbo Compressor System. The GCSM module is based on a block-oriented simulation language and contains logical, analog and other specific controllers. Each control block has up to four input variables. The output data, i.e. the generated control signal, can be returned to the TFD module as input for other models, for example to determine a valve position. However, the control signal can also serve as an input variable for another control block to describe more complex control circuits.
In addition, a special controller is available that provides an interface for the coupling of external simulation models, such as the containment model CONDRU.

2.4 Neutron Kinetics

The module NEUKIN describes the neutron kinetics of the core and calculates therefore the nuclear heat generation of the simulated plant. The prompt power from the fission, as well as the decay heat of short-lived fission products are calculated either with a point-kinetics model or with a simplified one-dimensional model that solves the time-dependent neutron diffusion equations. In addition, the decay heat from the long-lived fission products has to be added, in order to get the total reactor power. This decay heat is computed by multiplying the nominal reactor power with a factor, which becomes time-dependent in case of reactor scram and which is input via a tabulated GCSM signal.
For the conducted analysis, the point-kinetics module is applied. However, during the vast majority of the analyzed transient only the decay heat is of importance, since the reactor is scrammed when the initiating event occurs. Therefore, the NEUKIN module is only relevant during the steady-state calculation at the beginning of the simulation and to model the impact of the control rod insertion on the reactivity and thereby the corresponding heat input.

2.5 Component Models

Components can generally be modeled with thermo-fluiddynamic objects that can be coupled to heat conduction objects, which can both be described with the input data. However, certain elements need particular models. For boiling water reactors this includes for instance models for:

- Fills – A fill discharge or injection can be simulated at a junction at the edge of any system. The mass source or sink, as well as the corresponding enthalpy of the fluid are controlled by GCSM signals. This model is for example important to couple the model CONDRU of the wetwell, to the primary circuit of a BWR. Primary steam released through the safety and relief valves is simulated with a negative fill, whereas the equivalent is added to the wetwell by a positive fill.
- Pumps – A pump increases the pressure of the working fluid passing it, which is considered as an external momentum source $S_{e,m}$ in the momentum equation 2.5. Different pump models are available to account for different control strategies. However, the simulation of a pump is not important for the conducted analysis, due to their immediate failure caused by the station blackout.
- Valves – Valves are also junction related models and can represent any position between a fully opened and completely closed valve. The actual cross section area of the valve is determined via a GCSM signal. This cross section has a significant influence on the fluid's velocity, as well as the mass flow through the valve, which becomes zero as the valve closes. A valve increases the pressure drop due to the extra form loss that is added to Δp_{form}. This form loss coefficient is input by the user and weighted as a function of the open cross section.
- Water-steam separators – This special component consists of a pipe with a single control volume, but three junctions, i.e. one regular entrance junction, one exit junction for the water that enters the separator and one exit junction for the steam,

which requires a special separator differential equation for the determination of the mass flow.

- Turbines – Steam turbines can be simulated with an optional number of turbine stages, which are placed in a so-called turbine pipe. The resulting pressure drop is considered directly at the junction, whereas the power that is extracted from the fluid and actually converted into mechanical energy is removed in the subsequent control volume. The turbine model is described in detail in chapter 3.2.1.

3 Adaptation of ATHLET to Simulate the Turbo Compressor System

To enable the current ATHLET version 3.0 A [37], to model a sCO_2 driven Brayton cycle, several code extension were necessary. First of all, the fluid properties of the actual working fluid had to be introduced. ATHLET requires the specific volume, the enthalpy, the viscosity and the thermal conductivity to be functions of the state variables temperature and pressure, the corresponding implementation is described in chapter 3.1.1. Secondly, a correlation for the heat transfer has been added, to account for the specific behavior of supercritical fluids, chapter 3.1.2. The proceeding for the calculation of the pressure drop, due to wall friction, has been adopted from the original ATHLET version. Therefore, the method is described in more detail in chapter 3.1.3. Lastly, new component models for the simulation of radial turbines and compressors have been introduced. The original turbine model and the conducted adaptions are described in chapter 3.2.1, information about the compressor model can be found in chapter 3.2.2.

3.1 Implementation of Supercritical Carbon Dioxide as Working Fluid

Supercritical carbon dioxide has been implemented into ATHLET as additional working fluid. The user can select the new fluid for any thermo-fluid system, through the input data.
The behavior of supercritical carbon dioxide changes from fluid-like, at low pressures and temperatures to gas-like at high pressures and temperatures [53]. Exemplarily, this can be seen in Figure 3-1 which shows the density of four isobars of sCO_2. The density decreases for increasing temperatures, whereas the derivation of the density approaches infinity at the critical point, i.e. 30.978 °C and 7.3773 MPa.

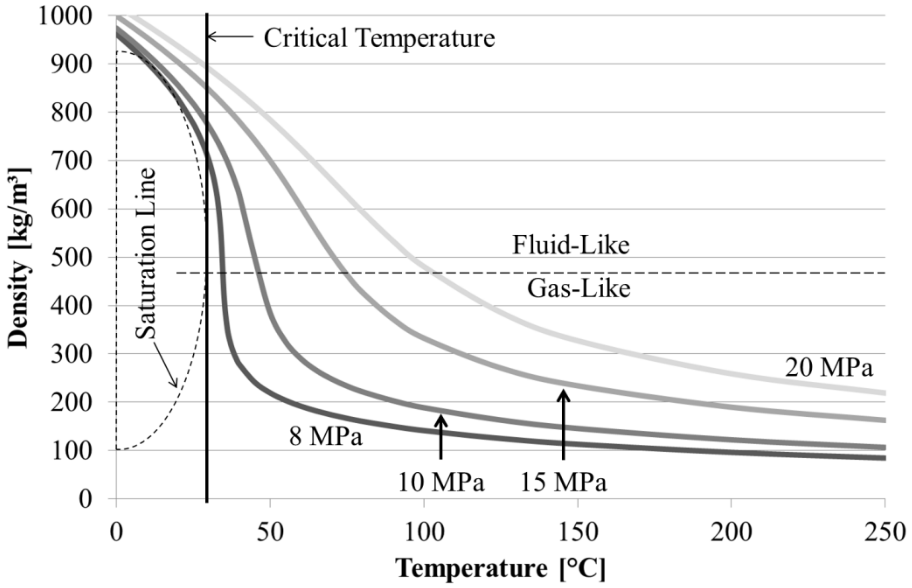

Figure 3-1: Temperature – Density Diagram of Supercritical Carbon Dioxide

Another prominent characteristic of supercritical carbon dioxide is a peak in the specific heat capacity, at the pseudocritical point. This behavior, as seen in Figure 3-2, is one of the reasons why the working fluid is well suited for the usage in thermodynamic cycles. Large changes in enthalpy are thereby accompanied by relatively small temperature gradients. However, the maximum value decreases, as the pressure increases. Furthermore, the pseudocritical temperature increases for higher pressures.

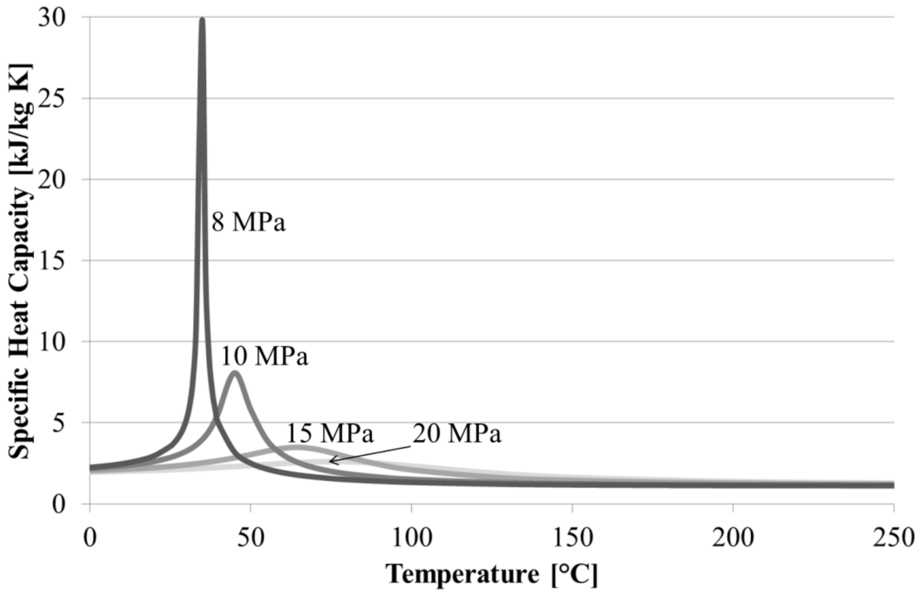

Figure 3-2: Temperature – Specific Heat Capacity Diagram of Supercritical Carbon Dioxide

Supercritical carbon dioxide is not hazardous and chemically inert in the applied temperature range. It is extensively used in other industries and under investigation as a primary coolant for generation IV reactors [29].

The lowest designated temperature of the analyzed system is 40 °C, with a system pressure no lower than 8 MPa. This means that the carbon dioxide is solely in the supercritical state and saturation and respectively condensation does not take place. It is therefore unnecessary to model phase changes and the supercritical carbon dioxide is accounted as single-phase fluid. It is defined as liquid in ATHLET, in order to facilitate the application of already existing models and correlations, for example for the calculation of the pressure loss due to wall friciton.

3.1.1 Fluid Properties

ATHLET needs the specific volume v and the enthalpy h of a working fluid to be a function of the state variables temperature and pressure, to utilize the 5-equation model. In addition, it requires the partial derivatives $\frac{\partial v}{\partial p}, \frac{\partial v}{\partial T}, \frac{\partial h}{\partial p}, \frac{\partial h}{\partial T}$, as well as $\frac{\partial v}{\partial h}$, i.e. the heat capacity, in order to calculate all thermodynamic properties. These derivatives have to be continuous, as the smoothness of the function of the state variables, as well as their derivatives, influence the computing time. This is due to the reason that the time integration algorithm decreases the time step, if the estimated error increases.

Even though ATHLET requires the fluid properties to be functions of temperature and pressure for the transient calculation, it performs the start calculation, for the determination of the steady state at the beginning of the simulation, on the basis of a 4-equation model. In contrast, this calculation is based on pressure and enthalpy, which means that also the fluid properties have to be a function of these variables. Compliance of both models has to be ensured.

3.1.1.1 Density & Enthalpy

The currently most accurate equation of state (EOS) for supercritical CO_2, formulated by Span and Wagner [52], is a function of the temperature and the specific volume and cannot be implemented into ATHLET directly. However, this EOS has been used to precompute 2,500 data points (ρ, p, T and h, p, T) to obtain density and enthalpy values for temperatures between 30 – 400 °C and pressures between 7.4 – 30 MPa, as a grid of equidistant nodes. These sets of data points are provided to an existing algorithm, for surface fitting with splines [8], in order to determine bicubic spline approximations. This algorithm choses the necessary number of knots and their positions iteratively, in order to limit the least square residuals to a selected value, which has been chosen in the range of the uncertainty of the original EOS. If the least square residual of any interval exceeds this boundary value, the interval is subdivided by placing an additional knot inside this interval. This procedure is iteratively repeated. Therefore, the approximation accounts for the specific behavior of the underlying function and a non-equidistant grid is formed. A grid of 13 x 11 has been selected for the approximation of the density values. The look-up table is generated with the algorithm and the 195 B-spline coefficients can be found in Appendix A. Likewise the approximation of the

enthalpy is based on a grid of 9 x 7. The look-up table and the 99 B-spline coefficients can also be found in the Appendix A.
Since the first and second derivative of a bicubic spline is continuous by definition [8], this approach fulfills the requirements of ATHLET on the thermodynamic property package [2].
For the verification of the implemented bicubic spline approximation and the evaluation of its accuracy, the basis 2,500 data points and the results of the spline approximations at these points have been compared. The maximum error for the enthalpy and density values is below 2% and in the range of low pressures and temperatures. This is due to strong variances of enthalpy and density values in the proximity of the critical point, i.e. 30.978 °C at 7.3773 MPa [36], which makes it more difficult to fit the data. In addition to the deviations of the implemented spline approximations, the uncertainty of the original EOS has also to be taken into account for the quantification of the entire uncertainties. For the density, it lies in the range of 0.1%, regarding the enthalpy the deviation is up to 2 % in the applicable pressure and temperature range [52].

3.1.1.2 Viscosity

In addition to the described thermodynamic properties, ATHLET requires two transport properties of each working fluid, i.e. the viscosity and the thermal conductivity. The latter has been implemented with a formulation of Fenghour et al. [18], which relates the viscosity to the fluid's density and temperature. In the utilized method, the dynamic viscosity μ is a combination of the viscosity in the zero-density limit μ_0, only dependent on the temperature, and the excess viscosity $\Delta\mu$, describing how the viscosity depends on the fluid's density

$$\mu(T,\rho) = \mu_0(T) + \Delta\mu(T,\rho) \tag{3.1}$$

Vesovic et al. [66] found an empirical correlation for the viscosity in the zero-density limit

$$\mu_0(T) = \frac{1.00697\sqrt{T}}{exp(\sum_{i=0}^{4} b_i(lnT_r)^i)} \tag{3.2}$$

To compute the overall viscosity μ, μ_0 can be added to another empirical correlation of Fenghour et al. [18], which describes the dependency on the fluid's density

$$\Delta\mu(T,\rho) = d_{11}\rho + d_{21}\rho^2 + \frac{d_{64}\rho^6}{{T_r}^3} + d_{81}\rho^8 + \frac{d_{82}\rho^8}{T_r} \tag{3.3}$$

The coefficients for equations 3.2 and 3.3 can be found in the Table 3-1.
This model is also recommended and utilized in the database of the National Institute of Standards and Technology (NIST) [36]. The uncertainty of the calculated values is up to 4% for the applicable temperature and pressure range.

Table 3-1: Coefficients for the Calculation of the Viscosity

$b_0 = 0.235156$	$d_{11} = 0.4071119 \text{ x } 10^{-2}$
$b_1 = -0.491266$	$d_{21} = 0.7198037 \text{ x } 10^{-4}$
$b_2 = 0.05211155$	$d_{64} = 0.2411697 \text{ x } 10^{-16}$
$b_3 = 0.05347906$	$d_{81} = 0.2971072 \text{ x } 10^{-22}$
$b_4 = -0.01537102$	$d_{82} = -0.1627888 \text{ x } 10^{-22}$
$T_r = T/251.196$	

3.1.1.3 Thermal Conductivity

The second transport property of carbon dioxide that is required by ATHLET is the thermal conductivity κ. It has been implemented in terms of a multi-parameter equation from Scalabrin et al. [47]. This empirical correlation utilizes the thermodynamic properties T and ρ of carbon dioxide, in order to calculate the conductivity

$$\kappa_r(T_r, \rho_r) = \sum_{i=1}^{3} n_i T_r^{g_i} \rho_r^{h_i} + e^{-5\rho_r^2} \sum_{i=4}^{10} n_i T_r^{g_i} \rho_r^{h_i} + n_c \kappa_{r,ce}(T_r \rho_r) \tag{3.4}$$

Where $n_c = 0.775547504$.

The thermal conductivity enhancement $\kappa_{r,ce}$ becomes more significant for boundary conditions close to the critical point

$$\kappa_{r,ce}(T_r, \rho_r) = \frac{\rho_r e^{\left\{-\frac{\rho_r^{a_1}}{a_1} - [a_2(T_r-1)]^2 - [a_3(\rho_r-1)]^2\right\}}}{\left(\left[\left\{\left(1-\frac{1}{T_r}\right) + a_4[(\rho_r-1)^2]^{1/2a_5}\right\}^2\right]^{a_6} + \left\{\left[a_7\left(\rho_r - \alpha(T_r)\right)\right]^2\right\}^{a_8}\right)^{a_9}} \tag{3.5}$$

Where

$$\alpha(T_r) = 1 - a_{10} arccosh\{1 + a_{11}[(1-T_r)^2]^{a_{12}}\} \tag{3.6}$$

The subscript r indicates the reduced parameters $T_r = T$ / 304.1282, $\rho_r = \rho$ / 467.6 and $\kappa_r = \kappa$/ 4.81384. The coefficients of equations 3.4, 3.5 and 3.6 can be found in Table 3-2.

The correlation is valid in the analyzed pressure and temperature range and the average absolute deviation between the underlying experimental data and the calculated values is 5.43% within the supercritical region.

Table 3-2: Coefficients for the Calculation of the Thermal Conductivity

i	g_i	h_i	n_i	a_i
1	0	1	7.69857587	3.0
2	0	5	0.159885811	6.70697
3	1.5	1	1.56918621	0.94604
4	0	1	−6.73400790	0.3
5	1	2	16.3890156	0.3
6	1.5	0	3.69415242	0.39751
7	1.5	5	22.3205514	0.33791
8	1.5	9	66.1420950	0.77963
9	3.5	0	−0.171779133	0.79857
10	5.5	0	0.00433043347	0.9
11	-	-	-	0.02
12	-	-	-	0.2

3.1.2 Heat Transfer Coefficients

The heat transfer of supercritical fluids depends on various aspects, such as the hydraulic diameter and the shape of the corresponding channel, the fluid and of course the applied boundary conditions. Also, varying fluid properties can influence the heat transfer, close to the pseudo critical temperature T_{pc}. The Eckert-Number Ec is an indicator, whether these property effects influence the heat transfer [40] with the corresponding pseudo critical temperature T_{pc}

$$Ec = \frac{T_{pc} - T_{bulk}}{T_{inner\ wall} - T_{bulk}} \tag{3.7}$$

The specific heat capacity has a maximum within a control volume, if 0 < Ec < 1. In this case, the drastic changes of the fluid properties near the wall, either through heating or cooling, have to be considered. For the anticipated operating conditions of the self-propelling heat removal system, the Eckert-Number is either greater than unity (cooling), or negative (heating). This means that the system operates outside the pseudo critical region [68] and the variation of the physical properties over the cross section can be neglected. Furthermore, the flow within the heat exchangers is always turbulent and the impact of different flow regimes can be ignored for the current analysis, due to the consistent fluid phase.

Therefore it is suitable to compute the Nusselt number by the Gnielinski correlation [24], which has been implemented in ATHLET. The correlation is applicable for forced convection in ducts with the Reynolds number Re between 2300 and 10^6 and the Prandtl number Pr ranging from 0.6 to 2000.

$$Re = \frac{\rho v D_h}{\mu} \tag{3.8}$$

$$Pr = \frac{\mu c_p}{\kappa} \tag{3.9}$$

Where the Nusselt number Nu [24] is calculated, with the friction factor ξ

$$Nu = \frac{\left(\frac{\xi}{8}\right)(Re - 1000)Pr}{1 + 12.7\sqrt{\left(\frac{\xi}{8}\right)}\,(Pr^{2/3} - 1)} \tag{3.10}$$

$$\xi = (1.82\,log(Re) - 1.64)^{-2} \tag{3.11}$$

This practice is applied to both, the heat flow from the fluid to the wall and vice versa.
The heat transfer enhancement through the entrance effect [24], has not been considered, since the diameter of the heat exchanger pipes of the investigated system is small compared to their length

$$f_{entrance} = \left(\frac{D}{l}\right)^{2/3} \tag{3.12}$$

Moreover, the minichannels, present in the compact heat exchanger and described in more detail in chapter 5.2.2, enhance the heat transfer, due to the small hydraulic diameter of the channels. Adams et al. [1] suggested for minichannels with a hydraulic diameter smaller than 1.09 mm, to multiply the determined Nusselt number with the factor

$$f_{channel} = 7.6 * 10^{-5}\,Re\left(1 - \left(\frac{D_h}{1.164}\right)\right) \tag{3.13}$$

However, this effect has also been neglected. Therefore, the implemented Gnielinski correlation is assumed to underestimate the values for the heat transfer coefficient htc, especially as the Reynolds number increases

$$htc = \frac{Nu(Re, Pr) * \kappa}{D_h} \tag{3.14}$$

There are correlations that have been developed especially for supercritical carbon dioxide with forced convection, for example from Krasnoschekov and Protopopov [31]. However, these focus on the heat transfer in the proximity of the pseudocritical point, which is not important for the current analysis.

Deviations between these two approaches are negligible in the considered pressure and temperature range [31] and the implemented approach is equally suitable [31]; [68].

3.1.3 Pressure Drop

Since supercritical carbon dioxide is a single phase fluid, equation 2.16, for the determination of the wall friction loss in ATHLET, can be simplified to

$$\Delta p_{wall} = -\lambda \frac{m\,|m|\,l}{2D_H A^2 \rho} \tag{3.15}$$

For turbulent flow conditions, which are present within the Turbo Compressor System throughout the entire simulation time, the Colebrook equation 2.17 is selected as a standard feature for the determination of the friction factor. This is in accordance with the literature [9], where the Colebrook equation has been recommended for supercritical carbon dioxide for both, minichannels and regular piping.

The second $\frac{1}{\sqrt{\lambda_{DW}}}$ of equation 2.17 is in ATHLET approximated with a preset value [2]

$$\frac{1}{\sqrt{\lambda_{DW}}} = -2\,lg\left(\frac{R}{3.7\,D_h} + \left(\frac{6.81}{Re}\right)^{0.9}\right) \tag{3.16}$$

Thereby, the pressure drop is calculated depending on the wall roughness R, which is an input parameter, the hydraulic diameter D_h and the Reynolds number Re

Since no drastic changes of fluid properties near heated or cooled surfaces are expected (Ec > 1 and Ec < 0), a correction factor for the scaling of the wall and form loss coefficients, as implemented in ATHLET for supercritical water, is not necessary.

3.2 Extension of the Model for the Turbomachinery

The simulation of the turbomachinery of the self-propelling heat removal system requires specific component models. A basic model for axial steam and gas turbines is already implemented in ATHLET Mod 3.0 A and has been adapted for the representation of radial turbines. Furthermore, a basic compressor model has been introduced.

3.2.1 Adaption to Model Radial Turbines

ATHLET models the pressure drop across a turbine Δp_t according to Stodola's cone law, which was originally derived from steam turbines. The approach is based on the relation between the in- and outflow pressures as well as the mass flow and their deviations from the design point values of the turbine, indicated by the subscript 0 in equation 3.17. In addition, a correction term for the deviation of the inflow density from the design point is included [3] [22].

$$\Delta p_t = p_{in} - \sqrt{{p_{in}}^2 - p_{in} \frac{p_{in,0}\left(1 - \left(\frac{p_{out,0}}{p_{in,0}}\right)^2\right)}{\left(\frac{m_0}{m}\right)^2 \frac{\rho_{in}}{\rho_{in,0}}}} \tag{3.17}$$

The basic equation of Stodola's cone law, which does not include the correction factor for the changing inlet density, expresses the relation between the in- and outlet pressure to the mass flow. It describes the lateral surface of the quarter of a cone, as seen in Figure 3-3. If one assumes a constant inlet pressure p_{in}, the mass flow is determined from the outlet pressure p_{out}. This relationship can be represented by an elliptical arc, parallel to the axis of the outlet pressure. On the other hand, for a constant outlet pressure, the mass flow through the turbine changes with the inlet pressure. This relationship can be displayed as a hyperbola parallel to the axis of the inlet pressure.

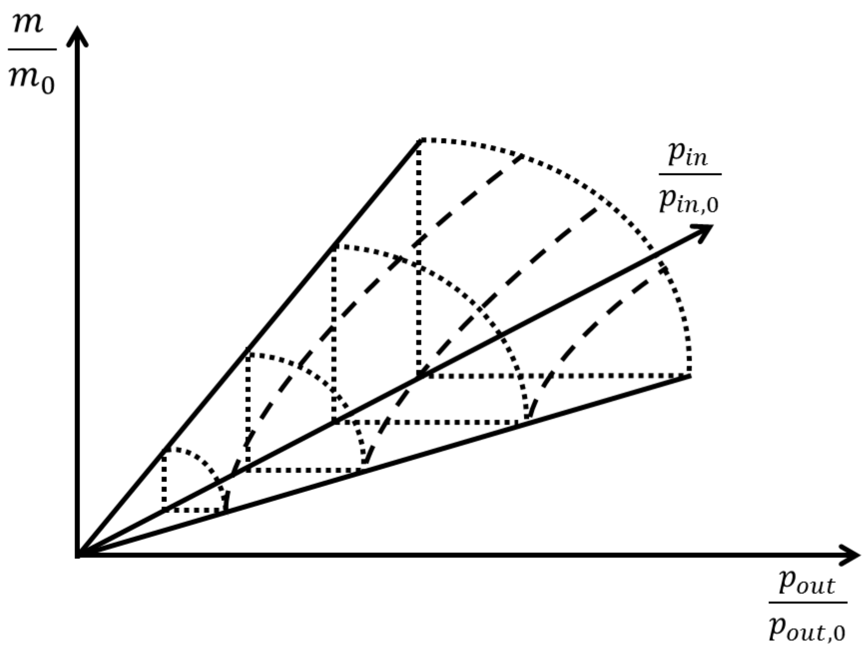

Figure 3-3: Stodola's Cone

The enthalpy drop across the turbine is determined by multiplying the isentropic enthalpy change Δh_{is} with the efficiency η. The isentropic enthalpy change is thereby calculated by dividing the pressure drop by an appropriate average density $\widetilde{\rho_t}$, based on the inflow and outflow densities. The weighting coefficient k, as well as $\widetilde{\rho_0}$ are determined during the steady state calculation with equations 3.20 and 3.21, at design point conditions

$$\Delta h = \eta \, \Delta h_{is} = \eta \, \frac{\Delta p_t}{\widetilde{\rho_t}} \tag{3.18}$$

$$\widetilde{\rho_t} = k \, \rho_{in} + (1 - k) \, \rho_{out} \tag{3.19}$$

$$k = \frac{\widetilde{\rho_0} - \rho_{out,0}}{\rho_{in,0} - \rho_{out,0}} \tag{3.20}$$

$$\widetilde{\rho_0} = m_0 \, \eta_0 \, \frac{\Delta p_0}{P_0} \tag{3.21}$$

Eventually the power P, which is extracted from the fluid and transferred into mechanical energy, can be calculated

$$P = \eta \, \Delta h_{is} \, m \tag{3.22}$$

The efficiency of the turbine at the design point has to be input by the user. However, the actual efficiency depends on the boundary conditions and decreases for off-design conditions. It changes for variations in the enthalpy difference or increasing or decreasing numbers of revolutions n of the turbine. The behavior is modeled with correlation 3.23 which describes the off-design behavior for axial steam turbines [44]

$$\eta = \eta_0 - 2\left(\frac{n}{n_0}\sqrt{\frac{\Delta h_{is}}{\Delta h_{is,0}}} - 1\right)^2 \tag{3.23}$$

However, the performance of radial turbines during off-design conditions differs significantly from axial turbines, which requires an adaption of the already included turbine model. The original model has been taken as the basis to calculate the pressure and the isentropic enthalpy differences. But, equation 3.23, which is utilized for the calculation of the efficiency parameter and is based on the behavior of axial turbines, has been replaced.
In order to include the influence of aerodynamic losses, as recommended by Dyreby et al. [12], the efficiency of the turbine under design point operation η_0 is scaled with the introduced efficiency parameter η_{aero}, such that the power extracted by the turbine, can be computed

$$\eta_{total} = \eta_0 * \eta_{aero} \tag{3.24}$$

Where

$$\eta_{aero} = 2u\sqrt{(1 - u^2)} \tag{3.25}$$

The velocity ratio u is further defined as the ratio of the rotor tip speed $U = D * \pi * n$ and the spouting velocity C

$$u = U/C \tag{3.26}$$

Where the spouting velocity is the velocity that can be obtained during an isentropic expansion and is a function of the isentropic enthalpy change Δh_{is} between turbine inlet and exit conditions [50]

$$C = \sqrt{2\,\Delta h_{is}} \tag{3.27}$$

Figure 3-4 gives an overview of the input and output variables of the adapted turbine model.

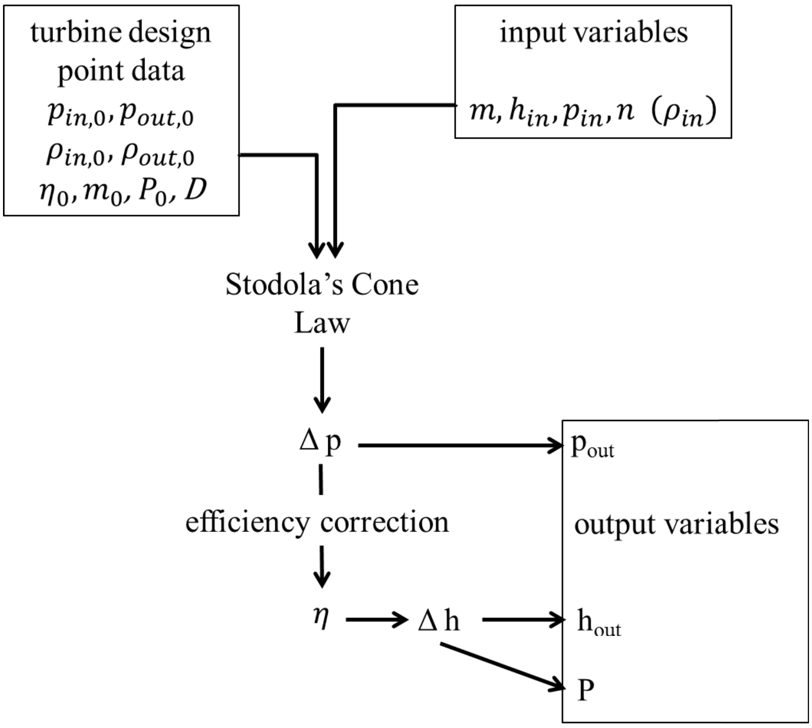

Figure 3-4: Adapted Turbine Model

It would be best to base the efficiency variation during off-design conditions on appropriate performance maps. However, they are not available at this time.

The turbine model allows the simulation of several turbines in parallel. However, the same rotational speed is applied to all of them, because it is assumed that they are located on a common shaft. Therefore, they cannot be turned off separately. An additional limitation of the modeling approach is that the turbine has to start under design-conditions.

3.2.2 The Implementation of a Compressor Model

Due to the lack of detailed design data for the radial sCO_2 compressor, a simple approach has been implemented to calculate the enthalpy difference between entry and exit conditions, as well as its efficiency and power demand. It has been assumed that the compressor provides a constant exit pressure, such that the pressure difference between the inlet and outlet can be computed. Equal to the approach included in the model for the axial steam turbine [3], the isentropic enthalpy change is calculated with

$$\Delta h_{is} = \frac{\Delta p}{\tilde{\rho}_c} \tag{3.28}$$

where the density $\tilde{\rho}_c$ is an appropriate average density, a function of the inlet density ρ_{in}, the outlet density ρ_{out} as well as a weighting coefficient w_0 to adjust the approach with respect to the design point

$$\tilde{\rho}_c = w\rho_{in} + (1-w)\rho_{out} \tag{3.29}$$

$$w = \frac{\left(\eta_0\, m_0 \frac{|\Delta p_0|}{|P_0|}\right) - \rho_{out,0}}{\rho_{in,0} - \rho_{out,0}} \tag{3.30}$$

The efficiency parameter of the compressor is further calculated, depending on the actual mass flow m

$$\eta_{total} = \eta_0 - \frac{\eta_0|m - m_0|}{2m_0} \tag{3.31}$$

Eventually, the necessary power input P can be computed

$$P = \frac{\Delta h_{is} m}{\eta_{total}} \tag{3.32}$$

Figure 3-5 shows the input and output variables of the compressor model.

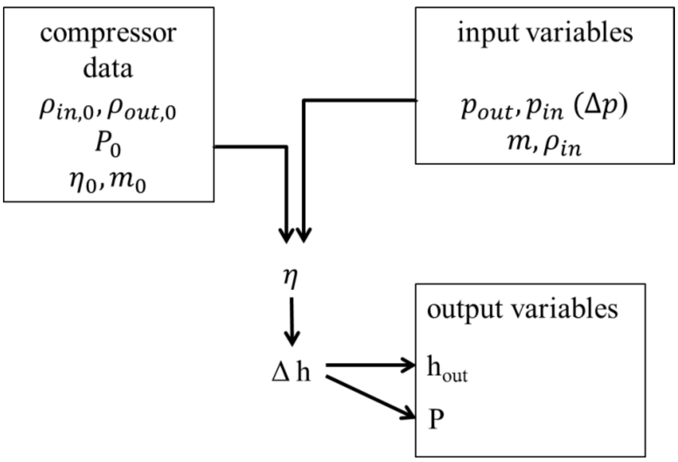

Figure 3-5: Implemented Compressor Model

A variable that represents the expansion work gained by the turbine minus the necessary compression work has been implemented as an additional GCSM process signal. This is necessary to simulate the interaction of the turbomachinery. The user is therefore able to include a control strategy of the system related to the power balance of the turbomachinery via the GCSM module, for instance to simulate the self-propelling behavior of the system and to bring it to a halt, once the necessary compression work cannot be provided by the turbine. Details about this procedure can be found in Appendix B.

4 Validation

The conducted code development, as described in the previous chapter, has been validated against experimental data, in order to confirm suitability of the implemented correlations and models to simulate a sCO_2 driven Brayton cycle. For one thing, the extended ATHLET version has been used to recalculate experiments, in which supercritical carbon dioxide was externally heated. The simulated heat transfer is thereby compared with the experimental values, which is shown in chapter 4.1. Secondly, the adopted wall friction model has been validated for the working fluid sCO_2. The calculated and experimentally measured pressure drops are shown in chapter 4.2. Lastly, the experimental setup of a closed Brayton cycle has been modeled. The implemented component models have been used to simulate the behavior of the turbomachinery under different boundary conditions, which is described in chapter 4.3.1. The comparison of the simulated and measured performance of the turbomachinery can be found in chapter 4.3.2.

4.1 Heat Transfer

Only very few experimental data regarding the heat transfer of purely supercritical carbon dioxide can be found in the literature. But some experiments of Walisch [68] qualify to validate the implemented heat transfer correlation and have therefore been recalculated with ATHLET.

The test section that has been investigated by Walisch is 1.512 m long and consists of a nickel-based alloy pipe with an inner diameter of 10 mm and an outer diameter of 11 mm. 23 experiments were carried out and recalculated, at a system pressure of 8 MPa and with mass flows varying from 5.22×10^{-4} kg/s to 2.2×10^{-2} kg/s. With inflow temperatures ranging from 64.2 °C to 85.8 °C, this leads to Reynolds numbers between 3000 and 1.4×10^{5}. Besides the mass flow rate and the system pressure, Walisch measured the entrance and exit temperature of the supercritical carbon dioxide as well as the outer wall temperature of the test section. The test section itself is a double pipe heat exchanger with saturated steam flowing through the annular gap that heats the sCO_2. The outer wall temperature of the test section has been measured with 13 thermocouples, nevertheless, only the averaged wall temperature has been stated in the literature. This value has been used as a given temperature boundary condition at the steam side. The saturated steam is generated in a boiler that is electrically heated. The heat input is recorded and an estimation of the heat loss of the overall system has been documented for different saturation temperatures.

4.1.1 Uncertainties of the Experimental Data of Walisch

Since the heat transfer coefficient or the Nusselt number itself cannot be measured experimentally, the heat input has been selected as the comparable quantity. Walisch suggested determining the actual amount of heat transferred to the carbon dioxide by means of an enthalpy balance between the test section in- and outlet

$$Q_{heat} = m\,(h_{out} - h_{in}) \tag{4.1}$$

This method achieves a high accuracy, also for lower heat inputs, as the uncertainty of the electric heater ($\Delta Q_{heater} = 5.2$ W) is quite high and the heat losses throughout the entire setup are not precisely known.
An uncertainty analysis has been conducted to assess the experimental results. It has been assumed that the uncertainty for the mass flow and enthalpy are uncorrelated

$$\Delta Q_{heat} = \sqrt{\left(\frac{\partial Q}{\partial m}\,\Delta m\right)^2 + \left(\frac{\partial Q}{\partial (h_{out} - h_{in})}\,\Delta(h_{out} - h_{in})\right)^2} \tag{4.2}$$

$$= \sqrt{((h_{out} - h_{in})\,\Delta m)^2 + (m\,\Delta(h_{out} - h_{in}))^2} \tag{4.3}$$

The uncertainty of the mass flow depends solely on the accuracy of the mass flow meter, i.e. ±0.2%. On the other hand, the uncertainty of $\Delta(h_{out} - h_{in})$ depends on several uncorrelated measurements: the in- and outlet temperatures, as well as the system pressure. These deviations can be summarized in a statistical error $\Delta(h_{out} - h_{in})_{stat}$

$$\Delta(h_{out} - h_{in})_{stat} = \sqrt{\left(\frac{\partial(h_{out} - h_{in})}{\partial T_{out}}\Delta T_{out}\right)^2 + \left(\frac{\partial(h_{out} - h_{in})}{\partial T_{in}}\Delta T_{in}\right)^2 + \left(\frac{\partial(h_{out} - h_{in})}{\partial p}\Delta p\right)^2} \tag{4.4}$$

$$= \sqrt{\left(c_p(T_{out})\Delta T_{out}\right)^2 + \left(c_p(T_{in})\Delta T_{in}\right)^2 + \left(\left(\frac{\partial h_{out}}{\partial p} - \frac{\partial h_{in}}{\partial p}\right)\Delta p\right)^2} \tag{4.5}$$

A highly accurate database of fluid properties [36], has been used to determine the enthalpy values as a function of pressure and temperature. Its accuracy was considered by means of a systematic error $\Delta(h_{out} - h_{in})_{sys}$. Table 4-1 summarizes the accuracy of the data.

$$\Delta(h_{out} - h_{in})_{sys} = \left|\frac{\partial(h_{out} - h_{in})}{h_{out}}\Delta h_{out}\right| + \left|\frac{\partial(h_{out} - h_{in})}{h_{in}}\Delta h_{in}\right| \tag{4.6}$$

$$\Delta(h_{out} - h_{in}) = \sqrt{\Delta(h_{out} - h_{in})_{stat}^{\ 2} + \Delta(h_{out} - h_{in})_{sys}^{\ 2}} \qquad (4.7)$$

For all 23 experiments, $\Delta(h_{out} - h_{in})$ lies within the range of $\pm$ 5.8 – 6.2 kJ/kg, where the uncertainties of Δh_{out} and Δh_{in} are most determining.
The term that mainly influences ΔQ_{heat} is $m\ \Delta(h_{out} - h_{in})$, therefore the accuracy of the heat input depends strongly on the mass flow. Considerably larger uncertainties have therefore to be taken into account for test series' with larger mass flows. The deviation is in the range of 6.8 – 23.3% with larger uncertainties for higher heat inputs.

Table 4-1: Uncertainties of the Experiment Regarding the Heat Input

Δh_{out}	0.6 %	accuracy of the NIST database [36]
Δh_{in}	0.6 %	accuracy of the NIST database [36]
ΔT_{out}	0.1 K	precision of the thermocouple
ΔT_{in}	0.1 K	precision of the thermocouple
Δp	30 kPa	precision of the gauge meter
Δm	0.2 %	precision of the mass flow meter

4.1.2 Uncertainties of the Simulation

ATHLET calculates the heat input for a control volume within a pipe via the heat conduction module HECU. The calculation of the heat conduction is thereby generally based on the assumption that the material of the component is homogeneous and isotropic over the entire heat conduction volume. It is furthermore anticipated that the temperature profile within each HCV is uniformly distributed, which leads to consistent material properties, such as a uniform heat conductivity λ. Therefore, the discretization of the test section has a strong impact on the overall heat input calculated with ATHLET and it will be underestimated for an insufficient fine nodalization. To exclude this cause of error in the validation, a sufficient spatial discretization is important. Therefore, an exemplary nodalization study has been performed for one experiment, selected due to its great temperature gradient. Seven simulations have been run for the same boundary conditions, whereby the test section has been divided into 10, 20, 40, 80, 160, 320 and 640 HCVs. The heat input increases for an increasing number of nodes, as seen in Figure 4-1 and asymptotically approaches an amount of inserted heat that is independent from the number of nodes. If the test section is divided into 40 or more HCVs, the difference to the heat input calculated with the nodalization of 640 HCVs is already less than 1 %.
To limit the uncertainty caused by the nodalization in the following validation, the test section has spatially been divided into 160 control volumes. The length of the control volumes is therefore less than 1 cm and the uncertainty of the heat input is significantly less than the experimental measuring inaccuracy, i.e. 0.13% for the analyzed experiment.

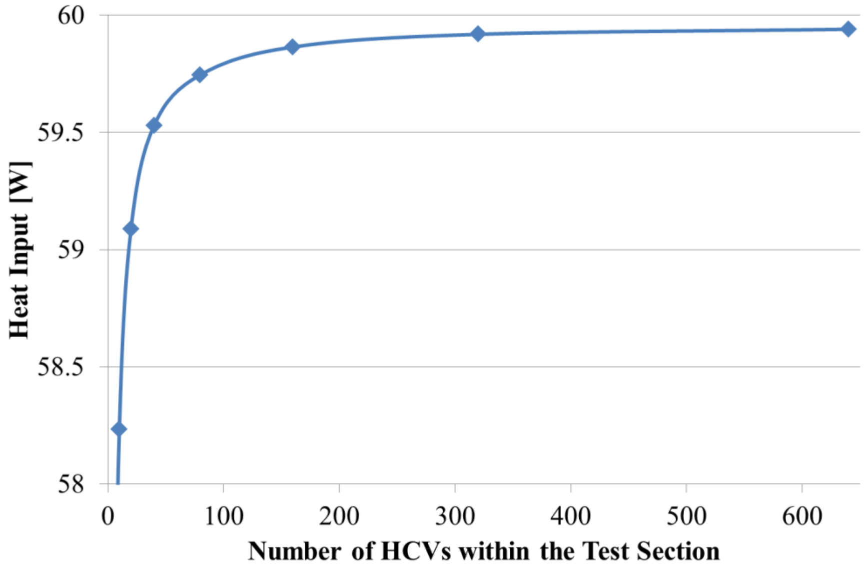

Figure 4-1: Comparison of the Simulated Heat Input for Different Nodalization Schemes

4.1.3 Comparison of the Experimental Data with the Simulations

The heat inputs of the experiments have been compared with the heat inputs that have been calculated by ATHLET.

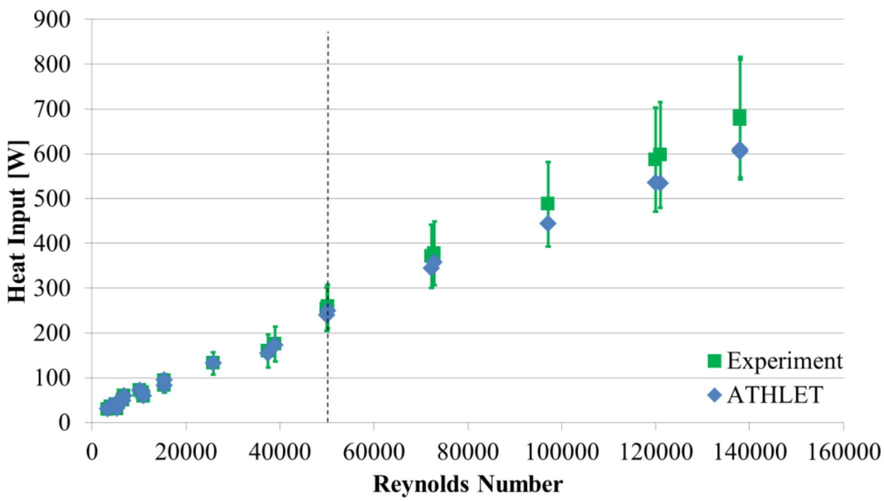

Figure 4-2: Comparison of the Experimentally Measured Heat Input with the Results Calculated with ATHLET against the Reynolds Number

As seen in Figure 4-2, the values show generally a good agreement and the calculated values are always situated within the error bar of the experimental values. For the 23 experiments a maximum deviation (Q_{ATH}/Q_{exp}) - 1 of 11.4% could be assessed for the heat input.

Especially for Reynolds number up to 50,000, which is the applicable range for the analyzed compact heat exchanger, ATHLET is able to simulate the heat input with a high accuracy, see Figure 4-3.

It should be mentioned that the Reynolds numbers on the x-axis of Figure 4-2 and Figure 4-3 are also subject to uncertainty. However, it has not been considered in the diagrams, since the Reynolds number is only used to for the representation and the alignment of the results.

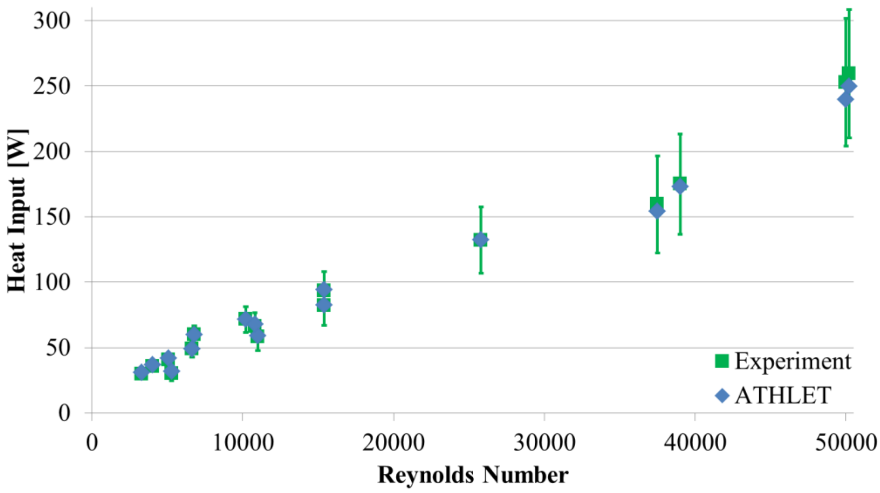

Figure 4-3: Comparison of the Experimentally Measured Heat Input with the Results Calculated with ATHLET against the Reynolds Number – Increased Scale

The differences of the calculated and measured heat inputs are shown in Figure 4-4. For Reynolds numbers up to 50,000 the deviation (Q_{ATH}/Q_{exp}) - 1 is less than 6%. For Reynolds numbers higher than 30,000, ATHLET tends to underpredict the heat input. This agrees with the assumption that the heat transfer coefficient is underestimated by the implemented Gnielinski correlation.

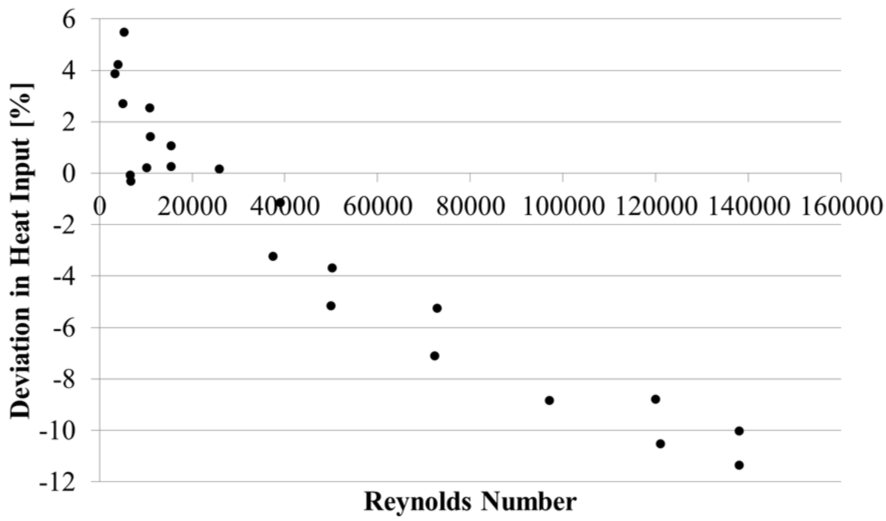

Figure 4-4: Deviation between the Measured and Calculated Heat Input against the Reynolds Number

4.2 Wall Friction

The validity of the friction factor determined by the Colebrook equation 3.16 has been examined by recalculating an experiment, conducted by Son et al. [51]. He performed some of the very few experiments to analyze the pressure drop characteristics of supercritical carbon dioxide. The test section is 6 m long and consists of a horizontal tube in tube heat exchanger, where CO_2 flows in the inside of a stainless steel pipe with an inner diameter of 7.75 mm and a wall thickness of 0.9 mm. Outside this test channel, water flows in an annular gap, which is divided into 12 equal subsections. Water cooling is provided in counter-current flow in every subsection. The sCO_2 mass flux is precisely documented, the inflow temperature is known to be between 90 and 100 °C and outflow temperature is around 25 °C. Unfortunately, certain information, such as the water temperature and mass flow, has not been recorded in the literature. Therefore, the modeling has been simplified and a constant temperature signal has been attached to the outer wall of the CO_2 channel. Test conditions and the stated temperature drop have been simulated, which is important, since the changing fluid properties have a strong impact on the actual pressure drop. In addition, the surface roughness of the test channel has not been documented, which is crucial for the determination of the wall friction. However, it is known that the test section is a stainless steel pipe. For new and untreated pipes of this category, the wall roughness R lies usually in the range of 0.02 to 0.04 mm [65]. Calculations have been conducted for R = 0.01, 0.02 and 0.04 mm.
8 experiments with mass fluxes between 200 and 500 kg/m²s and system pressures of 8.5 and 9.5 MPa have been recalculated. The results are shown in the Figure 4-5 and Figure 4-6.

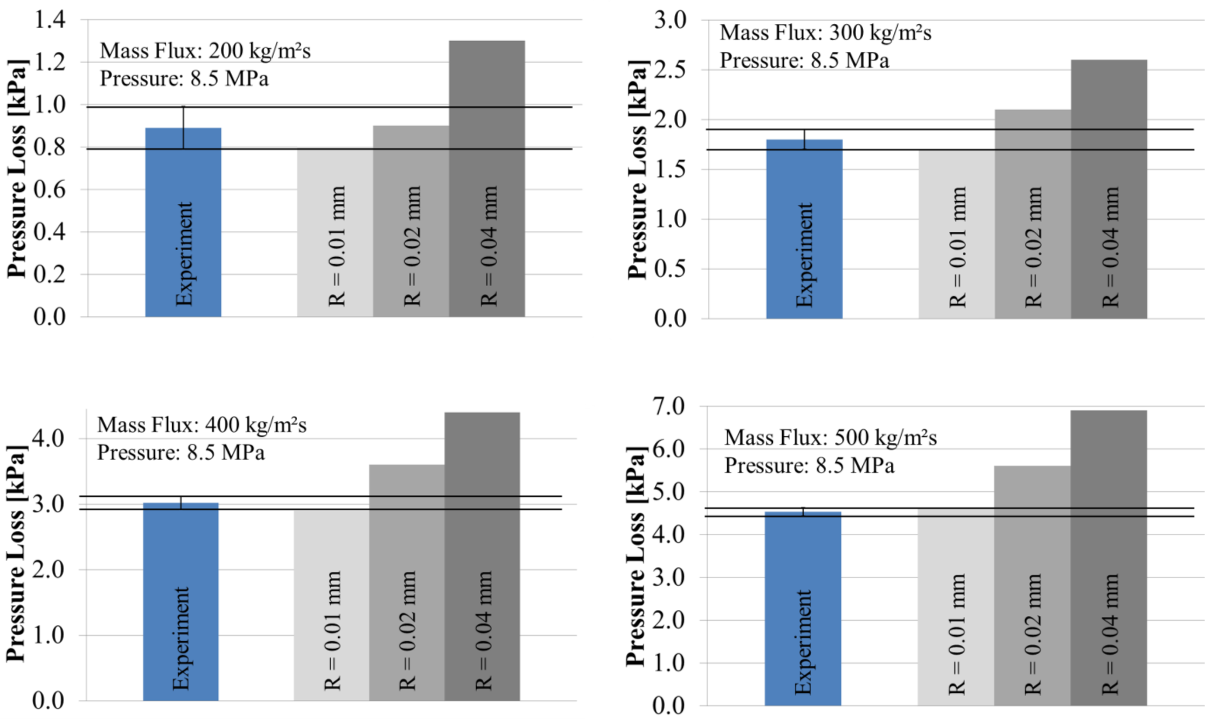

Figure 4-5: Comparison of the Experimentally Measured Pressure Loss with the Results Calculated with ATHLET for Different Wall Roughnesses – System Pressure 8.5 MPa

Especially, the pressure losses that have been modeled with the wall roughness R = 0.01 mm agree well with the experimental data. This data originates from a diagram published in the literature. The corresponding graphs have been read, whereby the read-off accuracy is limited and has been assumed to be 1 mm which results in an uncertainty of 90 Pa. Additionally, the accuracy of the pressure gauge, which is assumed to be a differential pressure transducer, is anticipated to be 10 Pa. All together this results in maximum tolerance of ±100 Pa, which is represented by an error bar in the diagrams. The uncertainties of the pressure drops calculated by ATHLET depend on the accuracy of the density, i.e. the deviation of the temperature and the pressure, the mass flow and the anticipated wall roughness. However, only the uncertainty of the wall roughness has been considered, since it has by far the greatest influence on the pressure drop.

For increasing mass fluxes, the correlation is able to predict increasing pressure drops. Furthermore, it correctly models lower pressure drops for higher system pressures. For the wall roughness R = 0.01 mm, the predicted pressure drops lie within the error bar of the experiments. The difference between the values, i.e. $(\Delta p_{exp}/\Delta p_{ATH})$ - 1 is less than 13 % for all mass fluxes. Nevertheless, the true wall roughness is not known to the author. If the wall roughness is actually higher, for instance R = 0.04 mm, the pressure losses are overpredicted by up to 52 %.

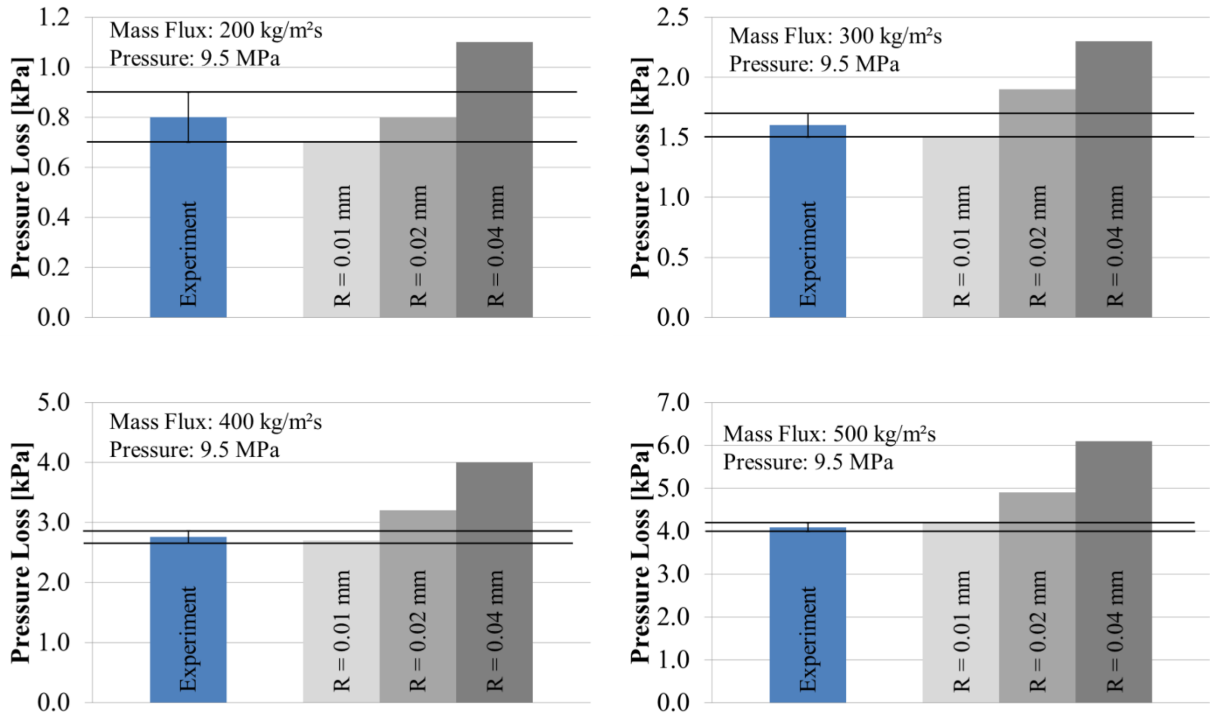

Figure 4-6: Comparison of the Experimentally Measured Pressure Loss with the Results Calculated with ATHLET for Different Wall Roughnesses – System Pressure 9.5 MPa

4.3 Experiments with Turbomachinery

Sandia National Laboratories have built a supercritical CO_2 Brayton cycle, in order to gain in depth insights and firsthand experience of such a power-producing loop [70]. The test section contains a radial turbine as well as a radial compressor and the detailed documentation of the test series makes it possible not only to evaluate the models for the turbomachinery, but to recalculate the entire cycle with ATHLET. The sCO_2 is electrically heated with up to 390 kW_{el} before it is expanded in the radial turbine. As seen in Figure 4-7, the carbon dioxide is further cooled down by a water cooled gas chiller with a capacity of 280 kW, by means of a printed circuit heat exchanger. Finally, the fluid is compressed in a radial compressor before it reaches the heaters again. The turbomachinery is assembled to a turbo-alternator-compressor (TAC) unit by means of a motor / generator. It can start the system by powering the compressor and can generate electricity, once the expansion work exceeds the necessary compression work. The temperatures and pressures at the turbine and compressor entries and exits have been measured and are recorded in terms of diagrams, as well as the rotational speed of the TAC and the mass flow.

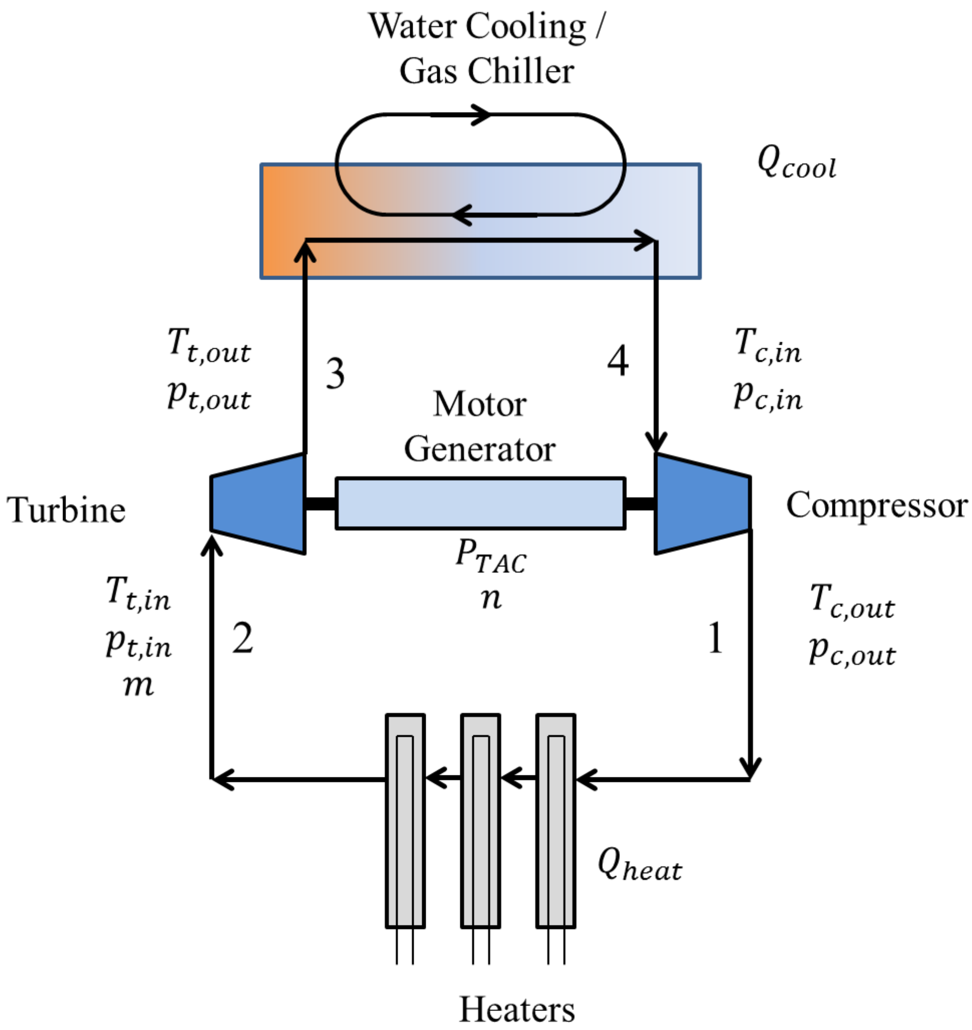

Figure 4-7: Supercritical CO_2 Brayton Test Cycle

The Brayton cycle has been modeled with ATHLET, Figure 4-8 shows the utilized nodalization scheme.

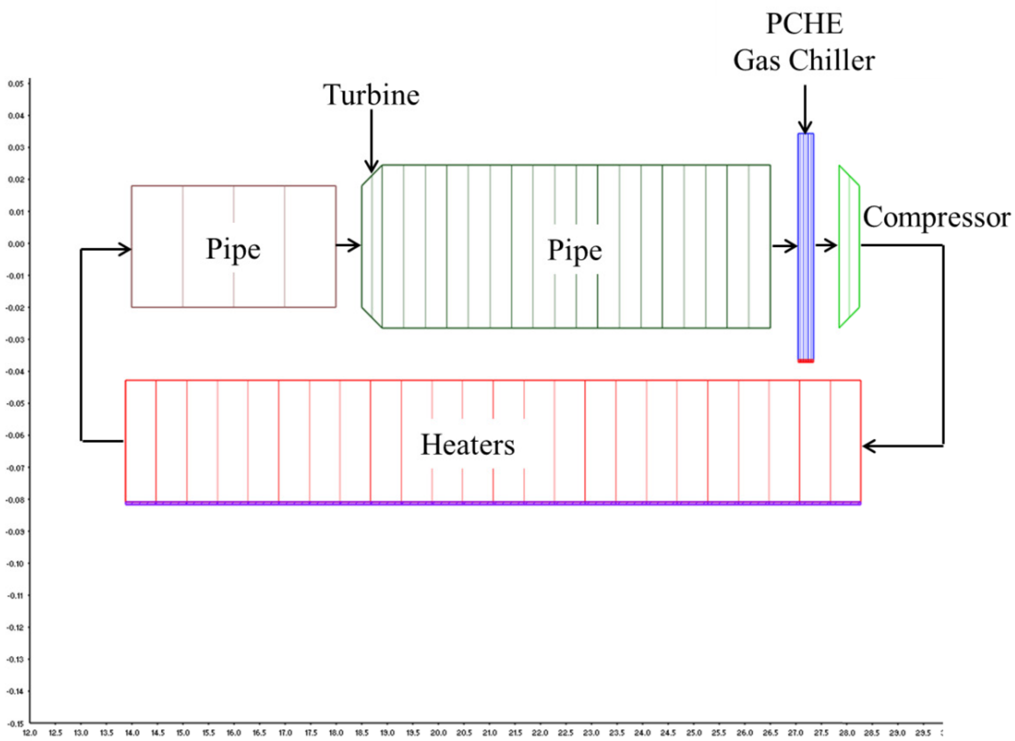

Figure 4-8: Nodalization Scheme of the Brayton Cycle

For the design point conditions of the turbomachinery [43], the efficiency parameters of the TAC and the turbine wheel diameter [67], the values listed in Table 4-2 have been used.

Table 4-2: Design Point Data of the sCO_2 Brayton Test Cycle

Design Point Data	
$p_{c,in}$ [MPa]	7.8
$p_{c,out}$ [MPa]	13.9
m_c [kg/s]	2.30
$h_{c,in}$ [kJ/kg]	473
η_c	0.70
$p_{t,in}$ [MPa]	13.5
$p_{t,out}$ [MPa]	7.9
m_t [kg/s]	3.15
$h_{t,in}$ [kJ/kg]	1025
η_t	0.87
D_t [mm]	67.6

Unfortunately, information about the piping, such as the length, the wall roughness and the number of bends are not given. However, the determined friction losses between turbine exit and compressor entry, as well as compressor exit to turbine entry strongly depend on this information. Therefore, the friction losses have been adapted to approximate the experimentally measured pressure drop. Nevertheless, this causes a small deviation on the input parameters of the turbine and compressor and has an influence on the overall result of the simulation.

Furthermore, facts of the gas chiller as well as the heaters are limited, wherefore the heat source and heat sink have been represented in ATHLET by heat conduction objects with fixed temperature signals on the outside. This way, $\vartheta_{t,in}$ and $\vartheta_{c,in}$ have been adjusted according to the experimental data. In addition, the revolving speed of the TAC has also been given as a boundary condition. The system's mass flow, the pressure information and the temperatures $\vartheta_{c,out}$ as well as $\vartheta_{t,out}$, have been determined by ATHLET.

The recorded experiment has been performed over more than 90 minutes, whereby the exit pressure of the compressor, the turbine inlet temperature and the number of revolutions of the turbine-alternator-compressor unit has been increased stepwise. Three representative operating points of the Brayton cycle have been selected and recalculated, at which the boundary conditions have been constant for at least 100 seconds. These conditions have been accounted as steady state for the conducted ATHLET simulations.

Table 4-3: Comparison of Experimentally Measured and with ATHLET Calculated Pressure and Temperature Values for Cases I - III

			I at t = 3,200 s	II at t = 4,000 s	III at t = 5,000 s
Boundary Conditions	n [1/min]		35,600	43,500	48,800
	$\vartheta_{t,in}$ [°C]		232	287	316
	$p_{c,out}$ [MPa]		9.89	11.38	12.4
	$\vartheta_{c,in}$ [°C]		32	33	33
Calculated Values	$p_{t,in}$ [MPa]	Experiment	9.59	10.93	11.96
		ATHLET	9.61	10.92	11.86
	$p_{t,out}$ [MPa]	Experiment	7.79	8.19	8.4
		ATHLET	8.37	8.78	9.23
	$\vartheta_{t,out}$ [°C]	Experiment	210	258	280
		ATHLET	221	267	292
	$p_{c,in}$ [MPa]	Experiment	7.54	7.70	7.70
		ATHLET	8.10	8.30	8.63
	$\vartheta_{c,out}$ [°C]	Experiment	47	56	60
		ATHLET	39	44	44

Table 4-4 summarizes the accuracy of the experimental data [70].

Table 4-4: Uncertainties of the Experimental Data

ΔT	1.5 K	precision of the experimental data
Δp	0.08 MPa	precision of the experimental data
Δm	0.02 kg/s	precision of the experimental data
Δh	0.6 %	accuracy of the NIST database [36]

4.3.1 Comparison of the Experimental and Simulated Behavior of the Turbomachinery

For the validation of the model, the pressure drop over the turbine, the pressure increase over the compressor, as well as the mass flow have been evaluated for the three configurations. Table 4-5, as well as Figure 4-9 show the predicted and measured pressure difference over the turbine and compressor. The error bars in Figure 4-9 account for the uncertainties of the experimental data regarding the pressure and the influence of possible temperature deviations on the enthalpy.

The pressure drop of the turbine is generally underpredicted, with a maximum deviation of 31.1 % for case 1. The pressure increase predicted by the compressor model depends strongly on the exit values of the turbine. The error is propagated and leads directly to an underpredicted pressure increase. This is why one can see a strong correlation between the turbine and compressor pressure drop difference between the calculated and measured values.

Table 4-5: Comparison of Experimentally Measured and with ATHLET Calculated Pressure Differences and Mass Flows for Cases I - III

			I	II	III
Comparative Validation Values	Δp_t [MPa]	Experiment	1.8	2.74	3.56
		ATHLET	1.24	2.14	2.62
		$\frac{\Delta p_{T,ATH}}{\Delta p_{T,exp}} - 1$	- 31.1 %	- 21.9 %	- 26.4 %
	Δp_c [MPa]	Experiment	2.35	3.68	4.70
		ATHLET	1.79	3.08	3.77
		$\frac{\Delta p_{c,ATH}}{\Delta p_{C,exp}} - 1$	- 23.8 %	- 16.3 %	- 19.8 %
	m [kg/s]	Experiment	1.75	2.14	2.63
		ATHLET	1.79	2.31	2.57
		$\frac{\dot{m}_{ATH}}{\dot{m}_{exp}} - 1$	2.3 %	7.9 %	2.3 %

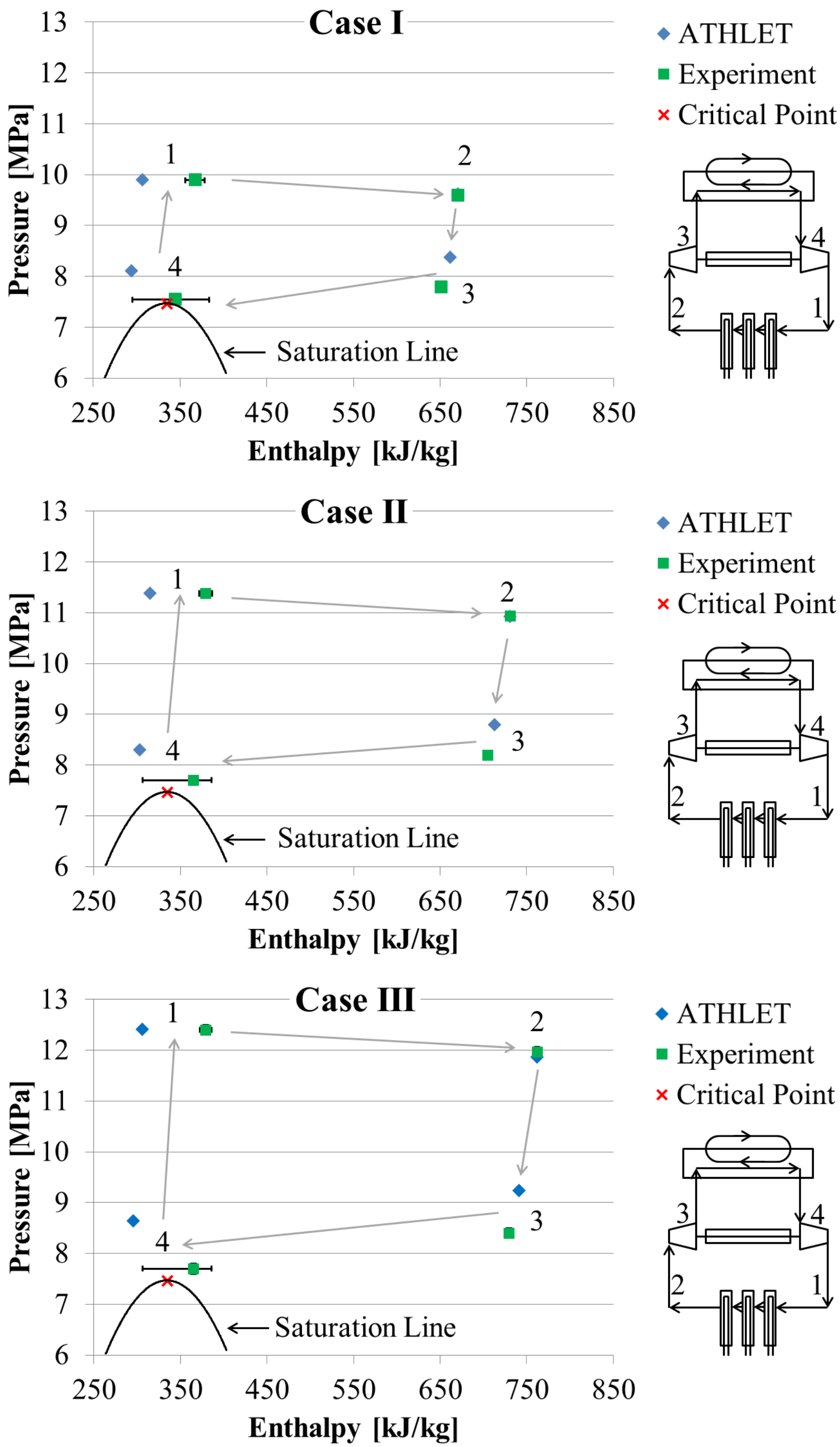

Figure 4-9: Comparison of the Experimentally Measured and with ATHLET Calculated p-h Data Points for Cases I – III

The system's mass flow is a solution variable and determined by ATHLET in accordance with the other thermohydraulic values. In comparison with the mass flows measured in the experiment, they deviate by at most 7.9 %.

Figure 4-9 shows that ATHLET is able to predict the basic behavior of the test cycle, regarding the pressure and enthalpy values. But, the deviations between the experimentally measured and with ATHLET calculated data are not negligible. One reason might be that the simulations have been performed as steady state calculations. However, it seems possible that in the experiment, a steady state is not reached after the boundary conditions have been constant for 100 seconds. Frumholtz [19] conducted a study about the thermal inertia of another sCO_2 test loop. He found that transient effects, due to the heat up of the test cycle and its components, can significantly influence the behavior of the system for more than 1 hour, in case of cold startup conditions. This could also be of importance for the analyzed test run of the Sandia loop. However, this impact has been ignored in the current simulations, because the information about the components of the Sandia loop is not sufficient to model the thermal inertia of the system.
Another reason for the differences between the measured and predicted pressure drops might be that the inlet conditions of the turbine are far from the mentioned design point. However, until additional validation data is available, close to and at the design point, the turbine model implemented in ATHLET will be utilized.

In the context of the experimental set-up, Sandia National Laboratories have also developed a model for radial turbines for supercritical carbon dioxide [67]. It separately accounts for phenomena in the volute, the nozzle, at the impeller and at the outlet. For this reason, the model needs very detailed knowledge of the turbines geometry, such as the height and the angles of the vanes.
The Sandia model was compared against experimental data from the same test facility. Unfortunately, the results of an alternative turbine alternator compressor unit have been used. This data has not been published and could therefore not be recalculated. Therefore, the two models cannot be compared directly.
The original approach from Sandia showed deviations of more than 50 % for the pressure drop. After the introduction of a multiplicative factor and the consideration of heat losses of the setup, the deviation of the pressure drop could be reduced to 30 % [67]. This confirms that the accuracy of the turbine model in ATHLET is at least in the same range than more complex approaches. However, more realistic models are necessary and have to be developed in the future to increase the accuracy of the pressure drop prediction.

4.3.2 Performance

The performance of the radial turbomachinery is examined, for the evaluation of equation 3.24 and 3.31, which determines the turbine's efficiency at boundary conditions off the design point. Since the efficiency is not measured directly, it has to be calculated

$$\eta_t = \frac{h_2 - h_3}{h_2 - h_{3,is}} \tag{4.8}$$

The same is true for the efficiency of the radial compressor

$$\eta_c = \frac{h_4 - h_{1,\mathrm{is}}}{h_4 - h_1} \tag{4.9}$$

Where the subscripts 2 and 4 represent the enthalpy at the turbine and compressor inlet, 1 and 3 the enthalpy at the outlet. The enthalpies are determined in dependency of the recorded pressure and temperature values, with the NIST database and are summarized in Table 4-6.

Table 4-6: Comparison of Experimental and with ATHLET Calculated Turbomachinery Efficiencies for Cases I – III

		I	II	III
$h_{t,in}$ [kJ/kg]	Experiment	671.0	731.1	762.1
$h_{t,out}$ [kJ/kg]		651.7	705.3	729.7
$h_{t,out,is}$ [kJ/kg]		652.8	702.5	725.3
η_t		0.90	0.90	0.88
	ATHLET	0.82	0.86	0.85
	$\frac{\Delta\eta_{T,ATH}}{\Delta\eta_{T,exp}} - 1$	- 8.9 %	- 4.4 %	- 3.4 %
$\Delta\eta_{t,stat}$		0.09	0.06	0.05
$\Delta\eta_{t,sys}$		0.43	0.30	0.24
$\Delta\eta_t$		0.44	0.30	0.24
$h_{c,in}$ [kJ/kg]	Experiment	344.8	365.1	365.1
$h_{c,out}$ [kJ/kg]		368.2	379.3	397.3
$h_{c,out,is}$ [kJ/kg]		349.9	374.1	376.3
η_c		0.22	0.63	0.79
	ATHLET	0.69	0.77	0.79
	$\frac{\Delta\eta_{c,ATH}}{\Delta\eta_{c,exp}} - 1$	213.6 %	22.2 %	0 %
$\Delta\eta_{c,stat}$		6.87	1.37	1.15
$\Delta\eta_{c,sys}$		0.12	0.20	0.21
$\Delta\eta_c$		6.87	1.38	1.16

As mentioned above, the experimental data itself is subject to uncertainty. Therefore, the effect of this on the calculated efficiency was also quantified. The deviation of the efficiencies $\Delta\eta_t$ and $\Delta\eta_c$ depend on the uncertainty of the pressure and temperature values, as well as the accuracy of the NIST database. The statistical error is thereby characterized by the uncertainties of the temperature and pressure measurements. Additionally, a systematic error is considered, in order to take the accuracy of the NIST database into account, which is 0.6 % [36] in the corresponding pressure and temperature range.

$$\Delta\eta_t = \sqrt{\Delta\eta_{t,stat}{}^2 + \Delta\eta_{t,sys}{}^2} \tag{4.10}$$

$$\Delta\eta_c = \sqrt{\Delta\eta_{c,stat}{}^2 + \Delta\eta_{c,sys}{}^2} \tag{4.11}$$

The entire errors computation can be found in Appendix C. Table 4-6 shows the results and summarizes the statistical error, the systematic error as well as the entire deviation, calculated with equations 4.10 and 4.11.

The turbine efficiencies calculated with ATHLET match the data obtained by the experiment quite well. The deviation $(\eta_{t,ATH}/\eta_{t,exp})$ - 1 is at the most 9 %. However, the uncertainty of the experimental performance is very high and the error for the turbine efficiencies has been calculated for configurations I-III. It is visible by means of the error bars in Figure 4-10 and a detailed tabulation can be found in Appendix C. The statistical error due to uncertainty of the experimental data is less than 10% for all three cases. However, the systematic error that is caused by the accuracy of the NIST database is up to 43 % in case 1 and mainly determines the overall uncertainty.

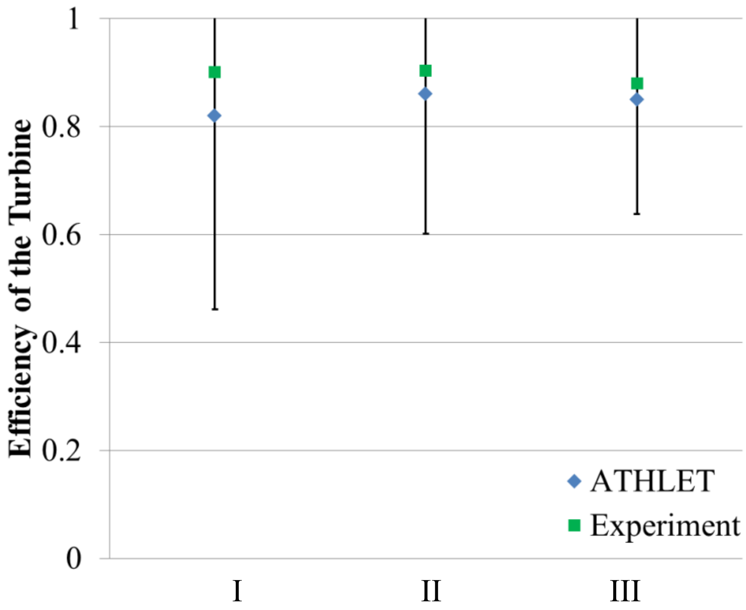

Figure 4-10: Comparison of the Experimentally Measured and with ATHLET Calculated Turbine Efficiency for Cases I - III

The compressor efficiencies calculated with ATHLET do not match the experimental data and the deviation $(\eta_{c,ATH}/\eta_{c,exp})$ - 1 even exceeds 200 % for case 1. The uncertainty of the compressor's performance is extremely high: The statistical error on its own, caused by the uncertainty of the experimental data, is more than 100 % for all cases. Since the inflow conditions are in the direct proximity of the critical point, temperature and pressure deviations have a strong influence on the enthalpy and hence on the efficiency. This effect is visualized in Figure 4-9, where the horizontal error bar is derived from the accuracy of the temperature data. Especially at the compressor inlet, i.e. point 4, the enthalpy values possess a very large uncertainty. Nevertheless, since the implemented approach computes quite realistic efficiencies, it is utilized for the conducted analysis. But, further experimental research is necessary, in order to provide qualitatively good data for a comprehensive validation of the performance model. In the future, data gained by experiments should be more precise, for example due to more accurate measuring devices. Alternatively, the uncertainty of the data would be reduced for experiments that are not conducted with boundary conditions in the direct proximity of the critical point, since the influence of temperature and pressure deviations on the enthalpy would be less.

CFD investigations, as in [45], are also helpful to get further insights into the phenomena within the compressor and to optimize its design. But additional model developments will be indispensable to further improve the prediction capability.

4.4 Discussion of the Model Validation

This chapter discusses the results of the model validation. It focuses on the relevance of the gained information on the simulation of a sCO_2 Brayton cycle and how possible deviations might influence the behavior of the self-propelling heat removal system.

The determination of the heat transfer coefficient is important for the calculation of the heat transferred through the compact heat exchanger that is utilized in the Turbo Compressor System. The validity of the Gnielinski correlation, to predict the Nusselt number for heated supercritical carbon dioxide, has been confirmed on the basis of 23 experiments. It was found that the heat transfer coefficient tends to be underestimated in the relevant operation regime. In addition, the small hydraulic diameter of the channels within the compact heat exchanger might further increase the actual heat transfer coefficient. But this effect is also neglected. The model shall be adjusted when more accurate correlations for the heat transfer in compact heat exchangers are obtainable. At this point in time this uncertainty is acceptable. The approach is conservative, which means that the heat removed from the primary circuit is likely to be underestimated. The Turbo Compressor System might be able to remove even more heat from the primary circuit than predicted.

In addition, the modeling approach of the printed circuit heat exchanger is an uncertainty source. The compact heat exchanger utilizes cross-flow, however, this cannot be simulated by ATHLET, within an acceptable computation time. Therefore, a co-current exchange mechanism is modeled, which has a lower efficiency. However, this is effect is not of great importance for condensation processes, as the vapor / water temperature is assumed to be constant. On the other hand, the number of nodes of the heat exchanger channels influences the amount of transferred heat, as shown in the exemplary nodalization study in chapter 4.1.2.

Nevertheless, the nodes have been limited, in order to achieve an acceptable computation time. Again this leads to an undervalued heat exchanger exit temperature of the sCO_2 and it is another indication that the heat transfer over the compact heat exchanger is underpredicted. Unfortunately, no applicable experimental data has been published in the literature, in order to validate the Gnielinski correlation for the cooling of supercritical carbon dioxide. However, as a first step, this aspect can be neglected for the simulation of the Turbo Compressor System. Air-cooling, as applied for the air-cooled heat exchanger, cannot explicitly be simulated by ATHLET, which is why the air-cooled heat exchanger modeling is simplified. A constant temperature signal is attached to a heat conduction object and is adjusted to establish the predetermined fluid temperature following the heat exchanger. Therefore, it is acceptable to use the correlation also for cooling, without an explicit validation.

The accuracy of the correlation for the determination of the pressure drop is uncertain, since the wall roughness of the test section is unknown. The simulated results show good agreement with the experimental data, for the assumed piping quality. However, if the wall roughness is actually higher as assumed, the pressure loss due to wall friction might be overpredicted. For the simulation of the Turbo Compressor System, this yields conservative results, since the necessary compression work could be overvalued. This would lead to an underprediction of the power balance of the turbomachinery. The heat removal system could be capable to operate self-propelling over a wider range of operating conditions and a greater amount excess electricity might be available. Therefore, further validation shall be executed, when appropriate experimental data becomes available.

The validation of the turbine model has revealed that the pressure drop for off-design conditions is slightly underestimated. For the simulation of the Turbo Compressor System this means that the achievable pressure difference and therefore the amount of expansion work obtained from the sCO_2 is undervalued. This is acceptable for this application, since it yields to conservative results and the power balance of the turbo-compressor-unit, might actually be higher than simulated. Furthermore, also the actual efficiency might be higher than simulated. Accordingly, the system could be self-propelling over a wider range of boundary conditions than anticipated. Once the detailed design of the turbomachinery is completed, performance maps shall be generated and implemented. This way, the accuracy of simulated behavior of the turbomachinery can be increased.

In addition to the uncertainties that originate from physical models and implemented correlations, as discussed above, some uncertainties come from the parameter selection of the user. For the simulation of a retrofitted boiling water reactor, this includes the time since reactor startup and shut-down, the temperature of the ambient air, as well as the TCS turbine, compressor and generator data. All of these values are input by the user. In the conducted study, they have been selected such that their uncertainties are covered by conservatism. The time since reactor startup has been selected as long as possible and the station blackout has been chosen as the initiating event such that the time since reactor shut-down is minimized. This leads to the maximum possible decay heat of the plant, which has been selected as the design criterion for capacity of the Turbo Compressor System. In addition, the temperature of the ambient air and respectively the sCO_2 temperature before the compressor is selected by the user. The value can be extremely different between summer and winter and does also vary over time, for example between day and night. This is certainly one difference between a simulated and a real scenario. In the conducted analysis the temperature of the ambient air is 37 °C, leading to the highest possible sCO_2 temperature entering the compressor. This is conservative because the amount of removed heat is minimized. Furthermore, the low density of the working fluid results in a reduced efficiency of the compressor and hence, an increased demand of power. In addition, data of the compressor, the turbine and the generator are selected by the user, such as the components' efficiencies at the design point. It is important that this data is in line with true values, in order to get a realistic power balance of the turbo-compressor-unit and the amount of excess electricity.

The conducted validation has confirmed that the extended version of ATHLET is able to represent sCO_2 Brayton cycles at least qualitatively. The model is able to predict the transient behavior of the Turbo Compressor System within an acceptable range of accuracy. In fact, it is likely that the amount of heat that is removed from the primary circuit is underestimated by ATHLET and that the Turbo Compressor System might be able to run independently over a wider range of operating conditions. Together with a conservative parameter selection of the user, for example regarding the turbomachinery data and the state of the plant, the simulation yields rather conservative results.

5 A BWR Retrofitted with a Self-Propelling Heat Removal System

A typical application of the self-propelling heat removal system is a retrofit measure for an existing boiling water reactor of generation II. This example has therefore been selected to demonstrate the feasibility of the extended ATHLET version to simulate the novel heat removal system, based on a sCO_2 driven Brayton cycle. For this reason the concept and the specific application of the system for a BWR is described in more detail in chapter 5.1. Assumptions regarding the boundary conditions are summarized in chapter 5.2, which have been taken as a basis, for a rough dimensioning of the system with respect to the required heat removal capacity. First thermodynamic cycle calculations have been conducted and the main components have roughly been dimensioned. Chapter 5.3 discusses the modeling approaches of the system and the components.

5.1 Concept

The Turbo Compressor System is designed to remove decay heat directly from the primary circuit. A bypass is attached to the main steam line and the feedwater line, which houses a heat exchanger. Natural circulation is utilized as the driving force and it is therefore advisable to place the heat exchanger as high as possible above the heat source, i.e. the core. However, it has to be located inside the containment, in order to ensure the confinement of the primary steam in case of containment isolation.

Comparable to the concept of an isolation condenser, primary steam flows upwards, to the heat exchanger. The vapor condenses and the water flows down, through the feedwater line and into the reactor pressure vessel, simply driven by gravity. The relative elevations of the system on the primary side can be seen in Figure 5-1. They have been chosen in accordance with the design parameters of a generic BWR, which has been taken as a basis for the conducted study.

The heat exchanger is separated from the main steam line during normal operation by four solenoid valves [59]. Two valves are placed in series, in order to avoid inadvertent opening. In addition, two of these series are placed in parallel, to guarantee opening if required. In case of a station blackout, the magnetic valves open automatically, due to the power failure.

Alternatively, for example in a loss of ultimate heat sink scenario, the valves are opened by the reactor protection system or manually by the operator.

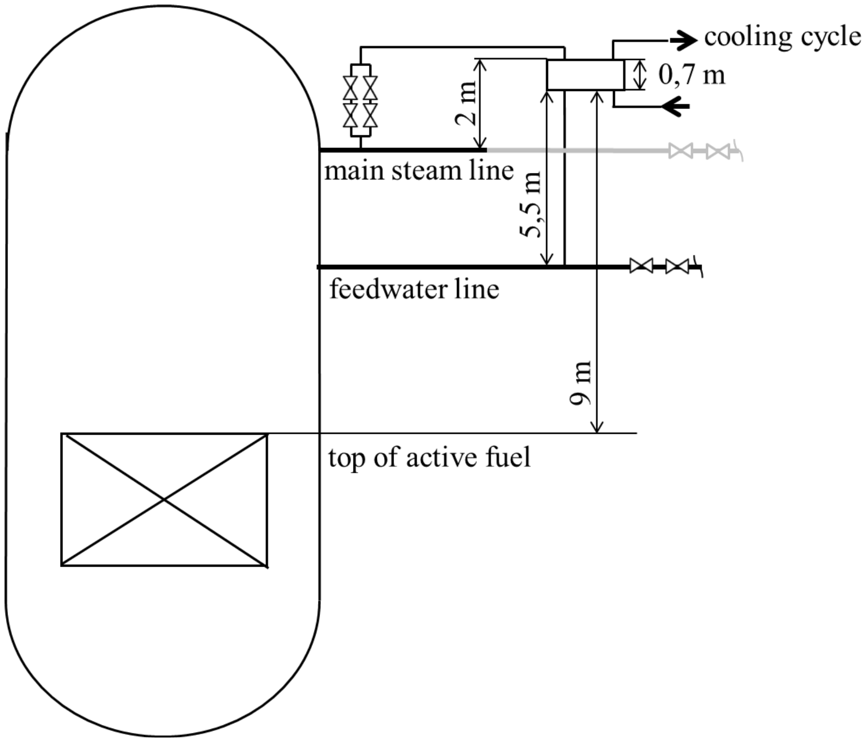

Figure 5-1: Relative Elevations of the Turbo Compressor System - Connection to the Primary Circuit

The heat is transferred from the primary circuit to an adjacent cooling cycle that can be seen in Figure 5-2. The supercritical carbon dioxide within this cycle is heated (1-2) and flows to a turbine (2-3) where it is expanded. The fluid continues to an air-cooled heat exchanger (3-4), which is located outside of the reactor building. The cooled sCO_2 proceeds to a compressor (4-1) where it is compressed, before it reenters the condenser. This concept is known as a Brayton cycle, which is widely used, for example in gas turbine engines.

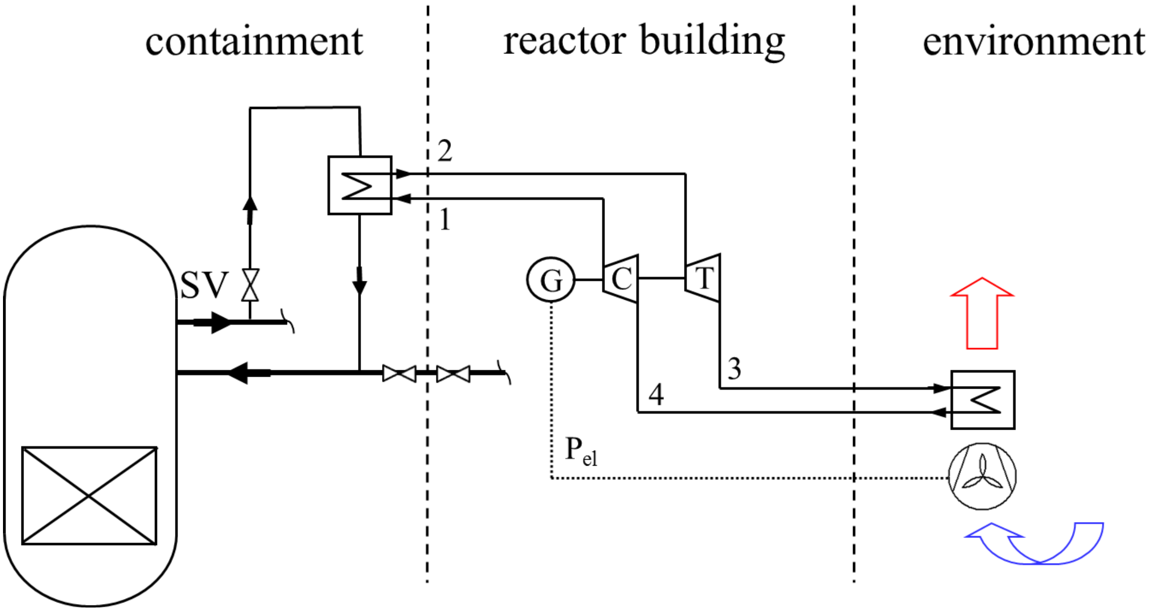

Figure 5-2: Conceptual Sketch of the Self-Propelling Cooling System

The turbomachinery works as the engine of the Turbo Compressor System and is placed on a common shaft. The implemented compressor is directly powered by the turbine. Radial turbomachinery has been selected as they operate efficiently over a wider range of boundary conditions compared to axial turbomachinery and are therefore more flexible throughout different accident scenarios. As the expansion work gained by the turbine actually exceeds the necessary compression work, it is possible to attach a generator to the shaft to produce electricity. Parts of this excess electricity can be used for various purposes throughout the plant, which can be extremely helpful during a station blackout. Nevertheless, the electricity is primarily intended to power air fans, in order to enhance the heat transfer of the air-cooled heat exchanger. The ambient air is utilized as alternative ultimate heat sink, which has the big advantage that the system is able to cope with the loss of ultimate heat sink scenario.

Special requirements apply for the heat exchanger that transfers the heat from the primary vapor to the sCO_2, since it is located inside the containment and the available space is limited. Therefore, a compact heat exchanger has to be used. More precisely, a printed circuit heat exchanger, as seen in Figure 5-5, has been selected for the current design, whose extremely high surface to volume ratio minimizes the required space. The heat exchanger consists of multiple plates, which house several hundred channels. These semicircular channels are chemically etched into the surface of the plates and have hydraulic diameters in the range of millimeters. The plates can be stacked crosswise and are connected by diffusion bonding. This joining technology enables the printed circuit heat exchanger to withstand high pressure differences and temperature gradients.

5.2 Design

Shortly after scramming a boiling water reactor with a nominal power of 3840 MW_{th}, its decay heat exceeds 200 MW_{th}. In order to remove the entire heat at this point in time, unreasonable huge installations of the self-propelling heat removal system would be necessary.

If the decay heat exceeds the quantity of removed heat, the amount of produced steam rises above the amount of condensed steam and the primary circuit pressure increases. The depressurization system limits the reactor pressure vessel pressure due to the intermittent blow down of steam into the wetwell via the safety and relief valves. On the one hand, this supports the heat removal system during the beginning of the scenario, but on the other hand it removes coolant inventory from the primary circuit. Furthermore, the coolant cannot be replaced, since all active injection systems are considered to be unavailable and external help is not anticipated. Therefore, the blow down of primary steam leads to a decreasing water level within the reactor pressure vessel. If a certain threshold value is reached, a low water level signal is activated and the depressurization system opens the safety and relief valves permanently, in order to facilitate external coolant injection and to avoid core degradation under high system pressures. To achieve long-term cooling via the heat removal system, this has to be avoided and a sufficient amount of water has to be kept within the isolated primary circuit.

Therefore, a feasibility study was conducted to determine the amount of heat that has to be removed, in order to achieve long-term coolability of the core. For this first evaluation, the input data deck of a generic boiling water reactor was simply extended by a heat sink. It has been attached with a bypass, connecting the main steam line and feedwater line, and the amount of heat that is removed was increased by 5 MW_{th} steps. The results of the feasibility study have shown that a heat removal capacity of 60 MW_{th} can be sufficient. Exemplarily, Figure 5-3 shows the amount of steam blown down into the pressure suppression pool for a heat removal of 50, 60 and 70 MW_{th}. The amount of steam that is blown into the wetwell increases stepwise. This is due to the intermittent opening of the safety and relief valves, which are triggered when the threshold value for the primary circuit pressure is reached. The intervals between these blow downs increase for larger heat removal capacities. A sudden increase of blown down steam can be seen after 3,300 seconds for the 50 MW_{th} case. This indicates that the low water level threshold value has been reached and the primary circuit is depressurized through permanently opened safety and relief valves.

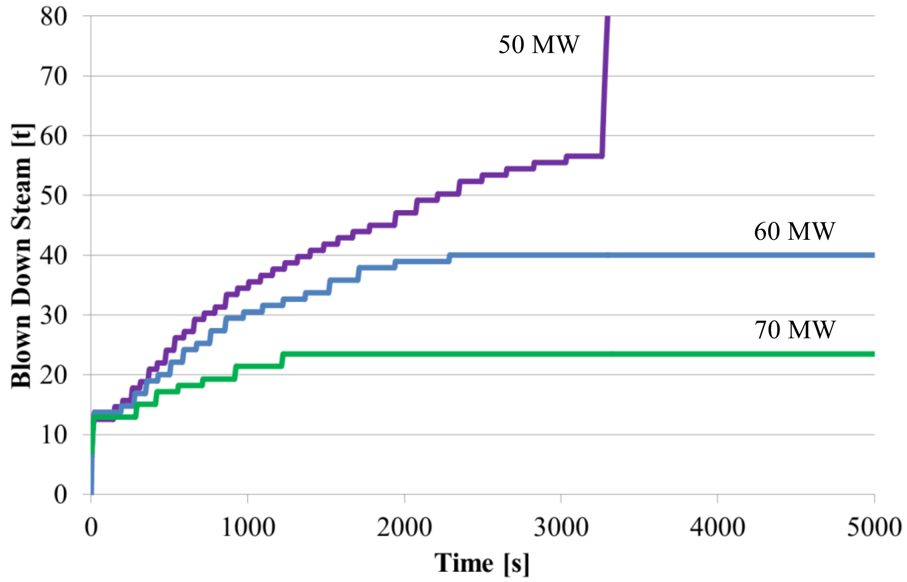

Figure 5-3: Amount of Steam Blown Down into the Pressure Suppression Pool over Time – for Different Heat Removal Capacities

Prior to the simulation of the Turbo Compressor System, a basic dimensioning of the incorporated components had to be done.

The boundary conditions, from which the component requirements have been deduced, are:

- the temperature of the ambient air: 37 °C, in accordance with the short-term temperature required by the EUR [16]
- the temperature of the primary steam during the beginning of the scenario: 286 °C, since normal operation under full load is anticipated when the initiating event occurs
- the amount of removed heat: 60 MW_{th}, in order to guarantee long-term coolability.

A minimum temperature difference of 5 K has been assumed for both heat exchangers to guarantee an efficient heat transfer. Hence, the minimum sCO_2 temperature is 42 °C and the maximum temperature was assumed to be 281 °C. Furthermore, these values have been selected as the design point temperatures for the turbomachinery, with isentropic efficiencies of $\eta_t = 0.85$ for the turbine and $\eta_c = 0.8$ for the compressor. A parameter study has been performed with a thermodynamic simulation tool that has been developed by RWE Technology [35]. The optimal pressure ratio of the Brayton cycle for the present boundary conditions has been computed to 1:2, with approximately 18 MPa on the high and 9 MPa on the low pressure side. With this information, a first analysis of the parameters of the Brayton cycle has been done without the consideration of friction losses, which can be seen in Table 5-1 and Figure 5-4.

Table 5-1: Calculated Values of the Brayton Cycle

Parameter	Value	Unit
Following the Compressor (1)		
Pressure	18	MPa
Temperature	81	°C
Enthalpy	391	kJ/kg
Entropy	1.55	kJ/kgK
Following the Condenser (2)		
Pressure	18	MPa
Temperature	281	°C
Enthalpy	708	kJ/kg
Entropy	2.28	kJ/kgK
Following the Turbine (3)		
Pressure	9	MPa
Temperature	219	°C
Enthalpy	658	kJ/kg
Entropy	2.31	kJ/kgK
Following the Cooler (4)		
Pressure	9	MPa
Temperature	42	°C
Enthalpy	367	kJ/kg
Entropy	1.54	kJ/kgK

The thermal efficiency η_{th} [17] of the Brayton cycle serves as a first indicator if the system is self-propelling:

$$\eta_{th} = \frac{\Delta h_t - \Delta h_c}{q_{heat}} = \frac{(h_2 - h_3) - (h_1 - h_4)}{(h_2 - h_1)} \tag{5.1}$$

Under design point conditions, the thermal efficiency turns out to be 8.3%. Even though this is comparably low, it proofs the potential of the system to operate completely independent. Furthermore, one has to keep in mind that the main task of the system is to transfer heat to the ambient air, for which a large q_{cool} is aspired.

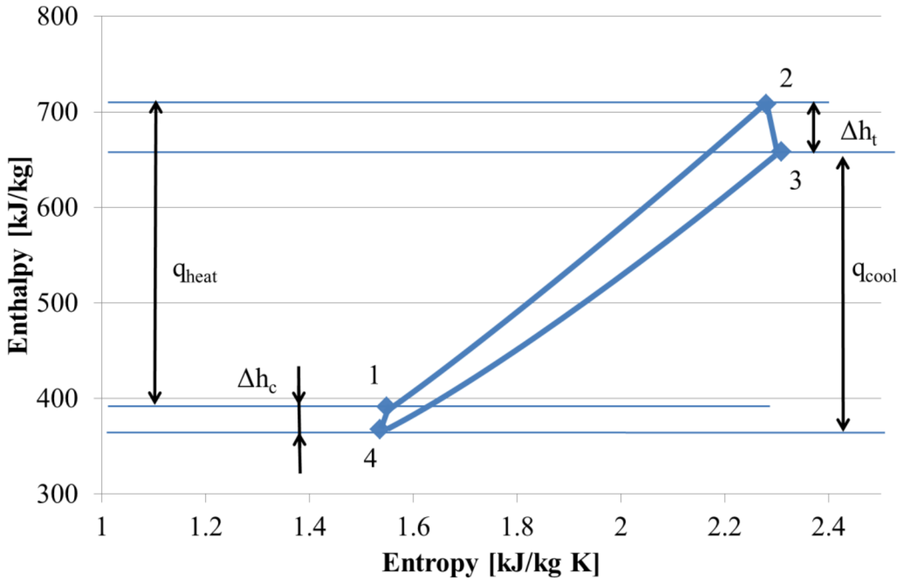

Figure 5-4: Enthalpy – Entropy Diagram for the Calculated Brayton Cycle

5.2.1 Turbomachinery

The mass flow of the Brayton cycle that is necessary to remove the desired 60 MW_{th} can be calculated for the given conditions, by means of an enthalpy balance

$$Q_{heat} = m * (h_2 - h_1) \tag{5.2}$$

Therefore, an overall mass flow of 189.3 kg/s has been selected as additional boundary condition for the design of the turbomachinery, which has been conducted by von Lavante [34]. Until now, a detailed design of the turbine and the compressor is not at hand. However, it was examined that the mass flow has to be reduced in order to achieve both, an efficient turbine and compressor with the same number of revolutions. In fact, four equivalent turbo-compressor-units and further, four separated cooling trains are placed in parallel to achieve the desired overall mass flow rate. Under the given conditions, von Lavante has proposed 60,000 1/min as the ideal number of revolutions with the turbine diameter $D_t = 0.0709$ m. This is comparable to values of turbo-compressor-units from the literature [70].

5.2.2 Compact Heat Exchanger

The heat exchanger that links the primary circuit to the cooling trains should be located within the containment, in order to keep the primary coolant within this boundary and to ensure activity retention. A compact heat exchanger is therefore required, since the available space within the containment is limited. A printed circuit heat exchanger has been selected, due to its high inner surface to volume ratio. 300,000 channels are currently postulated for the vapor / water and sCO_2 side, to transfer at least 60 MW_{th} under the given boundary conditions. An equal amount of plates with the same plate thickness and an identical channel length is assumed for both sides of the compact heat exchanger. Austenitic stainless steel SS316LN (X2CrNiMoN17-12-2) has been selected as the material of the diffusion bonded heat exchanger. This alloy has very good mechanical and corrosion resistance properties and has been discussed as a promising material for supercritical carbon dioxide heat exchangers that could be utilized in the nuclear industry [38]. To ease the construction process, the plates are arranged in cross flow with straight, semicircular channels. For the support of the natural circulation of the primary steam, the vapor/water channels are oriented vertically, to facilitate that the condensate drains downwards, as seen in Figure 5-5.

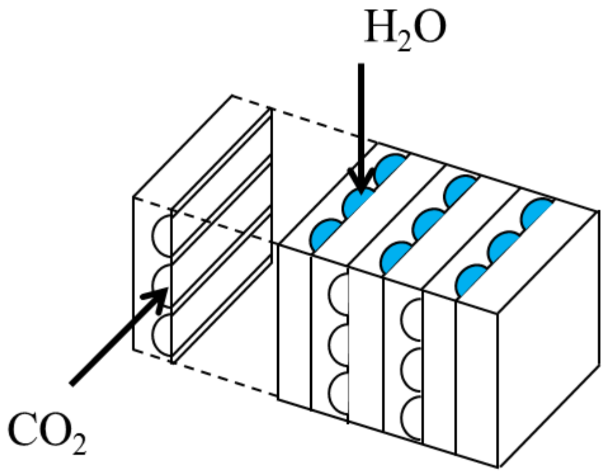

Figure 5-5: Printed Circuit Heat Exchanger – Orientation

It has been analyzed, if capillary forces influence the heat exchanger's performance as they can change the fluid's behavior in small channels. This effect is immaterial for supercritical fluids, as no phase change occurs, but might interfere the heat transfer on the vapor/water side. Teng et al. [56] have examined capillary blocking in small-diameter condensers and found that for co-current flows of fluid and vapor the liquid bridges do not block the flow. Either, these bridges are unstable and the hydrodynamic force breaks them up, or the vapor between the bridges condenses rapidly. Therefore, capillary forces have not been considered in the current analysis.

Typical channel diameters of a printed circuit heat exchanger are 1-2 mm [23]. Accordingly, the channel width for the vapor / water side has been selected as d_{H2O} = 2 mm, and a smaller diameter of d_{CO2} = 1.25 mm has been chosen on the supercritical carbon dioxide side, in order to guarantee turbulent flow for all applicable boundary conditions.

According to Hesselgreaves [23], the minimum wall thickness t_w, shown in Figure 5-6, can be estimated with equation 5.3:

$$t_w = \frac{1}{\left(\frac{\sigma}{\Delta p} + 1\right) n_f} \tag{5.3}$$

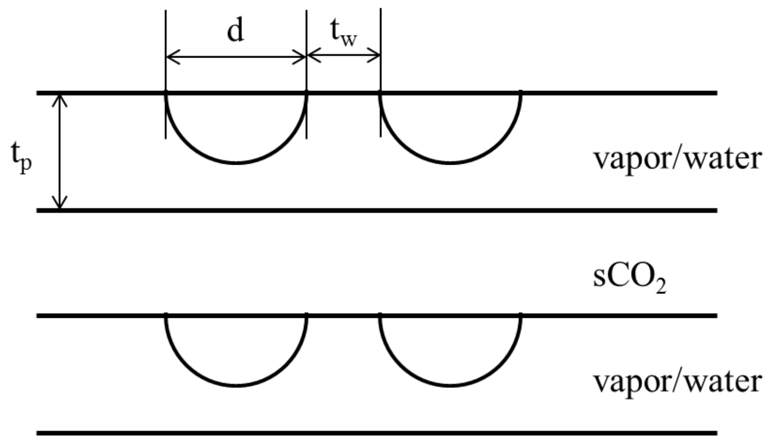

Figure 5-6: Printed Circuit Heat Exchanger - Dimensions

Where Δp is the maximum pressure differential that is 18 MPa, assuming full design pressure on the sCO_2 side and only atmospheric pressure on the vapor/water side. σ is the maximum allowable stress, which is taken as the proof strength of X2CrNiMoN17-12-2 at 300 °C, 120 MPa [7] and n_f is the number of fins. According to Dostal [9], this corresponds to the number of channel walls per meter, for a printed circuit heat exchanger

$$n_f = \frac{1}{d + t_w} \tag{5.4}$$

Therefore, the following equation can be obtained:

$$t_w = \frac{\Delta p}{\sigma} * d \tag{5.5}$$

Equation 5.3, for the estimation of the minimum wall thickness, originates from the design of plate fin heat exchangers. However, it is noted in the literature [9] that the formula can be transferred to printed circuit heat exchangers. Nevertheless, a conservative safety factor of 2.0 has been chosen to compensate for these uncertainties: This results in a wall thickness on the vapor / water side, i.e. the bar width $t_{w,H2O}$, of 0.6 mm. Furthermore, in consistence with the assumption of an equivalent amount of channels and the same number of plates for both fluids, $t_{w,CO2}$ is 1.35 mm.

In order to determine the plate thicknesses t_p, a basic stress analysis, of the radial stress σ_{rad}, as well as the tangential stress σ_{tan} has been conducted [11]. For a circumferential, thick-walled pressure vessel equation 5.6 and 5.7 are valid:

$$\sigma_{rad} = \frac{{r_{in}}^2}{{r_{out}}^2 - {r_{in}}^2}\left(-p_{ins} * \left(\frac{{r_{out}}^2}{r^2} - 1\right) - p_{outs} * \left(1 - \frac{{r_{in}}^2}{r^2}\right)\right) \tag{5.6}$$

$$\sigma_{tan} = \frac{{r_{in}}^2}{{r_{out}}^2 - {r_{in}}^2}\left(p_{ins} * \left(\frac{{r_{out}}^2}{r^2} + 1\right) - p_{outs} * \left(1 + \frac{{r_{in}}^2}{r^2}\right)\right) \tag{5.7}$$

The equivalent stress according to the maximum shear stress criterion is $\sigma_{sh} = \sigma_{tan} - \sigma_{rad}$ for the CO_2 side ($p_{ins} > p_{outs}$) and $\sigma_{sh} = \sigma_{rad} - \sigma_{tan}$ for the vapor / water side ($p_{outs} > p_{ins}$) [11]. For the plate housing the sCO_2 channels, the most stressed point at the inner radius $r = r_{in}$. With the primary circuit being at atmospheric pressure this results to

$$\sigma_{sh,CO2} = \frac{2{r_{out}}^2}{{r_{out}}^2 - {r_{in}}^2}\, p_{ins} \tag{5.8}$$

With a safety factor of 1.2 this leads to $r_{out,CO2} = 0.78$ mm, i.e. the plate thickness. Additionally, the vapor / water channel has to be examined under external pressure

$$\sigma_{sh,H2O} = \frac{2\,{r_{in}}^2}{{r_{out}}^2 - {r_{in}}^2}\, p_{outs} \tag{5.9}$$

Hence, $r_{out,H2O} = 1.17$ mm. Conservatively, the plate thickness is set to 1.2 mm.

ATHLET calculations have been run, in order to determine a sufficient channel length l (the modeling approach is described in chapter 5.3.1), where the length was iteratively decreased by 0.05 m. For the determined channel length of 0.7 m, the number of pair of plates n_p results to 1120.

$$n_p = \frac{300000}{n_{channel}} \tag{5.10}$$

$$n_{channel} = n_f * l \tag{5.11}$$

Overall, the volume of the compact heat exchanger core V is 1.9 m³.

$$V = n_p * 2 * t_p * l \tag{5.12}$$

If it is not possible to integrate the heat exchanger into the containment due to space limitations, it could be divided into modular arrangements, which could be placed between existing components.
The basic geometry of the printed circuit heat exchanger is summarized in Table 5-2.

Table 5-2: Dimensions of the Printed Circuit Heat Exchanger

Abbreviation	Parameter	Value	Unit
d_{H2O}	channel width	2	mm
d_{CO2}	channel width	1.25	mm
$t_{w,H2O}$	fin thickness	0.6	mm
$t_{w,CO2}$	fin thickness	1.35	mm
t_p	plate thickness	1.2	mm
n_f	number of channels per meter	384	1/m
$n_{channel}$	number of channels per plate	268	-
n_p	number of pair of plates	1120	-
l	channel length	0.7	m
V	volume of the HX core	1.9	m^3

5.2.3 Air-Cooled Heat Exchanger

The main task of the air-cooled heat exchanger is to transfer a maximum of 55 MW_{th} to the ambient air.

$$Q_{air} = m * (h_3 - h_4) \tag{5.13}$$

A basic design has been provided by the GEA Luftkühler GmbH [20], for comparable temperature and mass flow requirements. Twelve bundles of pipes, with 85 pipes each, have been suggested, which are ribbed on the outside. The heat exchanger has an overall surface area of more than 80,000 m^2 and twelve fans are intended, each with a nominal power of 55 kW, to guarantee the necessary heat removal. The footprint of the installation is approximately 540 m^2. At an earlier stage of this investigation, the natural circulation of ambient air has been considered, because of its passivity. However, as the heat transfer would be significantly lower, this would result in unpractically large installations. Therefore, the described air-cooled heat exchanger with forced convection has been chosen for the Turbo Compressor System. As the heat exchanger is separated into twelve bundles, it can easily be divided into four parts, such that each cooling train is connected to one quarter of the entire cooling device. Unfortunately, for the current design, the twelve air fans are arranged as in Figure 5-7. If three cooling trains are operating, ten fans would be needed, instead of nine. However, this problematic can be adjusted in a future design of the air-cooled heat exchanger and has been ignored in the current analysis. The number of operating fans is important in order to determine the power balance of the entire Turbo Compressor System and to evaluate if the excess electricity produced with the generator is sufficient to power the air fans.

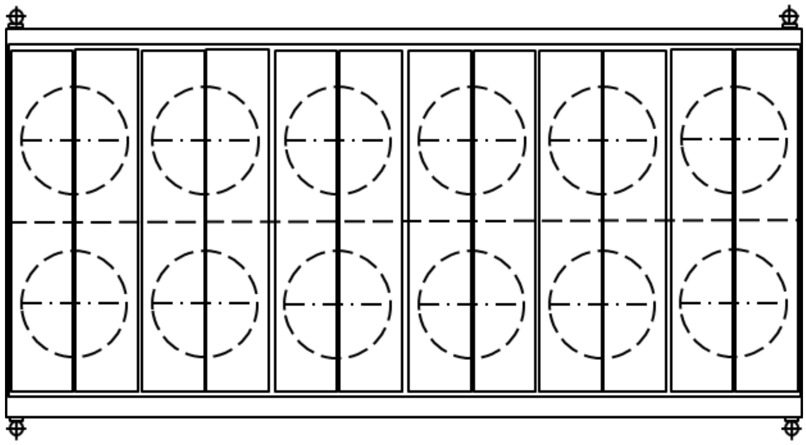

Figure 5-7: Air-Cooled Heat Exchanger – Arrangement of Fans, According to [20]

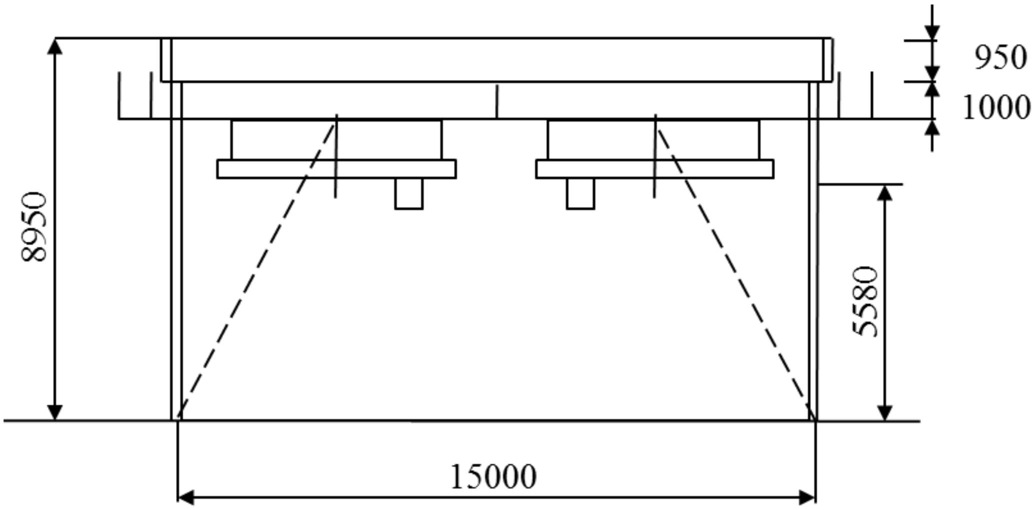

Figure 5-8: Air-Cooled Heat Exchanger – Dimensions, According to [20]

5.2.4 Starting Procedure

During the off-state of the system, the pressure within the entire cycle is 9 MPa, which corresponds to the entrance pressure of the compressor during design point conditions.

For the startup of the system, the movement of the working fluid has to be introduced, the windage has to be overcome and the rotating of all revolving parts has to be initiated. Secondly, as long as the gained expansion work is less than the necessary compression work, the turbine has to be supported. Furthermore, the air-fans have to be started and powered during the starting procedure, to ensure the heat transfer to the ambient air and to reach a low compressor inlet temperature. Therefore, it is necessary to temporarily provide power by a battery, until the number of revolutions has sufficiently been increased by a starting inverter and the system reaches break-even between the gained expansion work, the necessary compression work and the power needed for the air-fans.

A turbine bypass might be necessary, in order to guarantee positive flow through the compressor at the very beginning, which needs to be closed once the turbomachinery has gathered speed.

The required starting output is less than 2 MW per cooling train and will only be required for a couple of minutes during the startup. In fact, it is assumed in the following that it takes 50 seconds for the system to startup and to remove decay heat as anticipated. This time range is comparable to the startup time of other turbine driven systems, for instance the Reactor Core Isolation Cooling system. The necessary compression work has been determined as the main parameter in a rough estimation of the required starting output. During normal operation at design point conditions, the power demand P_c of one compressor is 1.14 MW.

$$P_c = \Delta h\, m \tag{5.14}$$

According to the affinity laws [49], the required power depends strongly on the compressor speed and is considerably lower during the speedup of the turbo-compressor-unit.

$$P_c \sim n^3 \tag{5.15}$$

However, the required power has been overestimated by considering the demand during normal operation at 60,000 revolutions per minute. Additionally, the expansion work obtained by the turbine has completely been neglected until break even, whereas the power required for the fans of the air-cooled heat exchanger is considered with $P_{fan} = 0.165$ MW. Therefore, a power supply that is able to provide 2 MW is sufficient for one train.
A consecutive starting procedure is also possible, whereby only one of the four cooling circuits needs the ability to black-start. The other circuits could then be powered by the gained excess electricity of the already running unit. The batteries shall be recharged after the startup by the gained excess electricity, in order to become capable to restart the system later on.

5.3 Modeling of a Supercritical Carbon Dioxide Brayton Cycle with ATHLET

For the simulation of the self-propelling heat removal system with ATHLET, four, and in one specific case two, cooling trains, are modeled separately. This allows switching them off individually, which is necessary to examine different operating procedures.

5.3.1 Compact Heat Exchanger

In case of four cooling trains in parallel, each incorporates one quarter of the compact heat exchanger. Each quarter again is represented by 75,000 copies of one sCO_2- and one vapor / water-channel. They are modeled in co-current flow, since ATHLET is currently not able to simulate cross-flow heat exchangers without an inacceptable increase in computation time. The total mass flow rate is anticipated to be evenly distributed to all channels and instead of semicircle channels they are modeled as round pipes, with the hydraulic diameter D_h as the inner width

$$D_h = \frac{4\,A}{\frac{\pi\,d}{2} + d} = \frac{4 * \left[\pi\left(\frac{d}{2}\right)^2\right]/2}{\frac{\pi\,d}{2} + d} = \frac{\pi\,d}{\pi + 2} \tag{5.16}$$

Where the denominator is the perimeter of the semicircle.
For the calculation of the pressure drop, the entry and exit losses are considered by ATHLET due to the calculation of the form loss

$$\Delta p_{form} = -\left(\left(\frac{1}{A_{pipe}{}^2} - \frac{1}{A_{HX}{}^2}\right)\frac{1}{2\,\rho_m}\,m\,|m|\right) \tag{5.17}$$

In addition the pressure drop due to wall friction is computed by ATHLET, for what the wall roughness has to be known. Mylavarapu [41] has measured the surface roughness on a chemically etched channel of a printed circuit heat exchanger. Thereby, the average roughness was determined to 242.6 nm and is conservatively set to 1 µm in the ATHLET calculations.

The heat transfer is computed with the module HECU. The compact heat exchanger is modeled as 75,000 copies of one heat conduction object (HCO), which connects one vapor / water channel, to one sCO_2 channel. The geometry of the HCO has been approximated as a plate, with a thickness equal to the average distance $\tilde{s}$ between two channels. It can be computed via the geometrical specification that $\tilde{s} = 0.56$mm.

$$\tilde{s} = \frac{\left(d_{H2O} * d_{CO2} * 2 * t_p\right) - \pi\left(r_{H2O}{}^2 r_{CO2} + r_{H2O} r_{CO2}{}^2\right)}{2 * \left(d_{H2O} * d_{CO2}\right)} \tag{5.18}$$

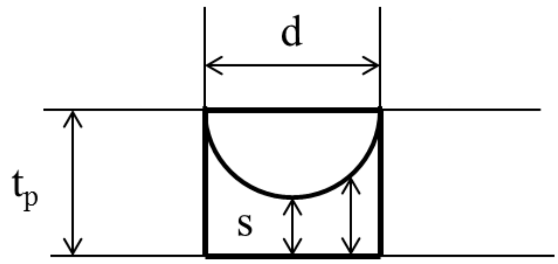

Figure 5-9: Printed Circuit Heat Exchanger – Averaged Plate Thickness

Furthermore, in order to determine the heat transfer between the fluids, the heat transfer area has to be known. A uniform heat distribution through the top and the bottom of the channel is assumed, considering an infinitely large heat exchanger, the heat transfer area can be approximated with

$$A_{HT} = 2\,d_{H2O}\,d_{CO2} n_{channel} \tag{5.19}$$

Since the length of the heat conducting plate equals the length of the channels, the width of the plate is adjusted to w_p =0.00192 m.

$$w_p = \frac{A_{HT}}{l} \tag{5.20}$$

5.3.2 Air-Cooled Heat Exchanger

Similar to the modeling approach of the compact heat exchanger, the model of the air-cooled heat exchanger is also subdivided into four parts, corresponding to the four cooling trains placed in parallel. Therefore, each quarter is represented by 255 copies of one heat conducting object. Since air-cooling cannot be simulated with ATHLET explicitly, the modeling had to be adapted. The heat conducting object connects one pipe, with a diameter of 25.4 mm, to a GCSM signal that represents the temperature at the outer wall of the object. Again, it is assumed that the total mass flow rate is distributed likewise through all pipes. The temperature of the outer wall of the pipe was adjusted, to match the targeted exit temperature of 42 °C. The surface roughness was not provided but is necessary for the determination of the friction losses. Therefore, it has been selected in order to obtain a pressure drop within the range of the one provided by the GEA Luftkühler GmbH [20], 25 kPa.

It is anticipated that the Turbo Compressor System needs a certain startup time before it operates as intended. However, the startup process cannot be modeled with ATHLET, since it is not possible to simulate the starting of the turbomachinery with the currently implemented component model. Therefore, 50 seconds are allowed before the air-cooled heat exchanger starts to cool the supercritical carbon dioxide as planned, to imitate the reduced heat removal capacity during the starting procedure.

5.3.3 Turbomachinery

The turbomachinery can be modeled with a special component model. It needs design point information about the entry and exit pressure, the mass flow and the enthalpy, in order to determine the averaged design point density. Furthermore, the isentropic efficiency and the number of revolutions per minute have to be entered.

Figure 5-10 shows the nodalization scheme of one of the four cooling cycles of the Turbo Compressor System, Table 5-3 summarizes the most important parameters of the main components. The ATHLET input description for one cooling train can be found in Appendix D.

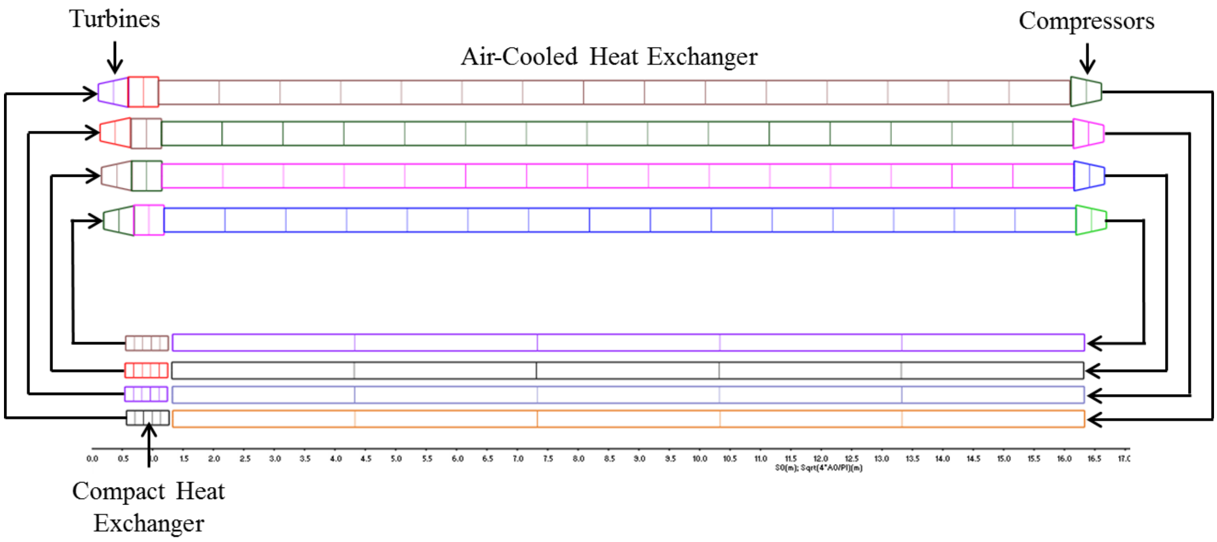

Figure 5-10: Nodalization Scheme of one Cooling Train of the Turbo Compressor System

Table 5-3: Nodalization of the Turbo Compressor System

Component	Number of nodes	Length
Turbine	4	0.5 m (turbine pipe)
Compressor	2	0.5 m (compressor pipe)
Compact heat exchanger	5	0.7 m
Air-cooled heat exchanger	15	15 m

6 Simulation of Station Blackout and Loss of Ultimate Heat Sink Scenarios

The Turbo Compressor System has been simulated as a potential retrofit measure for a generic boiling water reactor with the extended version of ATHLET. The impact of the self-propelling heat removal system on the plant during a combined station blackout and loss of ultimate heat sink scenario has been evaluated. Different configurations and control strategies have been anticipated and the results have been compared with each other as well as to the reference case, i.e. the plant's behavior without the retrofitted system.

6.1 Modeling of the Generic Boiling Water Reactor

The input deck that has been utilized for the current analysis is based on a generic boiling water reactor with four loops and 3840 MW thermal power. It is generally used, for example by the GRS for the analysis and evaluation of potential incidents in comparable plants.

6.1.1 The Thermohydraulics

All major components that influence the behavior of the plant are included in the input deck. It consists of over 300 thermo-fluiddynamic and more than 120 heat conduction objects, to model for example the reactor pressure vessel and its connection to the main steam line (MSL) and the feedwater line (FWL). Figure 6-1 shows the interconnecting TFOs, as well as the nodalization scheme of the interior of the RPV. It includes for example the core, the downcomer, the steam-water separator and the dome. For the clarity of the outline, only one connecting main steam line and feedwater line are displayed. However, all of the four loops are simulated separately and the self-propelling heat removal system has been attached to one of them. Several valves are incorporated, such as the isolation valves, attached to the MSL and the check valves, installed at the FWL, to simulate the isolation of the containment. Furthermore, the input data includes the safety and relief valves, as well as the diversified pressure relief valves. If primary steam is blown down through one of these valves, it flows into the wetwell which is modeled by the module CONDRU. The input deck includes further all emergency cooling systems, as well as safety injection systems that are usually implemented in a generic boiling water reactor. However, due to the postulated power failure they do not run in the conducted analysis. The only means to inject water into the reactor pressure vessel (RPV) is via the feedwater tank, once the pressure in the feedwater system overcomes the RPV pressure and the check valves open. Some parts of the balance of plant, such as the steam turbine is demonstrated by means of GCSM signals.

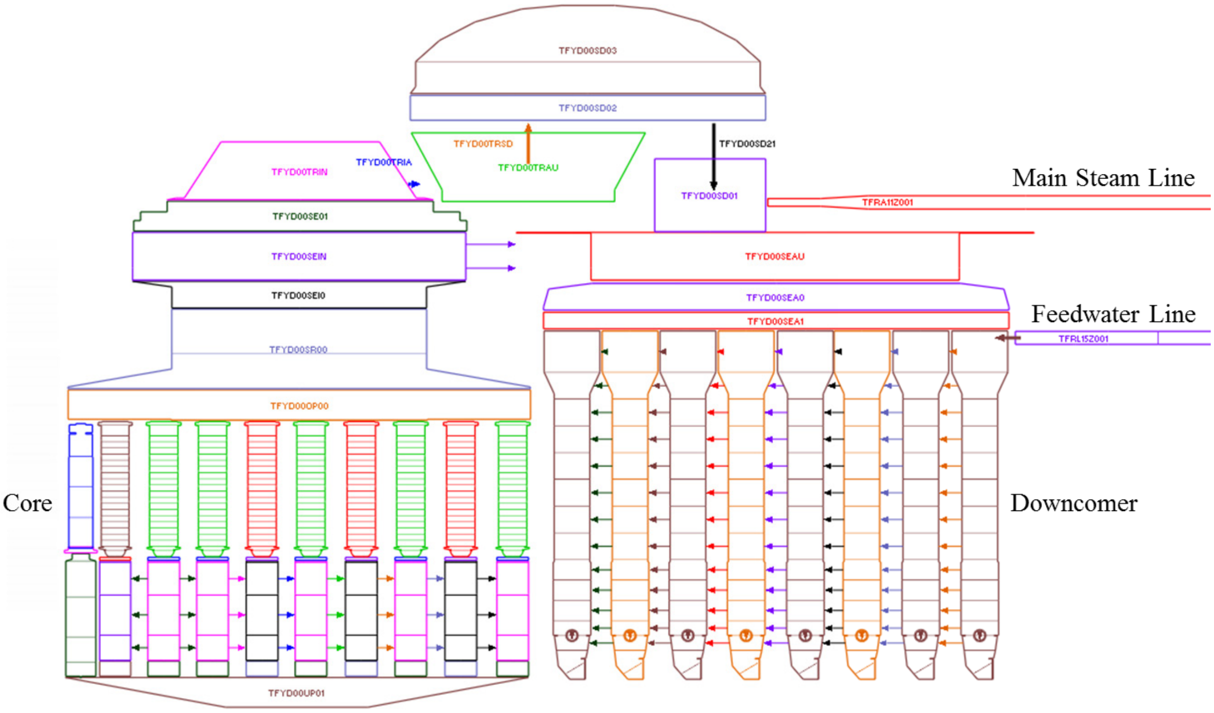

Figure 6-1: Nodalization Scheme of the RPV with Core and Downcomer

The thermal power of the reactor is calculated via a pointkinetics model during normal operation. However, after the reactor is scrammed, the heat is no longer calculated with the module NEUKIN. The resulting decay heat is determined by multiplying the nominal reactor power, i.e. 3840 MW_{th} with a time-dependent factor that is provided via a GCSM signal. For the available input deck, the user has the option to choose between three tables, based on the time since reactor startup. For the conducted analysis, the maximum amount of decay heat, i.e. after 300 days of operation, was selected.

6.1.2 The Instrumentation and Control System

The purpose of the simulation of the instrumentation and control (I&C) system is twofold. On the one hand it is necessary to determine deducted parameters, such as the water level within the reactor pressure vessel, which serve as boundary conditions for several safety systems. On the other hand, it is essential for the simulation of the safety systems themselves, for example the reactor protection system. It activates the shutdown of the reactor, or opens and closes the safety and relief valves, based on the water level and the pressure within the RPV.

For the current analysis, the station blackout is chosen as the initiating event. Therefore, the failure of load rejection to auxiliary station supply is anticipated. Simultaneously, the back-up grid, the foreign grid and all five emergency diesel generators become unavailable, which is

simulated via a time-dependent GCSM signal. However, the reactor protection system is supposed to be available throughout the entire time, since it is backed up with batteries.
The scenario that is anticipated in the following simulations is a long-term station blackout together with a loss of the ultimate heat sink. The combination of these events is very unlikely and considered beyond design basis. Some adaptions on the input data of the generic boiling water reactor have been necessary to simulate this rare scenario such as an independent closure of the isolation valves due to the decreasing control oil pressure after power failure. It is considered that the valves close 12 seconds after the initiating event, which has been implemented as a time-dependent signal. Additionally the opening logic of the safety and relief valves has only been implemented for the simulation of a turbine trip without subsequent reactor scram. However, a reactor scram has a strong influence on the control strategy of the depressurization of a boiling water reactor. The opening time is reduced, in order to limit the amount of steam blown into the pressure suppression pool and to moderate the primary circuit pressure drop, which would cause the isolation of the containment and results in the loss of the primary heat sink (even though the loss of the ultimate heat sink is anticipated in the current scenario). The opening time of the safety and relief valves triggered by the turbine trip has therefore been reduced from 120 to 20 seconds.

In the framework of the conducted study, five different cases have been analyzed and the results are described in the following.

- **Reference Case**: A reference case is presented, in which the performance of a generic boiling water reactor is demonstrated under the combined station blackout and loss of ultimate heat sink conditions. A brief simplification of the accident sequence, as well as present threshold values are introduced.
- **Retrofitted BWR**: The previous case, but retrofitted with the self-propelling heat removal system. Its influence on the overall plant behavior is evaluated and compared to the reference case.
- **Retrofitted BWR with Adapted Depressurization System**: The previous case, with an adapted depressurization system. The diverse blow-off valves are deactivated, in order to avoid the partial depressurization during the beginning of the accident sequence.
- **Retrofitted and Adapted BWR with Control Strategy**: The previous case, with a simple control strategy for the turbo-compressor-units of the self-propelling heat removal system. Two of the four cooling trains are successively shutdown.
- **Turbo Compressor System Combined with a Reactor Core Isolation Cooling System**: A generic boiling water reactor, equipped with a reactor core isolation cooling system, is retrofitted with the self-propelling system, but with a reduced heat removal capacity.

6.2 Reference Case

In the reference case, the performance of a generic boiling water reactor of generation II has been simulated under the named conditions. Figure 6-2 shows a brief simplification of the accident sequence, as well as present threshold values.

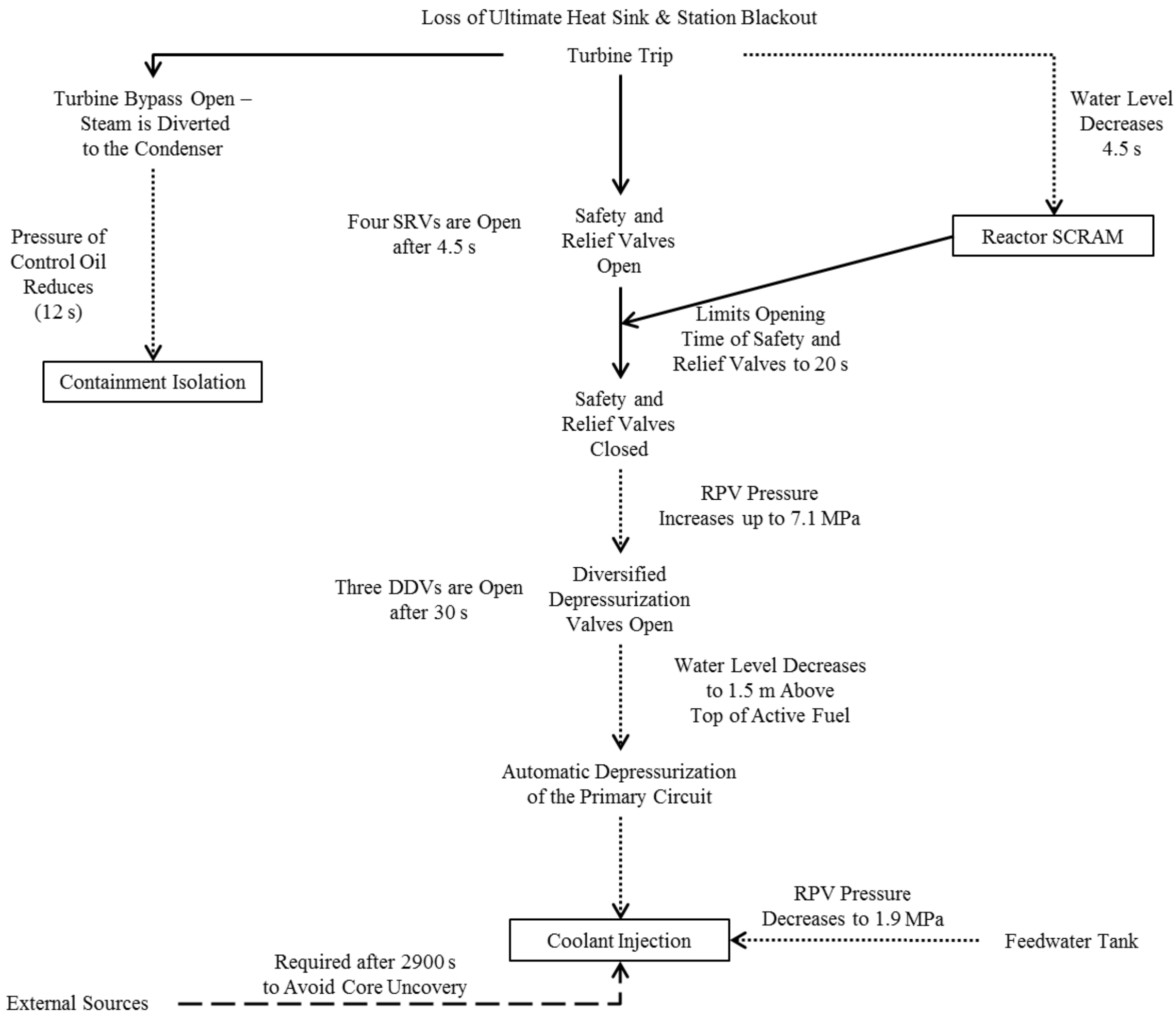

Figure 6-2: Accident Sequence of a Station Blackout, Combined with the Loss of Ultimate Heat Sink

In order to achieve an entire loss of electrical power supplies, it is assumed that the load rejection to auxiliary station supply fails and that the station blackout is therefore directly accompanied by a turbine trip. The diverter valves of the turbine bypass are pressure controlled and open subsequently to the turbine trip, which enables the majority of the primary steam to flow directly to the condenser. However, not the entire amount of steam can be diverted through the turbine bypass. The remaining vapor has to be released into the wetwell through the safety and relief valves, in order to keep the primary system pressure within the designated threshold values. These valves are triggered by the reactor protection system as a consequence of the turbine trip.

Generally, turbine trips can be controlled without a reactor scram. In this case, the thermal power is reduced with the control rods. However, due to the station blackout, the feedwater pumps run out and the water level within the reactor starts to decrease. Within a couple of

seconds, the level falls below a certain threshold value and the reactor protection system initiates the reactor scram. The control rods are completely inserted into the reactor core to ensure the first safety objective, the control of the reactivity.
The reactor scram strongly influences the depressurization concept. Firstly, the control strategy of the safety and relief valves, previously determined by the turbine trip, is changed and the opening time and therefore the amount of blown off steam is reduced. The valves close. Secondly, the scram triggers the opening of the diversified depressurization valves (DDV), which open due to increasing RPV pressure. Similar to the safety and relief valves, primary steam is blown off through these diversified valves, into the pressure suppression pool.
During normal operation, the isolation valves are hold open by a high pressure control oil. However, due to the station blackout, the pressure of the control oil cannot be maintained. After around twelve seconds the pressure has dropped to the point that the isolation valves close automatically and the containment is isolated.
Primary steam is continuously blown off into the pressure suppression pool through the diversified depressurization valves. This results in a declining water level. After a certain time the water level has fallen under a threshold value and the slow depressurization of the primary circuit is activated. Therefore, some of the safety and relief valves are reopened. Since no means for coolant injection are at hand, the water level continues to decrease and the reactor protection system calls upon the so-called fast depressurization. Additional safety and relief valves are opened and the primary circuit pressure is further reduced, in order to facilitate any kind of coolant injection.
When the primary circuit pressure falls below the pressure in the feedwater tank and the corresponding feedwater piping, water can flow through the check valves and can be inserted into the reactor pressure vessel. Without any means of active cooling, coolant injection through external sources is the only option to achieve heat removal.

The accident progression of a typical boiling water reactor was simulated and the results of a plant without additional heat removal are represented in the following graphs. They provide the reference data, in order to evaluate the plant behavior retrofitted with the Turbo Compressor System in the following chapters.

The combined SBO & LUHS, i.e. the initiating event, occurs at 0 seconds. The reactor pressure vessel pressure drops slightly, as shown in Figure 6-3, because the safety and relief valves are opened due to the turbine trip. More primary steam is removed over the turbine bypass and a low water level signal activates the reactor scram. Subsequently, the safety and relief valves close, whereas the diverse blow-off valves are opened. The amount of steam that is removed over the diverse blow-off valves is lower, compared to the ordinary safety and relief valves. Therefore, the RPV pressure increases again and stays almost constant for around 750 seconds. The intention of the diversified blow-off valves is a very slow depressurization through continuous steam removal, until the primary circuit pressure falls below a certain threshold value, which would cause the valves to close successively. However, before this limiting value is reached, the slow automatic depressurization is triggered by a low water level signal. Certain safety and relief valves are opened and the RPV pressure drops significantly. This procedure should facilitate coolant injection. However, since it is anticipated that no means of safety injection are available, the water level falls further, which activates the fast automatic depressurization at 1,100 seconds and even more safety and relief valves are opened, in order to accelerate the depressurization.

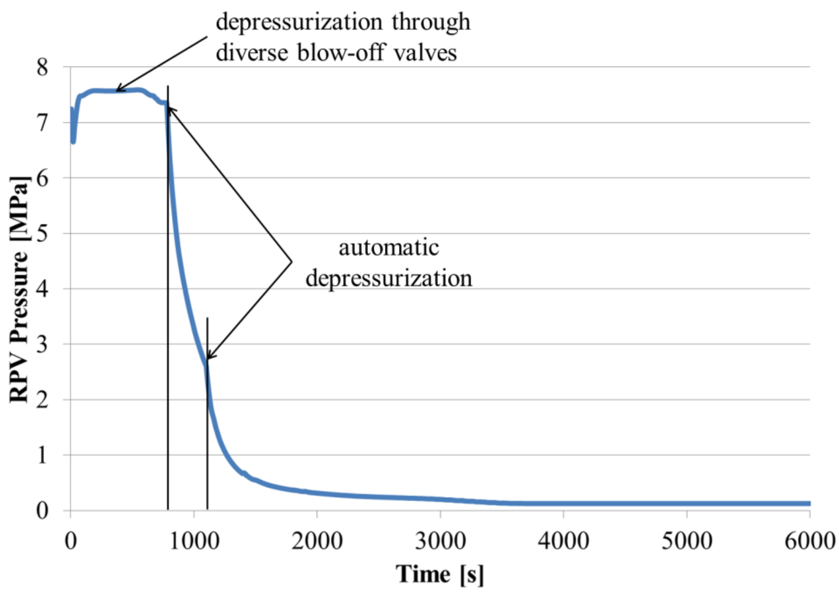

Figure 6-3: Plot of the RPV Pressure against Time – Reference Case

Figure 6-4 shows the coolant inventory within the isolated primary circuit. One can see a sudden drop at the very beginning of the scenario, caused by the steam removal via the turbine bypass and the safety and relief valves. The coolant loss is then limited as the safety and relief valves are closed and steam is further removed only through the diverse blow-off valves. This results in the almost linear reduction of the total mass until the automatic depressurization is activated at 750 seconds, due to the low water level signal. The opened safety and relief valves significantly accelerate the depressurization of the primary circuit, which comes along with a drastic reduction of the remaining coolant inventory. However, due to the decreased primary circuit pressure, the pressure difference before and after the isolating check valves becomes large enough, so that water from the feedwater tank and the connected piping flows passively into the RPV.

Nevertheless, after 3,500 seconds, the total mass is already reduced by more than 50%, compared to the coolant inventory of 280,000 kg at the beginning of the scenario.

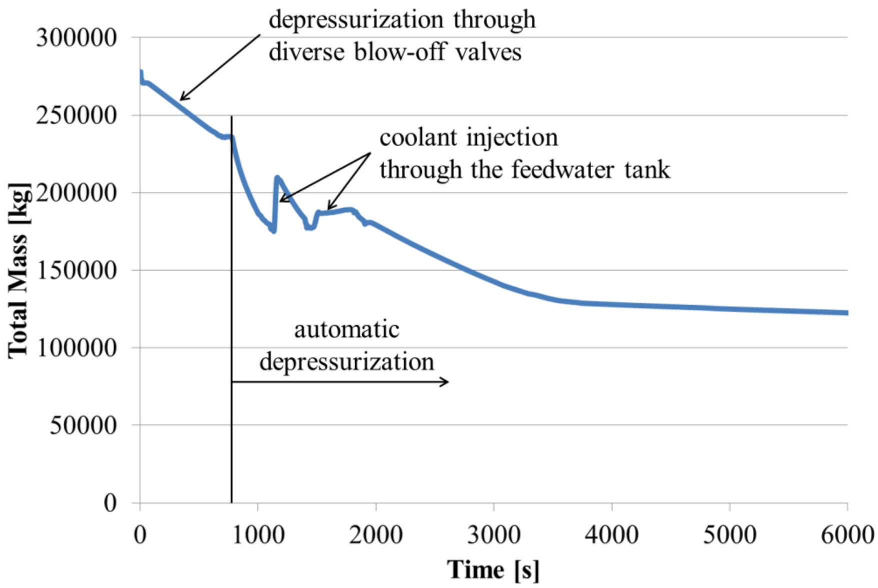

Figure 6-4: Plot of the Water Inventory against Time – Reference Case

The temperature profile of the water / vapor in a central channel in the upper region of the core is shown in Figure 6-5. During the beginning of the scenario, the temperature corresponds to the saturation temperature under the given system pressure. It stays constant until the automatic depressurization causes a significant pressure drop, which also results in the reduction of the saturation temperature. However, after 2,900 seconds, the temperature starts to increase. This indicates that the core starts to uncover and the decay heat cannot be removed sufficiently. Since the thermo-hydraulic code ATHLET does not consider core degradation, the development, after temperatures reached values higher than 1200 °C, is not realistic, due to missing models. Nevertheless, the calculation demonstrates that first core degradation processes start, under the given extreme conditions, about 1 1/4 hours after the station blackout occurred.

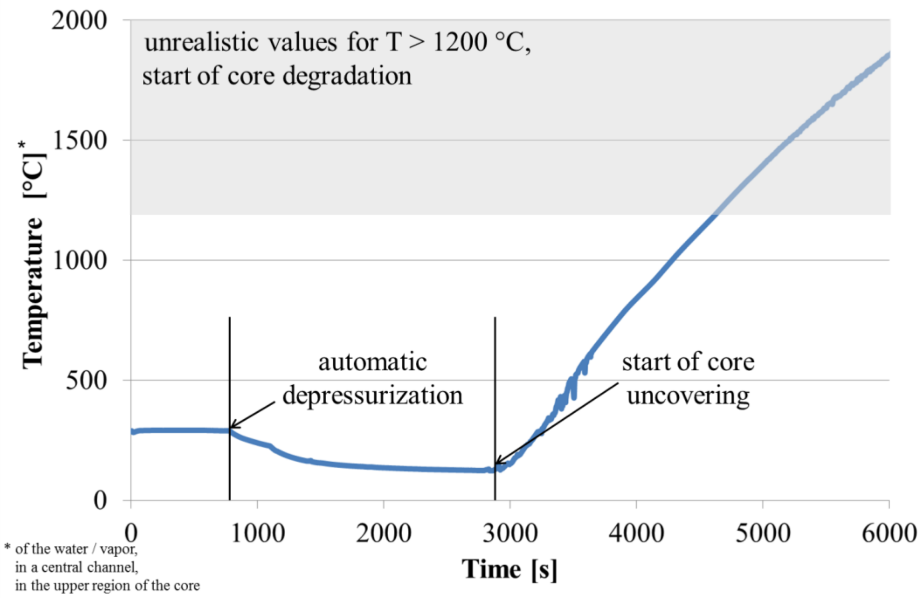

Figure 6-5: Plot of Water / Vapor Temperature in a Representative Channel in the Core against Time – Reference Case

If external sources of coolant injection are available, the heat removal can be prolonged. However, without the recovering of an actual heat sink, it is impossible to control the scenario over a longer period of time. Figure 6-6 shows the temperature of the water inventory within the wetwell that is initially around 25 °C. It increases steadily due to the primary steam that is released through the diverse blow-off valves or the safety and relief valves, and that is condensed in the water inventory of the wetwell. The temperature reaches 75 °C after 3,500 seconds so that some more steam could be condensed. However, most of the capacity of the water inventory has already been utilized. It will therefore be necessary to actually remove decay heat from the containment within time and to establish an ultimate heat sink.

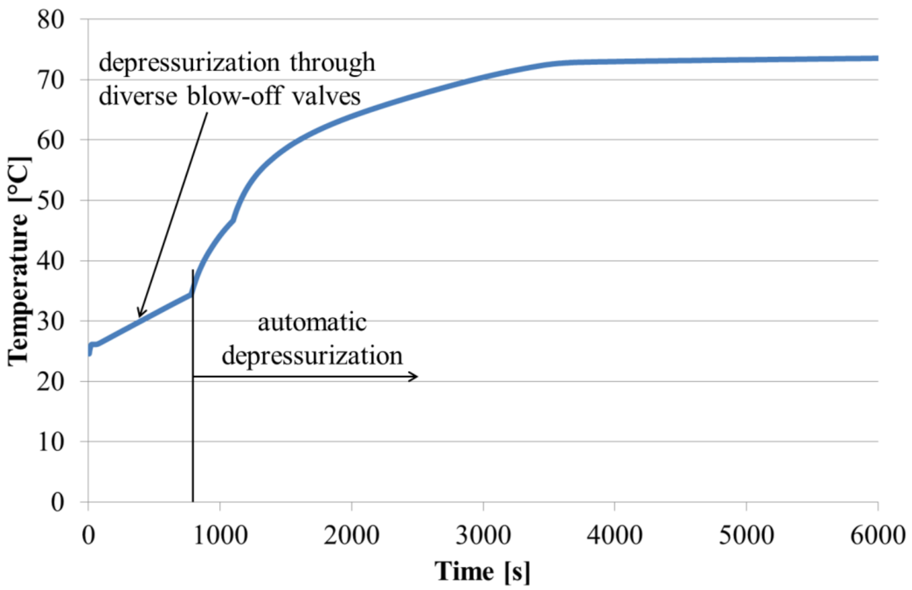

Figure 6-6: Plot of the Wetwell Temperature against Time – Reference Case

6.3 Retrofitted BWR

The input deck of the generic boiling water reactor has been extended by the self-propelling heat removal system, as described in chapter 5. The nodalization scheme in Figure 6-7 shows the connection of the printed circuit heat exchanger and the corresponding piping to the main steam line and the feedwater line. The horizontal position of the TFOs is original, whereas the vertical position of the feedwater line is shifted for a better visualization. The printed circuit heat exchanger is actually subdivided into four equal parts, one for each cooling train. Exemplarily, two separated heat exchangers are displayed in the outline. In order to maximize the driving force of the natural circulation within the primary circuit, the heat exchanger is placed as high above the RPV as possible, according to design restrictions of the plant.
The temperature of the ambient air is assumed to be 37 °C for all simulations. Additionally, all TFOs except the heat exchangers are considered as adiabatic, such that heat losses through structures and components are neglected in the simulation.

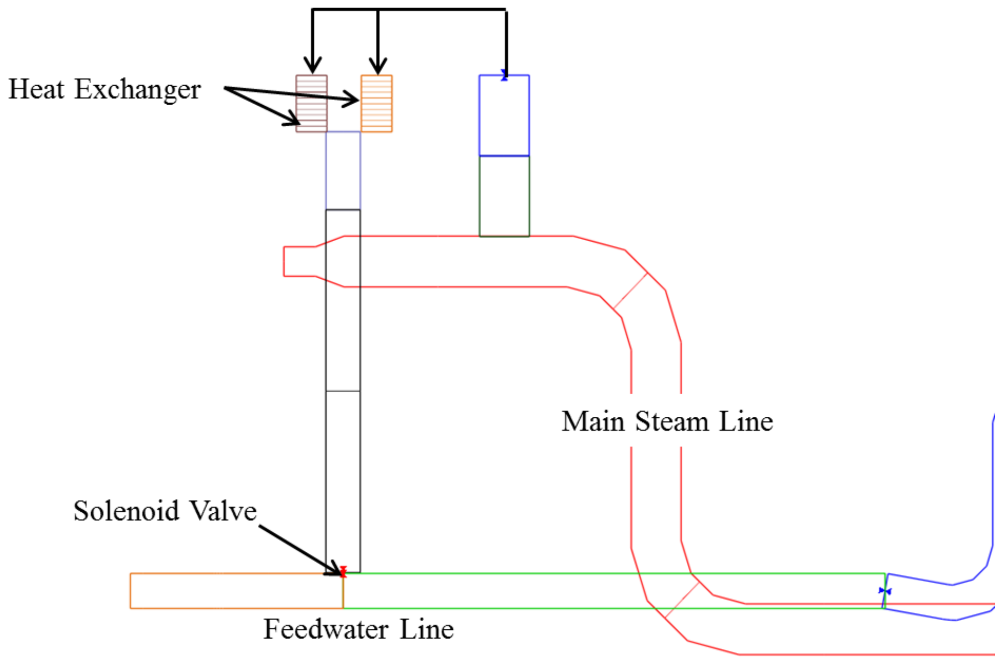

Figure 6-7: Nodalization Scheme of the Turbo Compressor System – Primary Side

The normal power operation is not influenced by the Turbo Compressor System. The impact of the system on the overall behavior of the plant is analyzed and compared to the reference case.

In both situations, the turbine trip triggers the safety and relief valves, followed by the reactor scram and the initiation of the partly depressurization through the diverse blow-off valves. In addition the magnetic valves open automatically, due to the power failure, and a natural convection between the main steam line and the feedwater line evolves. Thereby, the sCO_2 is heated. The rotating of the turbomachinery is initiated over the battery, whereby the self-propelling heat removal system is started. 50 seconds are considered in the simulations, before the heat removal system achieves its full capacity. This is comparable to the startup time of other turbine driven systems, such as the reactor core isolation cooling system, which is described in chapter 6.6.

The development of the RPV pressure against elapsed time is shown in Figure 6-8. Primary steam is simultaneously condensed through the heat removal system and blown into the pressure suppression pool through the diverse blow-off valves. In contrast to the reference case, these measures achieve a reduction of the primary circuit pressure at the beginning of the scenario. Two of the three diverse blow-off valves close, after their set-points have been reached, at around 250 and 450 seconds. With one diverse blow-off valve staying open, steam is constantly removed from the primary circuit. Before the closing set-point of the last blow-off valve is reached, the water level within the RPV has decreased so far that firstly the slow, and secondly the fast automatic depressurization is activated. The safety and relief valves are opened and the RPV pressure decreases rapidly, after 1500 seconds.

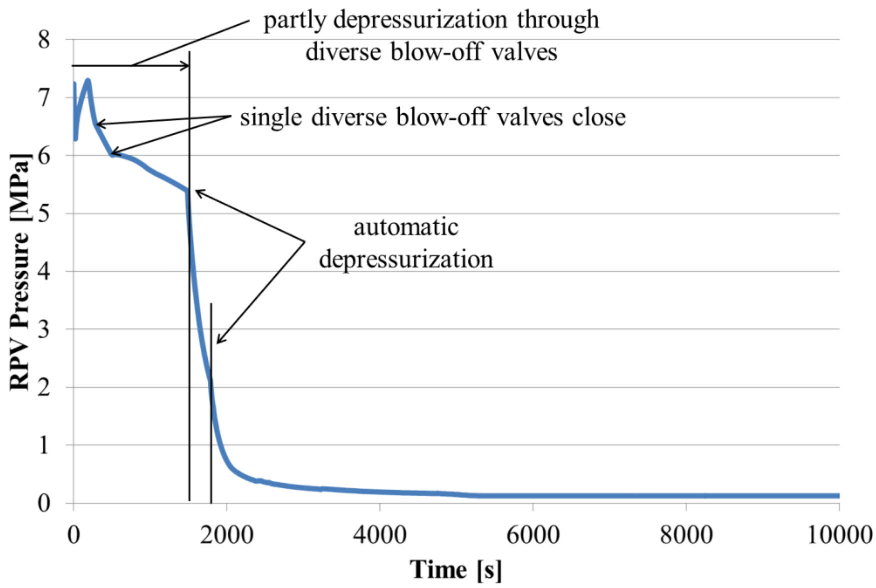

Figure 6-8: Plot of the RPV Pressure against Time – Retrofitted BWR

The amount of primary steam released into the pressure suppression pool is reduced for the retrofitted boiling water reactor, compared to the reference case. This is shown in Figure 6-9. For one thing, this is caused by the closure of two of the three diversified blow-off valves. Secondly, the reduced primary circuit pressure also decreases the amount of steam blown off, because it depends on the pressure difference between the pressure suppression pool and primary circuit. Nevertheless, the constant loss of primary steam results in a decreasing water level within the RPV, which finally triggers the automatic depressurization. As seen in the reference case, the low system pressure allows for a passive coolant injection through the feedwater tank.

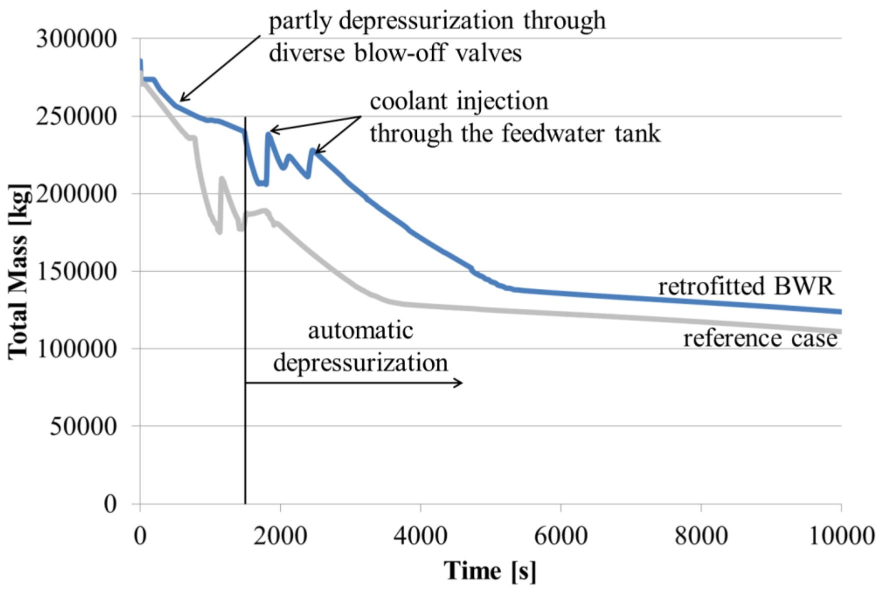

Figure 6-9: Plot of the Water Inventory against Time –
Comparison of a Retrofitted BWR and the Reference Case

The amount of heat that is removed by the self-propelling cooling system is displayed in Figure 6-10. The maximum capacity of 60 MW is only reached at the very beginning of the scenario. As the primary circuit pressure and accordingly the saturation temperature decreases, the carbon dioxide within the Brayton cycle cannot be heated as anticipated. Since the self-propelling system is driven by the temperature difference between the heat sink and the heat source, the amount of removed heat decreases slowly. The full heat removal potential can only be exploited under high pressure conditions.

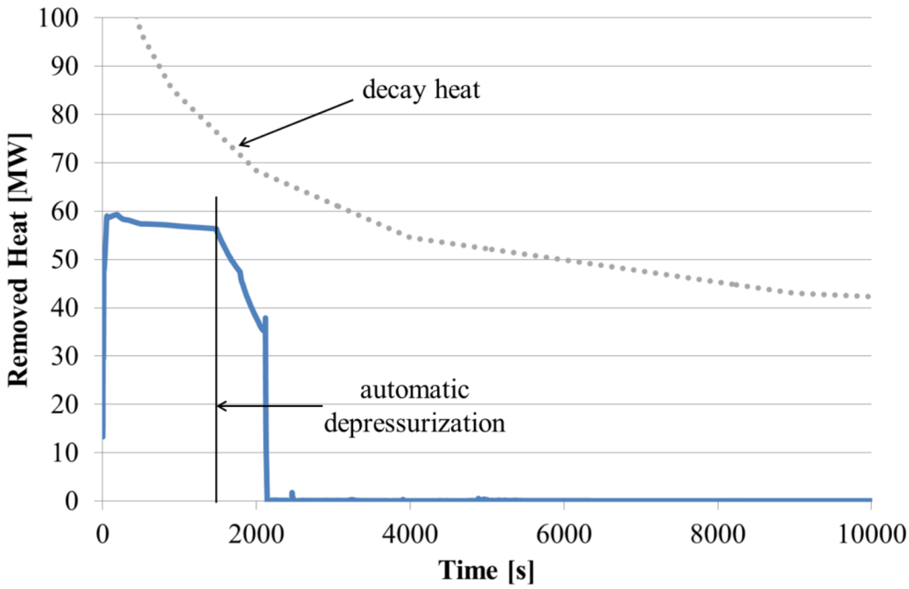

Figure 6-10: Plot of the Removed and Produced Heat against Time – Retrofitted BWR

In addition, the primary circuit pressure is rapidly reduced after 1,500 seconds, due to the automatic depressurization, which further reduces the ability of the system to remove heat. Subsequently, the heat removal stops completely, which will be discussed in the next chapter in more detail.

This highlights the dependence of the amount of removed heat on the RPV pressure. It shows that depressurizing the primary circuit is counterproductive for the heat removal system and that the self-propelling system works most effectively under high pressure conditions.

The graphs shows also that it takes more than 3,000 seconds for the decay heat to fall below the maximum capacity of 60 MW. Until this point, the decay heat clearly exceeds the amount of removed heat.

Figure 6-11 shows the water / vapor temperature in a central channel in the upper region of the core against the time elapsed since the initiating event occurred. The temperature profile of the retrofitted BWR looks comparable to the reference case, only shifted by approximately 1,800 seconds. Therefore, the retrofitted, self-propelling heat removal system is able to extend the grace period by around 30 minutes.

The core starts to uncover 4,750 seconds after the station blackout. At this time, the decay heat has already decreased up to the point where the heat removal system would be able to remove it completely, but only under high pressure conditions.

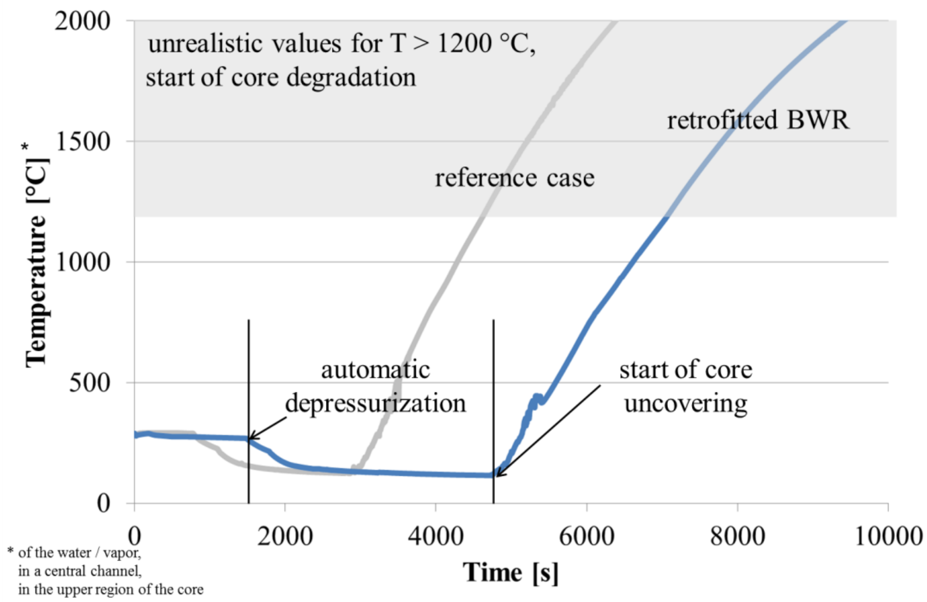

Figure 6-11: Plot of Water / Vapor Temperature in a Representative Channel in the Core against Time – Comparison of a Retrofitted BWR and the Reference Case

The diverse blow-off valves are intended to partly depressurize the primary circuit. To do so, steam is continuously blown into the pressure suppression pool. Anticipating that no means of coolant injection are available, this reduces the coolant inventory and decreases the water level within the RPV. Before the partly depressurization is completed and the closure set point of the third diverse blow-off valve is reached, the water level already fell below the threshold value that triggers the automatic depressurization. Once the automatic depressurization is triggered, the safety and relief valves are opened and fixed in this position by holding magnets. The coolant inventory in the primary circuit decreases further and even more rapidly. The heat removal system stops to operate.

It is common sense to depressurize the primary circuit of a boiling water reactor following a station blackout or loss of ultimate heat sink, in order to facilitate the coolant injection either by an implemented system or external measures like a fire pump. However, to extend the grace period with the addition of a self-propelling cooling system significantly, it might be necessary to rethink, if the depressurization of the primary circuit should be requested. The control strategy of the blow-off valves should respect the operating range of Turbo Compressor System. Otherwise the depressurization can jeopardize core coverage, despite the implemented heat removal system. Through the removal of residual heat, depressurization may be deferred and shall be favorably considered, when the plant conditions are stable again, power supply is restored and / or external support is accessible.

6.4 Retrofitted BWR with Adapted Depressurization System

In order to operate the self-propelling cooling system close to its design point and to acquire its maximum heat removal capacity, the diverse blow-off valves have been deactivated in the subsequent cases, to avoid the partial depressurization, which is classified as an operational action. This is in accordance with the BWR Owners Group, who recently recommended adapting the RPV depressurization, as a station blackout enhancement: "*Core cooling is highest priority. If RPV depressurization will result in loss of systems needed for core cooling: Terminate depressurization*" [69]. However, the control strategy of the safety and relief valves has been hold, in order to avoid changes in safety-related systems and to keep the RPV pressure within acceptable limits. This way, more coolant can be retained within the isolated primary circuit, which is important, because no means for coolant injection are supposed to be operable.

In the beginning of the scenario, the Turbo Compressor System works at its maximum capacity and removes around 60 MW from the primary circuit. However, the decay heat that is still produced in the beginning is around 200 MW, which causes the RPV pressure to increase. Once a certain threshold value is exceeded, the reactor protection system opens one safety and relief valve, to limit the system pressure. Primary steam is blown into the pressure suppression pool and the RPV decreases again. As shown in Figure 6-12, this behavior is repeated for some time, until, after around 2,500 seconds, the heat removal is sufficient to stop the raise of the RPV pressure. In fact, the pressure starts to decrease continuously, as more heat is removed by the Turbo Compressor System than is produced. This depressurizes the primary circuit slowly, even though all blow-off valves are closed. Suddenly, after 42,000 seconds, the heat removal stops. Subsequently to the halt of the self-propelling system, the primary circuit pressure increases again, up to the point where the safety and relief valve has previously been triggered to limit the RPV pressure. Coolant is repeatedly removed from the primary circuit and blown into the pressure suppression pool. The low water level signal activates the automatic depressurization after 58,000 seconds.

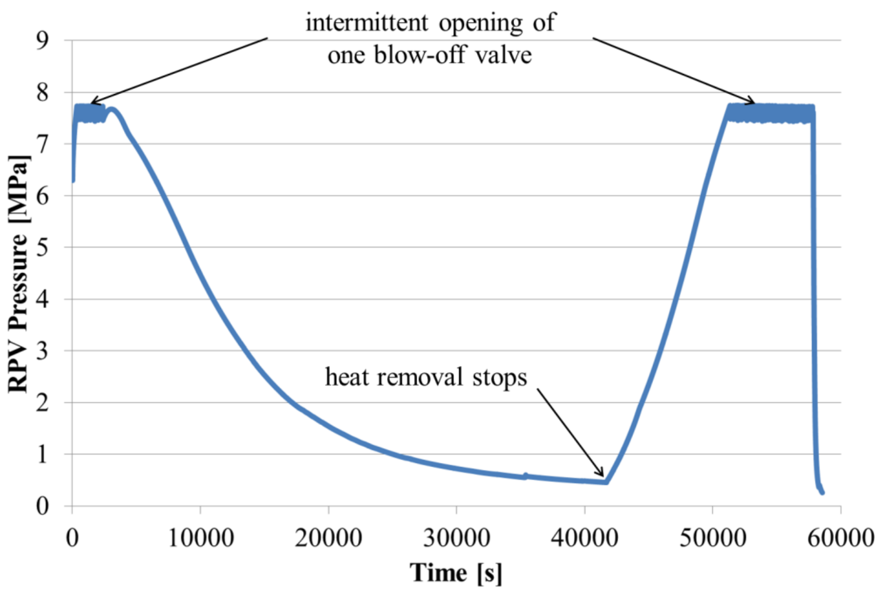

Figure 6-12: Plot of the RPV Pressure against Time – Retrofitted BWR with Adapted Depressurization System

Figure 6-13 shows the amount of heat that is removed with the self-propelling heat removal system, as well as the decay heat. At the beginning of the scenario, the decay heat exceeds the amount of removed heat, which causes the primary circuit pressure to increase. However, after around 3,000 seconds the decay heat becomes smaller than the amount of removed heat, which is the reason for the decreasing RPV pressure. The graph confirms that the heat removal stops after 42,000 seconds, which indicates that the Turbo Compressor System comes to a halt. Again, one can see that the amount of removed heat decreases, as the primary circuit pressure reduces.

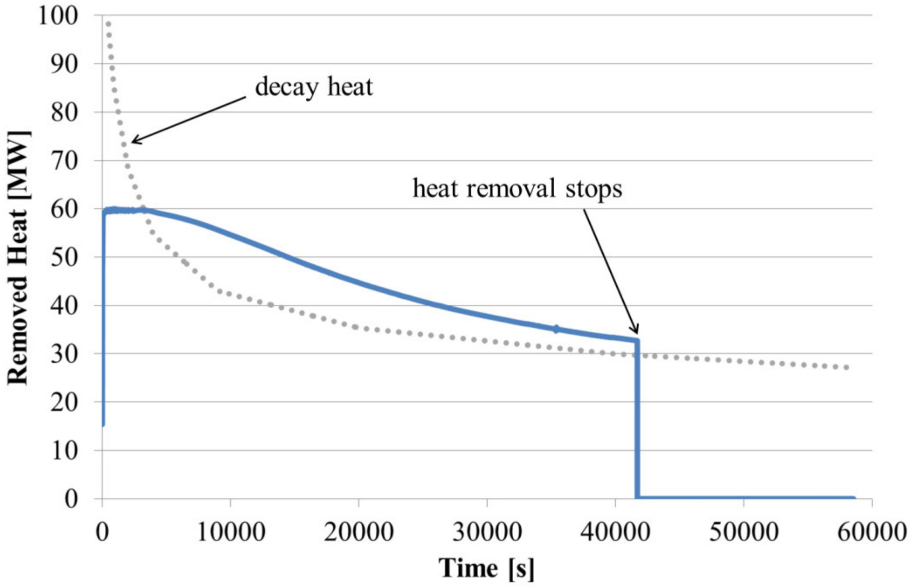

Figure 6-13: Plot of the Removed and Produced Heat against Time – Retrofitted BWR with Adapted Depressurization System

The decreasing RPV pressure goes along with a declining steam temperature, as shown in Figure 6-14. This influences directly the sCO_2 temperature after the compact heat exchanger, which determines the performance of the turbine. Additionally, the smaller temperature gradient between the vapor and the sCO_2 decreases the efficiency of the heat transfer, which further lessens the sCO_2 temperature.

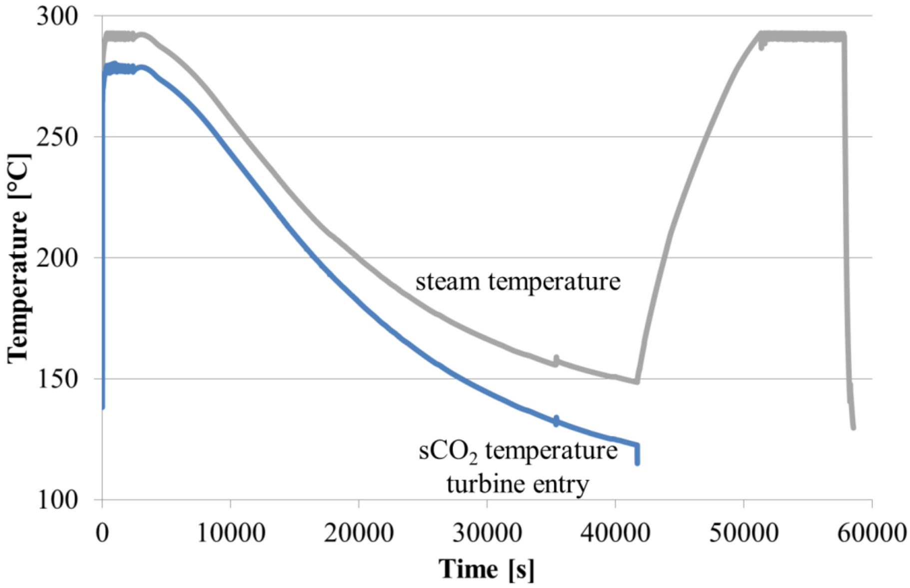

Figure 6-14: Plot of Maximum Steam and sCO_2 Temperature against Time – Retrofitted BWR with Adapted Depressurization System

The performance of the turbine is strongly affected by the temperature drop. This is also reflected in the pressure difference that is realized over the turbine, as shown in Figure 6-15. The entrance pressure stays constantly at 18 MPa and the turbine exit pressure increases from 8.9 MPa to 9.7 MPa. This reduces the amount of energy that the turbines can extract from the supercritical carbon dioxide.

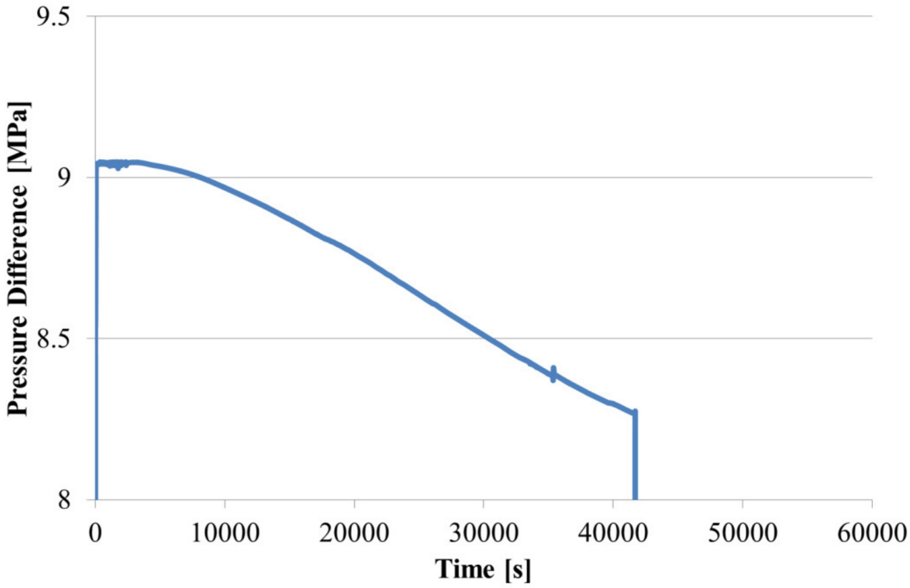

Figure 6-15: Plot of the Pressure Difference over the Turbine against Time– Retrofitted BWR with Adapted Depressurization System

Figure 6-16 shows the energy extracted from the fluid and additionally the power that is needed to run the compressors. The remaining energy is utilized to generate excess electricity via a high speed generator. This electricity is essential to power the air fans, which need 0.7 MW_{el} to operate.

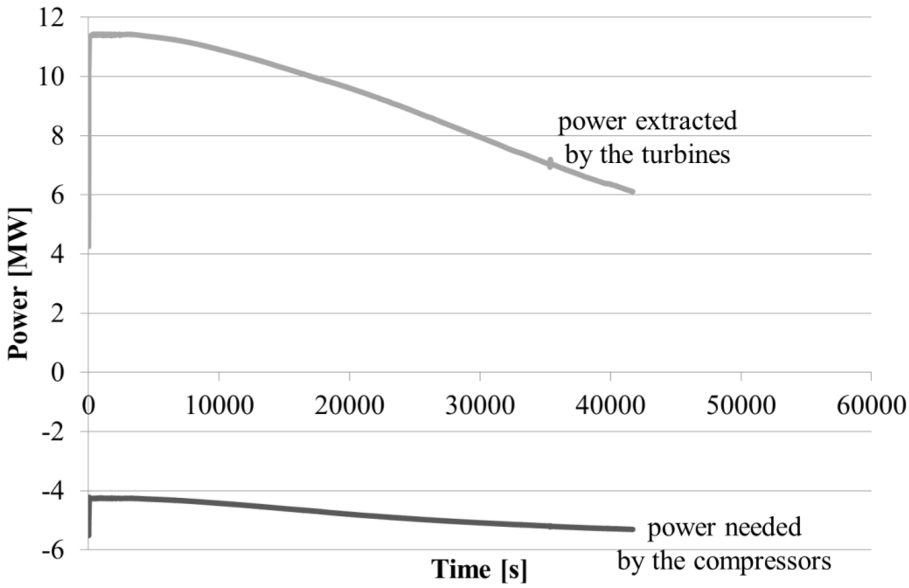

Figure 6-16: Plot of the Power Extracted by the Turbines and Needed by the Compressors against Time – Retrofitted BWR with Adapted Depressurization System

In the early stage of the scenario, the power gained by the turbines (11.5 MW) significantly exceeds the power needed for the compressors (4 MW) and the air fans (0.7 MW). Therefore, the system is truly self-propelling. However, the energy that is extracted by the turbines constantly decreases, as the entry temperature of the turbines reduces. Additionally, the energy consumption of the compressors raises over time, as the sCO_2 mass flow increases and its efficiency decreases. This effect will be discussed later in this chapter.
Eventually, after around 42,000 seconds, more power is needed by the compressors and the air-fans than can be provided by the turbines. Once the motors of the air-fans are not sufficiently supplied with electricity, the temperature of the supercritical carbon dioxide will remain higher as anticipated. Consequently, the compressors will need even more power in this working condition to raise the pressure, which will finally cause the system to halt. The cooling cycles are no longer self-sufficient.

This observation can also be confirmed by Figure 6-17, which shows the excess electricity, i.e. the electricity produced with the generator, minus the electricity needed for the air fans. During the beginning of the scenario, around 5.5 MW_{el} can be provided by the Turbo Compressor System to ensure for example lighting and ventilation, even during a station blackout. After consultation with plant operators, the electricity would be sufficient to power small high pressure pumps. For instance, the pumps that provide sealing water or alternatively, the pumps that supply the rinsing water for the control rods, could be utilized. These pumps can be valuable options for high-pressure coolant injection during a station blackout scenario and are already part of many severe accident guidelines in BWRs.

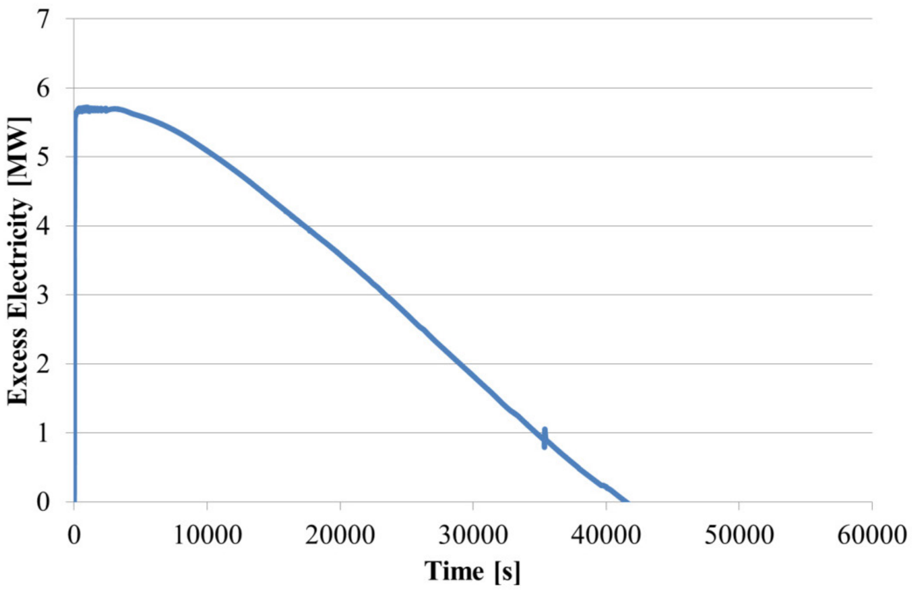

Figure 6-17: Plot of Excess Electricity against Time – Retrofitted BWR with Adapted Depressurization System

However, one can also see that the overall power balance of the system continuously decreases. This is due to the fact that the operating conditions of the turbomachinery move away from their design point. After 42,000 seconds the excess electricity is diminished, up to the point that the air-fans can no longer be supplied with electricity and the system is not self-sufficient anymore.

Currently, the control of the self-propelling cooling system is rudimentary. A consistent pressure is appointed on the high pressure side of the Brayton cycle leading to a constant compressor exit pressure. In addition, the number of revolutions is unchanged during the entire simulation, accompanied by a constant volume flow rate.
The temperature of the ambient air is fixed for the entire simulation, which results in a constant sCO_2 temperature at the compressor inlet. With the increasing pressure on the low pressure side, the sCO_2 density at the compressor inlet increases over time. At a constant number of revolutions and a constant volumetric flow this leads to an increased mass flow. Consequently, the amount of heat that can be removed from the primary circuit under the given temperature constraints, is increased. According to this, the RPV pressure decreases even faster, this accelerates the process.
Therefore, the self-propelling heat removal system is not self-adapting. Moreover, this behavior is even counterproductive and leads to an earlier system failure. In order to achieve long-term heat removal, the system has to be equipped with active control measures. The increasing power demand of the compressors that is displayed in Figure 6-16 is also due to the increasing sCO_2 mass flow.

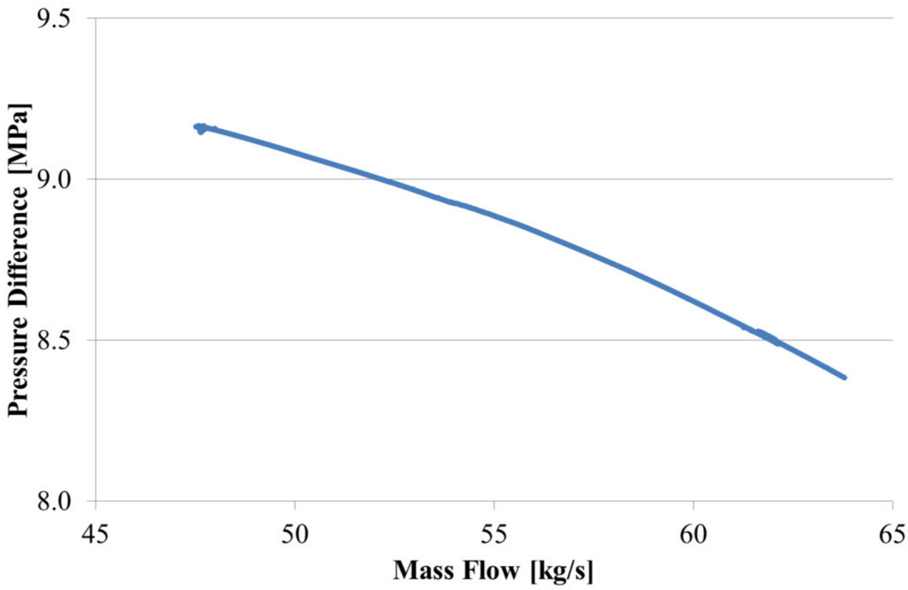

Figure 6-18: Plot of the Pressure Difference over the Turbine against sCO_2 Mass Flow – Retrofitted BWR with Adapted Depressurization System

The grace period of a retrofitted BWR with the adapted depressurization system is in the range of 15 hours. It has been extended considerably, compared to the previous case, the retrofitted BWR. However, the analysis has shown that the system does not automatically adapt to the amount of decay heat and has to be controlled in order to fully exploit its potential. Currently, a restart of the system is not considered.

6.5 Retrofitted and Adapted BWR with Control Strategy

A simplified control strategy for the retrofitted heat removal system has been developed, in order to reduce the difference between the produced and removed heat [62]; [64]. The operating time of the Turbo Compressor System is thereby maximized and the entire potential of the system can be evaluated.
As in the previous cases, all four Brayton cycle start to remove decay heat immediately after the initiating event. However, two cooling trains are successively switched off and only two of the four cooling circuits continue to operate during the entire simulation time, which has been limited to 260,000 seconds.

Figure 6-19 shows the development of the primary circuit pressure over time. At the very beginning of the scenario, the self-propelling heat removal system operates at its maximum capacity, with all four cooling trains running. Still, the decay heat exceeds the amount of removed heat and one safety and relief valve is intermittently triggered to limit the RPV pressure. This is the same pattern as seen in the previous case, the retrofitted BWR with an adapted depressurization system. The primary circuit pressure starts to decrease after 3,000 seconds and follows an increasing / decreasing behavior, subsequently to the shut-down of the single cooling circuits. The points in time, when the single trains are shut-down are selected as early as possible, in order to maximize the primary circuit pressure, but as late as necessary, in order to avoid a further opening of the safety and relief valves, to keep most of the coolant inventory within the primary circuit. In the presented case, the first cooling train is deactivated with a time-dependent signal after 4,500 seconds and the second cooling train after 16,000 seconds.
These points in time depend strongly on the particular situation of the plant and are determined from the specific amount of decay heat. For an actual implementation of the system in a BWR, passive mechanisms have to be evaluated in the future, to determine the optimal point in time to switch the Brayton cycles off. However, the development of such as system is outside the scope of this work.

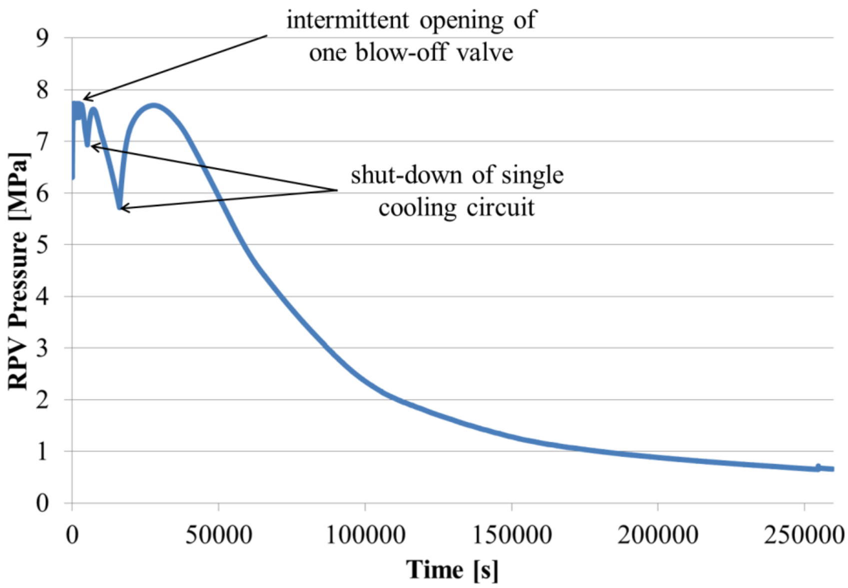

Figure 6-19: Plot of the RPV Pressure against Time – Retrofitted and Adapted BWR with Control Strategy

The increasing / decreasing RPV pressure is caused by the difference between produced and removed heat, which is both shown in Figure 6-20. The primary circuit pressure increases, as long as the decay heat exceeds the amount of removed heat and vice versa. The shut-down of the first single cooling circuit, at 4,500 seconds in this case, results in a rapid reduction of removed heat. However, as the decay heat reduces over time, less heat must be removed to equalize it. After the shut-down of the second cooling train at 16,000 seconds, the amount of removed heat still decreases over time, from 30 MW_{th} after 20,000 seconds to 20 MW_{th} after 200,000 seconds. This reduction is solely caused by the pressure dependency, i.e. the decreasing temperature difference between the heat sink and heat source. One can see that this effect causes the amount of removed heat to approach the amount of decay heat in the long term. Therefore, the shutdown of single cooling circuits results in almost self-adapting behavior, since the amount of heat removed by Turbo Compressor System equals the amount of heat that is produced. This is desirable, as it enables the system to work continuously for at least three days.

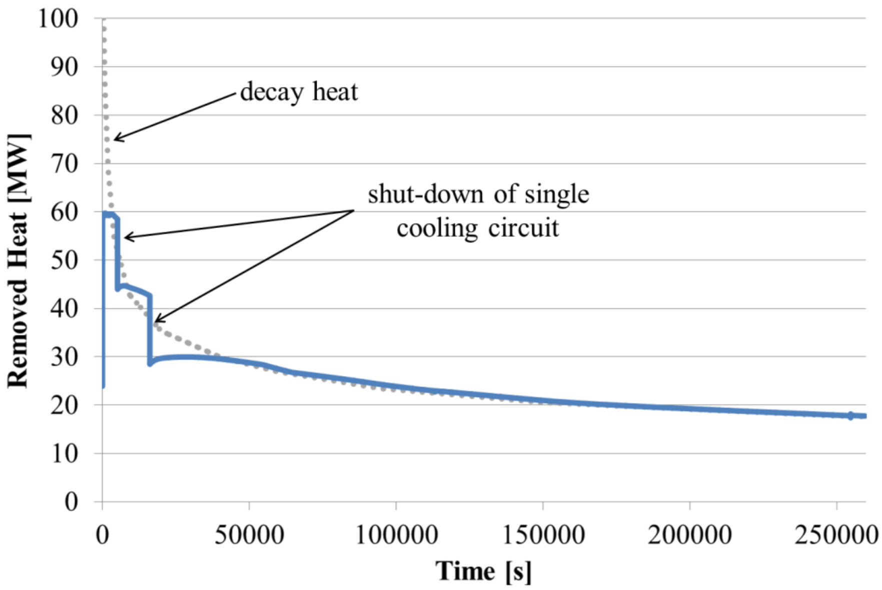

Figure 6-20: Plot of the Removed and Produced Heat against Time – Retrofitted and Adapted BWR with Control Strategy

The excess electricity that is produced with the generator of the operating Brayton cycles, deducted by the power needed for the air-fans, is shown in Figure 6-21. The shut-down of the single cooling circuits results in a rapid reduction of excess electricity, on the other hand, this measure secures its availability in the long run. It enables the system to operate over a longer period of time, compared with the previously discussed cases and to serve as an independent AC power source.

The availability of electricity can be advantageous as it provides a plant with more flexibility to cope with long-term station blackouts. It could, for instance, power existing, small high pressure pumps, which might be required for other accident scenarios or different reactor designs.

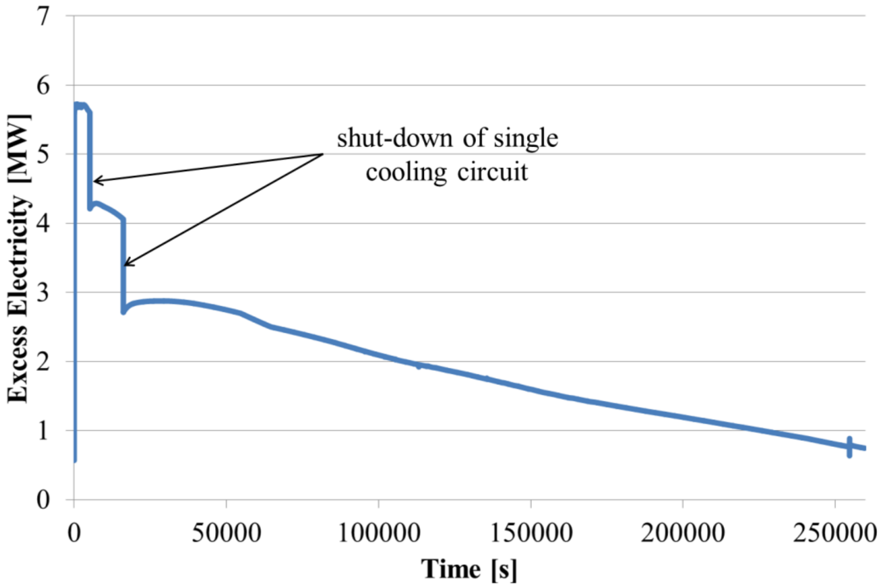

Figure 6-21: Plot of Excess Electricity against Time – Retrofitted and Adapted BWR with Control Strategy

In this scenario, the safety and relief valves open after the turbine trip and limit the RPV pressure through intermittent opening during the beginning of the scenario. Another function that is not activated is the automatic depressurization, which can be triggered by the low water level signal. The threshold value is reached, when the water level above the core falls below 1.5 m. Figure 6-22 shows the changes of the water level over time. Measured is thereby the mixture level of water and vapor, which serves also as the reference for the reactor protection system. At the beginning of the scenario the water level drops significantly. This is due to the decreasing void fraction after the reactor scram and the actual reduction of the coolant inventory, caused by the removal of primary steam during the first 2,500 seconds after the turbine trip. At this point in time, the total cooling mass within the isolated primary circuit reaches its minimum and stays constant afterwards, until coolant is passively injected from the feedwater tank. Nevertheless, the water level continues to vary, where the increasing / decreasing behavior of the water level after the shut-down of the single cooling circuits mirrors the manner of the RPV pressure. The rising and falling of the water level occurs due to the changing system pressure and the varying saturation temperature, as this determines the water and vapor densities. The water density increases for falling system pressures, which causes the water level to get lower, even though the coolant inventory stays constant. The water level comes alarmingly close to the threshold value for the low water level signal. This is even more concerning because it is quite unknown if the point in time and the amount of coolant injected from the feedwater tank is accurate. In case the threshold value is reached and the automatic depressurization is triggered, this would lead to a rapid reduction of the coolant inventory and would bring the self-propelling cooling system to a halt, as discussed in chapter 6.4. As long as power cannot be recovered and the RPV cannot be reflooded, this would jeopardize core cooling and shall be avoided under all circumstances. Therefore, the threshold values of the depressurization system should be adapted for station blackout scenarios, in order to maximize the benefit of such a retrofitted system. However, it goes without saying that for certain situations a depressurization of the primary circuit is inevitable for safety reasons.

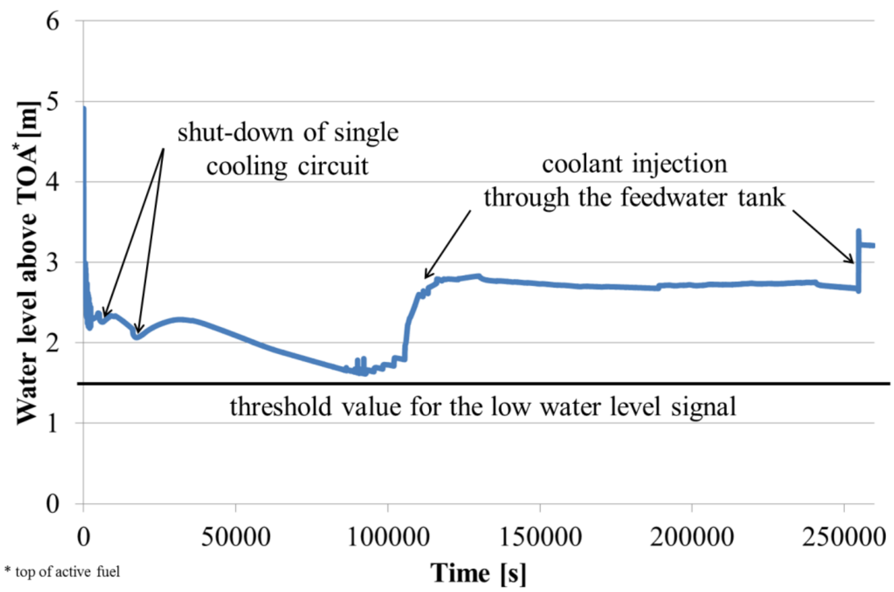

Figure 6-22: Plot of the Water Level above the Core against Time – Retrofitted and Adapted BWR with Control Strategy

The current evaluation shows that the Turbo Compressor System has the potential to extend the grace period during a combined SBO & LUHS scenario significantly. A retrofitted BWR becomes capable to counter such a design basis exceeding event independently for at least 72 hours. However, the adaptation of the operational, partial depressurization is a prerequisite for a successful long-term operation of the system. Furthermore, a manual intervention is necessary twice, in order to shut-down two single cooling trains. This reduces the amount of removed heat and holds the operating conditions closer to its design point.

The timing for the shut-down of the single Brayton cycles is crucial, but depends strongly on the particular situation at the plant, for example how long the reactor has been operating since its startup. For the conducted analysis, a maximum amount of decay heat was considered, with the core being at the end of its cycle. For a new core that has just started operation, the decay heat would be smaller, which in turn would require an earlier shut-down of the cooling circuits. Passive mechanisms shall be evaluated in the future, to determine the optimal point in time to switch the Brayton cycles off. This would further increase the reliability of the system.

6.6 Turbo Compressor System Combined with a Reactor Core Isolation Cooling System

Some BWRs are standardly equipped with a so-called reactor core isolation cooling system (RCIC). Such a system consists of steam-driven turbo pump that injects water from the wetwell into the reactor pressure vessel, powered by primary steam. It is completely independent from external AC power sources and does not need any water from outside the containment. It is therefore predestinated to operate under station blackout conditions and in cases where the containment is isolated and the ultimate heat sink is lost. In fact, the RCIC was one of the very few safety systems that were available in the Fukushima accidents [58]. However, the system is only meant to provide an interim period to recover active safety

systems, which can ensure long-term core cooling. The operating time of the RCIC is limited, because it can only transfer heat from the primary circuit into the pressure suppression pool, but is unable to remove heat out of the containment. Therefore, the water temperature in the wetwell increases, up to the point where the turbo-pump and hence the RCIC system fails [30].
It is evaluated in the following how the two steam-driven systems, the RCIC and the self-propelling heat removal system interact with each other. The performance of the systems and possible interferences [63], due to the sharing of working steam, are investigated.

6.6.1 Description and Modeling of the Reactor Core Isolation Cooling System

The Reactor Core Isolation Cooling system (RCIC), as seen in Figure 6-23, is intended to slowly depressurize the primary circuit and to provide coolant. It can be activated by a station blackout or a low water level signal. The turbine is powered by high-pressure primary steam and directly drives the pump. The exhaust steam of the turbine is forwarded into the pressure suppression pool, where it completely condenses. Additionally, water is taken from the wetwell and can be provided to the reactor pressure vessel, via the feedwater line. The loss of primary steam, through the safety and relief valves or due to the loss of the driving steam of the RCIC, can therefore be compensated.

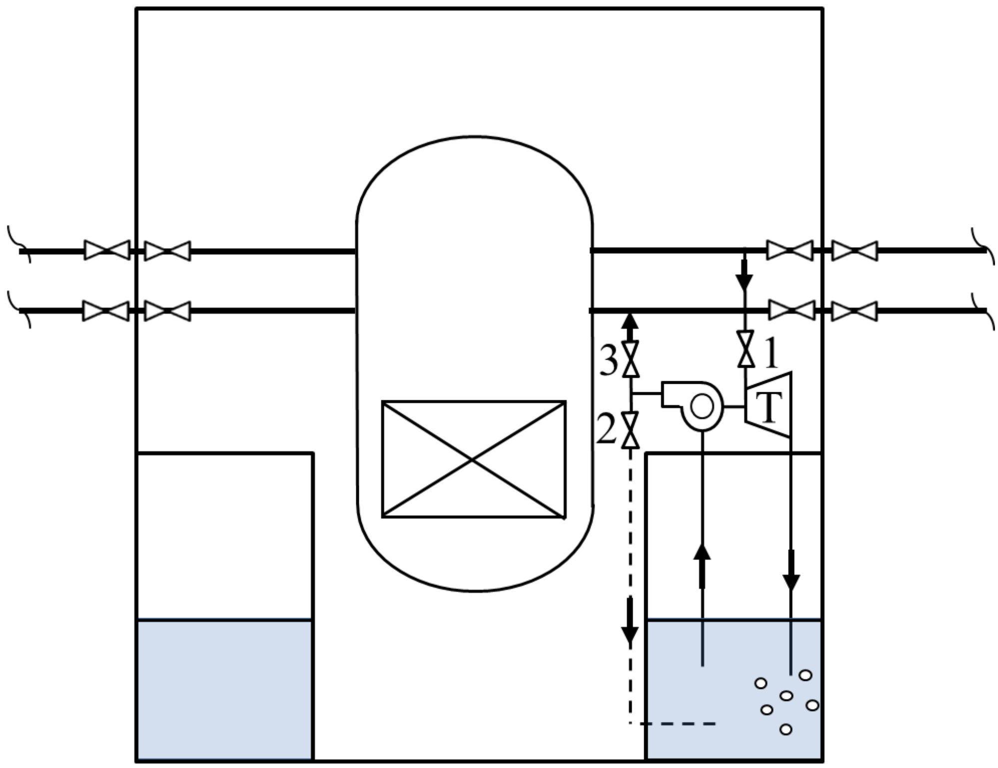

Figure 6-23: Schematic Sketch of the Reactor Core Isolation Cooling System

Table 6-1: Control Parameter of the Implemented Reactor Core Isolation Cooling System

Parameter	Value	Unit	start signal	stop signal	comment
water level	2.3	m	x		starts the system (in case of off-state) water injection is started, below activating signal for active injection systems, sufficiently before activation of the automatic depressurization
water level	4.41	m		x	water injection is stopped, same threshold value as for other injection systems
wetwell temperature	75	°C		x	system is shut-down, pump begins to cavitate
Primary circuit pressure	1	MPa		x	minimum pressure to achieve sufficient turbine performance
battery				x	provides the control energy for the turbine, lasts for three hours
reactor scram			x		starts the system, water injection is started (+50 seconds)

Once the system is started, valve 1 opens and the turbine runs continuously throughout the entire operating time of the RCIC. An almost constant amount of steam is thereby removed from the primary circuit. In case the water level within the RPV falls below a certain threshold value, valve 2 closes and valve 3 opens, to enable the pump to supply water to the primary circuit. To avoid overfeeding, valve 2 reopens and valve 3 closes, if the low water level signal is reset. The pump continues running and recirculates a minimum quantity of water into the wetwell. Since the turbine steadily transfers steam to the wetwell, the wetwell temperature increases over time. The system will be stopped, in order to avoid cavitation of the pump, if the wetwell temperature reaches 75 °C. Below this temperature, the system continues operating, as long as the primary circuit pressure exceeds 1 MPa and the corresponding battery is able to provide control energy for the turbine. The control parameters are summarized in Table 6-1.

ATHLET assumes that all turbines are placed on a common shaft, more precisely the same number of revolutions is considered for all turbines within one data set. However, the revolving speed of the steam-driven turbine is significantly slower than of the radial sCO_2 turbines. Therefore, it is currently not possible to simulate the turbines of the self-propelling heat removal system and the RCIC simultaneously. Since the mass flows of steam and water are almost constant during the RCIC operation, they are simulated by a fill model that accounts for the mass and related energy sources and sinks, as shown in Figure 6-24. The containment model CONDRU models the wetwell, based on the mass flow and the enthalpy and accounts for the steam and the water in- and out-flow.

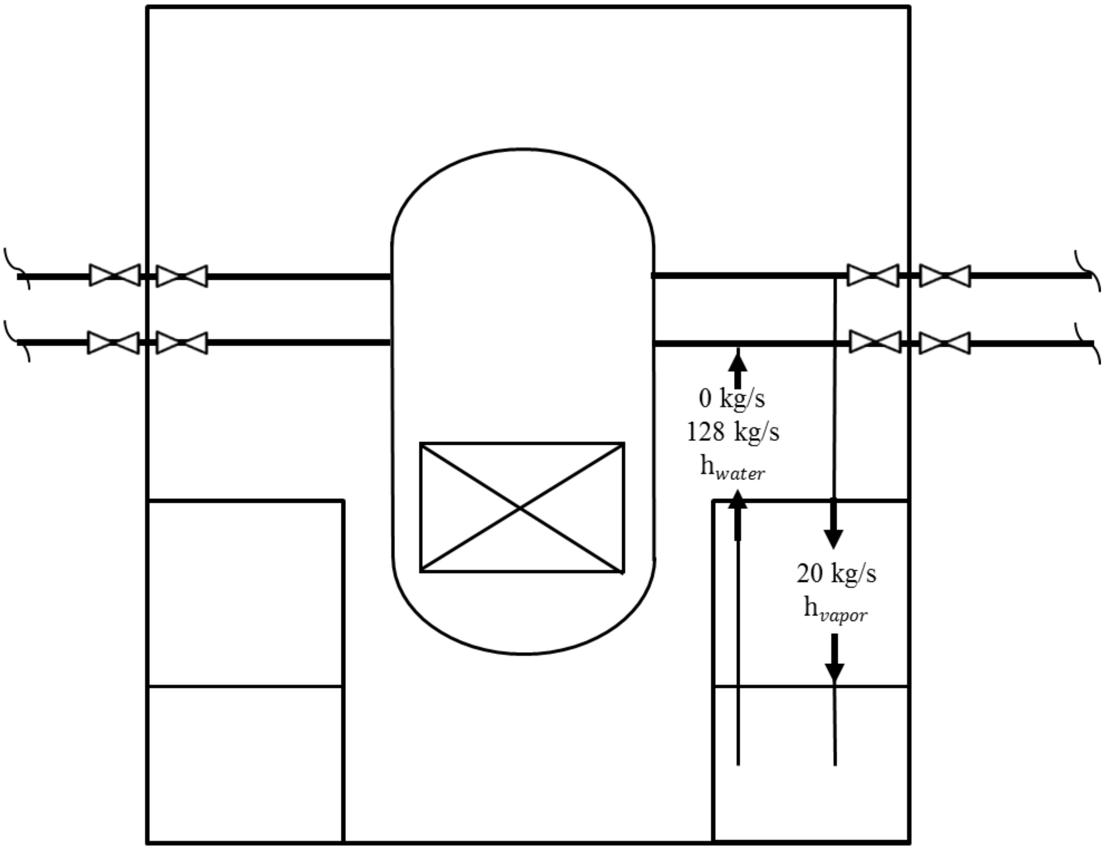

Figure 6-24: Modeling of the Reactor Core Isolation Cooling System

The heat removal capacity of the self-propelling cooling system has been reduced by 50 %, in comparison with the previously discussed cases in chapter 6.2-6.5. Hence, only two cooling trains are assumed to be retrofitted in the current simulation, with a maximum heat removal of up to 30 MW_{th}.

6.6.2 Thermohydraulic Analysis

The initiating event is, as in all other simulations, the station blackout, which activates the Turbo Compressor System, as well as the reactor core isolation cooling system. The turbine trip triggers the safety and relief valves to limit the RPV pressure and the reactor is scrammed. The self-propelling cooling system starts to remove heat. In addition, primary steam is removed from the primary circuit via the RCIC turbine. However, the RCIC system needs around 50 seconds for its startup and to get ready to inject coolant into RPV.

Figure 6-25 shows the development of the reactor pressure vessel pressure during the first 10,000 seconds of the accident. The increased timescale has been chosen to facilitate the evaluation of the RCIC behavior. The water level decreases rapidly after the reactor scram, due to the collapsing steam bubbles. Therefore, the low water level signal immediately triggers the coolant injection, once the RCIC pump is started. Relatively cold water from the wetwell is inserted into the RPV, which further reduces the void fraction. As seen in Figure 6-25, this goes along with a quick reduction of the primary circuit pressure. The first coolant injection stops after 550 seconds, when the water level within the RPV reaches a certain threshold value and the low water level signal is reset. However, the steam removal through the RCIC turbine continues, which limits the pressure increase. The water level decreases a second time and falls below the threshold value after 3,700 seconds, causing the coolant injection to restart. Again, this results in a significant RPV pressure drop. The second injection period lasts for about 600 seconds until the low water level signal is reset. At that point in time, the decay heat has already decreased so far that less steam is produced, than is removed through the RCIC turbine and is condensed by the Turbo Compressor System. Accordingly, the primary circuit pressure decreases. A third injection period is triggered 9,200 seconds after the initiating event. However, it lasts less than 100 seconds since the RPV pressure drops to 1 MPa, which is the minimum operating pressure for the RCIC turbine. The turbine comes to a halt, which causes the RCIC system to stop. In the current analysis, it is not considered to restart the system.

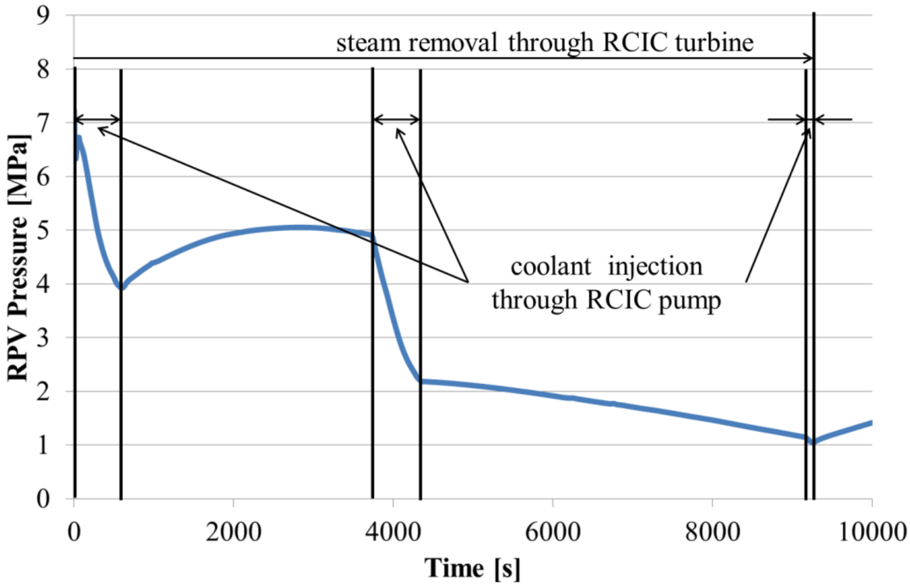

Figure 6-25: Plot of the RPV Pressure against Time – Retrofitted BWR with RCIC, Increased Timescale

It is unusual for the RCIC system to stop due to low primary circuit pressure. Usually, the RCIC shuts down either due to a high wetwell temperature or after the battery that provides the control energy for the turbine, is exhausted. Therefore, the low primary circuit pressure, which causes an early interruption of the third injection period, is a first indicator for the interaction between the TCS & RCIC. Since the self-propelling cooling system removes continuously heat from the primary circuit, it contributes to the decreasing RPV pressure, and hinders the RCIC to complete its third injection period. However, as the control energy for the turbine is intended to last for three hours, which includes usually three injection periods, this is only a minor drawback.

Figure 6-26 shows the development of the RPV pressure over the entire simulation time, which has been limited to 260,000 seconds. Subsequently to the RCIC stop, the self-propelling cooling system remains as the only available heat removal system. The primary circuit pressure starts to increase again, because the decay heat that is still produced, overcomes the heat removal capacity of the Turbo Compressor System. Eventually, a safety and relief valve is triggered, in order to limit the RPV pressure. As the decay heat reduces, the amount of removed heat actually exceeds the amount of produced heat, which causes the primary circuit pressure to decrease slowly.

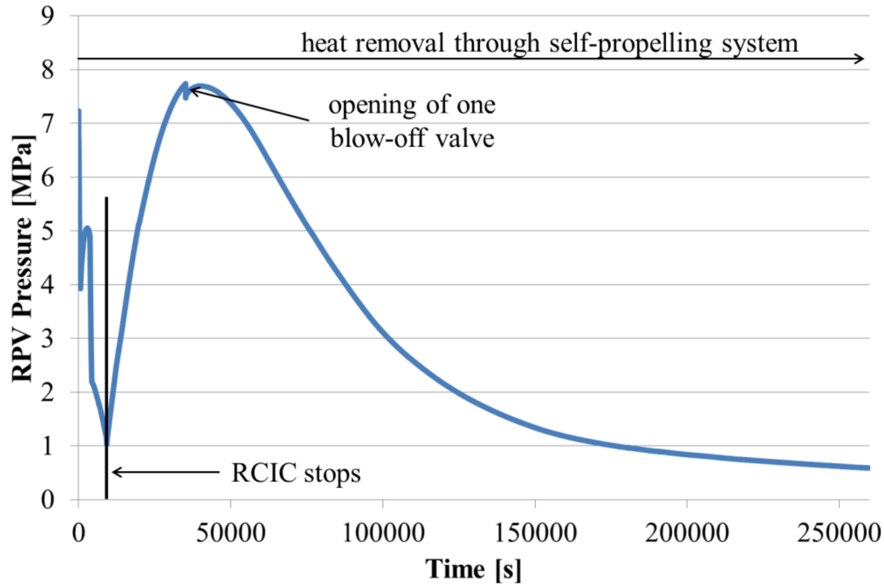

Figure 6-26: Plot of the RPV Pressure against Time – Retrofitted BWR with RCIC

Figure 6-27 shows the amount of heat removed by both systems and the Turbo Compressor System alone, compared to the decay heat. One can see that the system is unable to realize its maximum heat removal capacity of 30 MW_{th} during the beginning of the scenario. Moreover, the amount of heat decreases as long as the RCIC system is operating, but recovers afterwards. This behavior is caused by the dependency of the amount of removed heat on the RPV pressure, or more precisely, on the saturation temperature of the primary vapor. Since the RCIC rapidly reduces the primary circuit pressure, its operation negatively influences the heat removal capacity of the Turbo Compressor System.

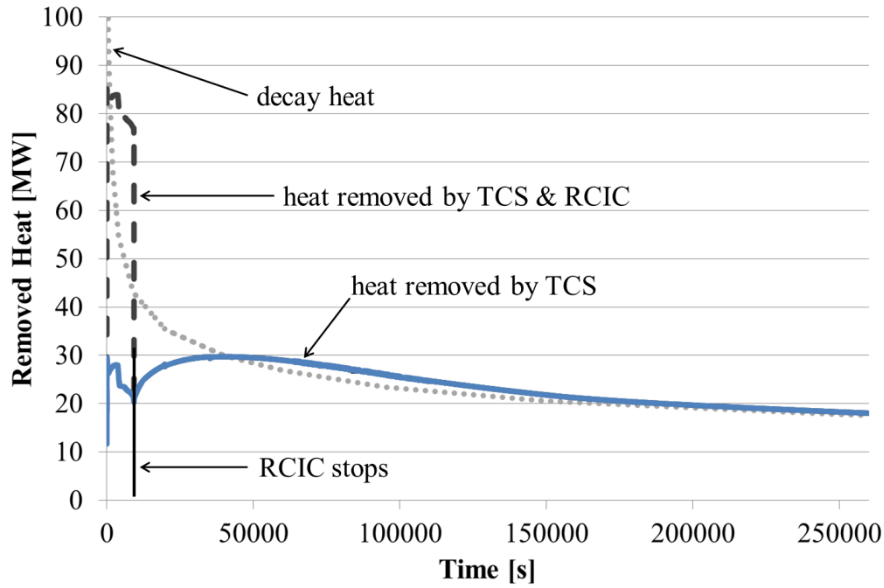

Figure 6-27: Plot of the Removed and Produced Heat against Time – Retrofitted BWR with RCIC

The same pressure dependency causes on the other hand the self-regulating behavior of the system, as the amount of removed heat approaches the amount of decay heat during the later phase of the accident. For the combination of the Turbo Compressor System with the reactor

core isolation cooling system, manual intervention and a complex control strategy becomes unnecessary, which is a big advantage.
The significant difference between the decay heat and the heat that is removed with the self-propelling cooling system, during the beginning of the scenario, is compensated by the reactor core isolation cooling system to a large extent. Therefore, both systems work very well together, as the RCIC supports the TCS especially during the beginning of the scenario, when the decay heat is at its height.

Figure 6-28 shows the excess electricity, generated with the Turbo Compressor System, which can be utilized for various purposes throughout the plant. It starts off at around 2.8 MW_{el}, which is half of the electricity provided in the previous cases. This is due to the fact that only two, instead of four, turbo-compressor-generator units are considered in the current configuration. The excess electricity depends strongly on the system's performance, which is determined by the temperature difference between the primary steam and the ambient air. Hence, it is also influenced by the severe pressure drop of the primary circuit. In fact, the amount of excess electricity reduces to 1.4 MW_{el} as long as the RCIC is operating. Subsequently, it starts to rise again. Overall, the consistently positive power balance underlines that the self-propelling heat removal system operates independently throughout the entire simulation time of 260,000 seconds and is therefore self-sufficient.
It seems reasonable to supply the RCIC system with excess electricity to prolong the option of independent operation under station blackout conditions beyond the usual battery capacity. This would enable the system to be restarted and provides more flexibility for the control of beyond design basis accidents.

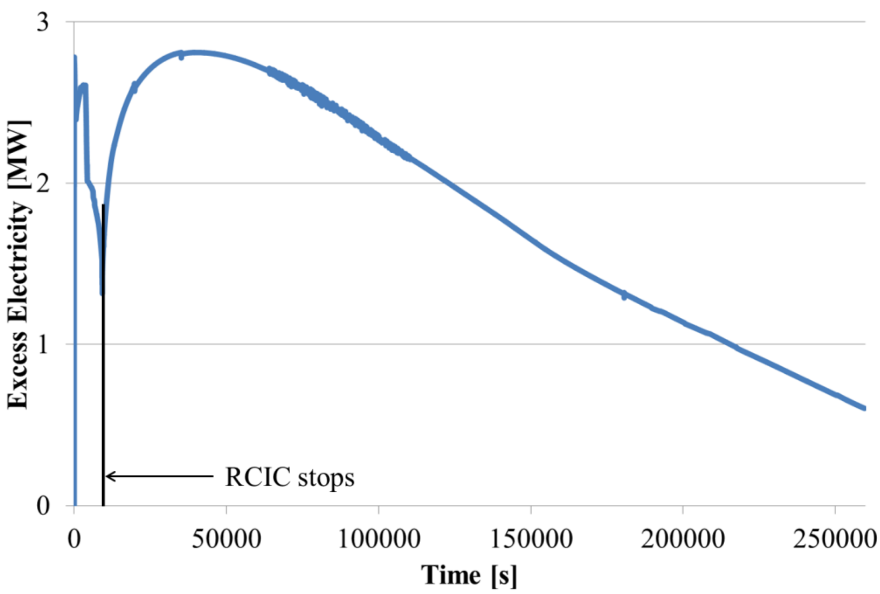

Figure 6-28: Plot of Excess Electricity against Time – Retrofitted BWR with RCIC

Steam that is released from the primary circuit has to be condensed in the available water inventory of the wetwell, in order to limit the pressure increase within the containment. This is mainly due to the steam that drives the RCIC turbine. However, the same is true for the steam that is blown-down into the pressure suppression pool through the safety and relief valves, directly after the turbine trip. Therefore, the temperature within the wetwell increases, especially during the beginning of the accident scenario, as shown in Figure 6-29. The maximum water temperature of 62 °C is reached directly after the RCIC stops operating. It decreases slightly over time, as heat is transferred into the surrounding structure. The water inventory within the wetwell serves as a heat buffer and is able to balance the peak in decay heat, at the beginning of the scenario. Since the RCIC pump is considered to work properly for water inlet temperatures up to 75 °C, the system's performance is not influenced by the increasing wetwell temperature. Nevertheless, the capacity of the water inventory is mostly utilized.

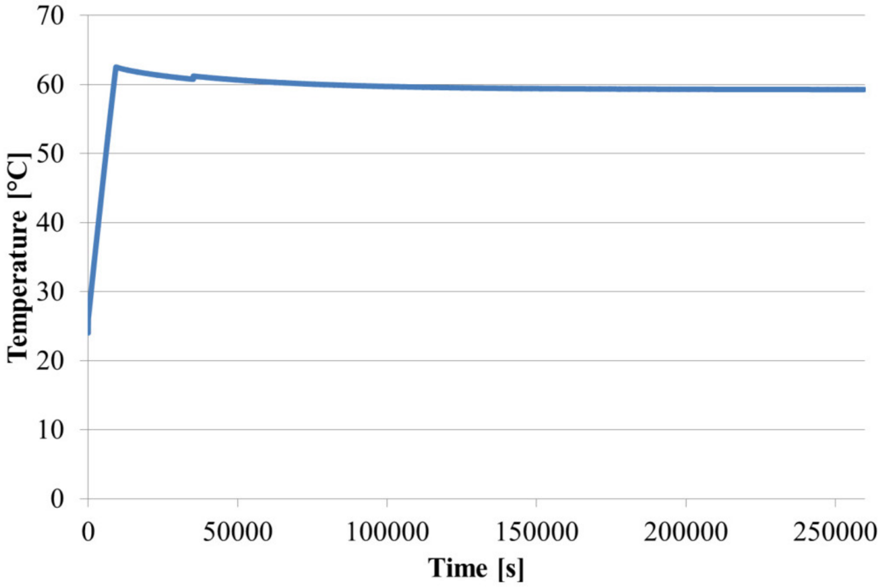

Figure 6-29: Plot of the Wetwell Temperature against Time – Retrofitted BWR with RCIC

The above evaluation showed that the self-propelling heat removal system works well together with the steam-driven reactor core isolation cooling system. These two systems are able to maintain the fundamental safety functions for a combined SBO & LUHS scenario for at least three days. Only minor interferences have been detected during the beginning of the scenario due to the accelerated depressurization. This is caused by the simultaneous steam removal, via the RCIC and steam condensation, via the Turbo Compressor System. On the one hand, the accelerated depressurization interrupts the last injection period of the RCIC, as the primary circuit pressure falls below the operating range of the turbine and therefore lessens the amount of inserted coolant. On the other hand, the reduced RPV pressure decreases the amount of heat removed by the self-propelling cooling system and negatively influences the system's performance and electricity generation.

Typically, a RCIC is intended to bridge the time during a station blackout, until external emergency procedures are implemented or power is regained. It transfers heat from the primary circuit to the pressure suppression pool, but cannot remove the heat from the containment itself. Therefore, its operating time is limited to a couple of hours. However, the system is able to realize the potential of the wetwell, to serve as a heat buffer. It can balance the peak of the decay heat during the beginning of the scenario, which is extremely beneficial. This is the reason, why the self-propelling cooling system can be designed 50 % smaller, compared to the cases presented in chapters 6.2-6.5.

However, a coordinated operating strategy would further maximize the synergy of the two steam-driven systems, especially under the assumption that excess electricity can be provided to the RCIC and that the system can be restarted during the entire time. It would be best, to stop the RCIC system subsequently to an injection period, in order to maximize the water inventory within the primary circuit. Vice versa, it should be avoided that the RCIC is shut-down right before an injection period is triggered, in order to prevent an unnecessarily low water inventory. In the long run, this could lead to an insufficient water level within the RPV and could jeopardize core cooling.

Furthermore, an aligned operating strategy could reduce pressure fluctuations within the isolated primary circuit, which helps to decrease the stress for the components.

7 Summary and Conclusion

The cooling of nuclear fuel is one of the three main safety objectives [26] in nuclear safety and has to be ensured under all circumstances. Redundant safety systems are implemented in nuclear power plants, to guarantee decay heat removal during design basis events. However, design basis exceeding events may require the implementation of external emergency procedures to maintain the core cooling function. The accidents of Fukushima have underlined, how important it is to deal with events, like the station blackout, combined with the loss of the ultimate heat sink. Therefore, it has been recommended that regulators should consider retrofit measures, to account for a potential unavailability of numerous safety systems and the isolation of the site [15]. A novel system that has the potential to significantly increase the grace period during such an event is the Turbo Compressor System. This self-propelling cooling system is based on the concept of a Brayton cycle, powered by the decay heat, which makes the system independent from external supplies, such as water or AC power. However, the transient analysis of the system and the evaluation of its impact on the plant behavior cannot be simulated with existing system codes. Therefore, a thermohydraulic simulation tool is needed.

A model has been developed, in order to extend the thermohydraulic system code ATHLET for the simulation of sCO_2 Brayton cycles for temperatures between 30 – 400 °C and pressures between 7.4 – 30 MPa. Supercritical carbon dioxide has been implemented as an additional working fluid, by adding its specific fluid properties in the before mentioned range. In addition the heat conducting and heat transfer module HECU has been extended by an appropriate heat transfer correlation. The model for the turbine has been adapted for the simulation of radial turbines and ATHLET has been enabled to simulate a compressor.

The heat transfer correlation and the determination of friction losses have been validated against experimental data, for systems with the working fluid sCO_2. The same is true for the models of the turbomachinery. The validation has shown that the developed model is able to simulate the behavior of a sCO_2 Brayton cycle within an acceptable range of accuracy.

A typical application of the Turbo Compressor System as a potential retrofit measure for a boiling water reactor has been selected to demonstrate that the modified version of ATHLET is suitable to simulate the heat removal system. A feasibility study has shown that a maximum heat removal capacity of 60 MW_{th} is sufficient in order to control a combined SBO & LUHS scenario. According to the temperature conditions present at the beginning of the scenario, the pressure ratio of the Brayton cycle has been determined and the main components have been roughly dimensioned. An existing input data deck of a generic BWR with 3840 MW_{th} has therefore been extended with the cooling system that has a modular design and consists of four equivalent cooling trains build in parallel.

For the conducted analysis, a station blackout, combined with the loss of the ultimate heat sink has been assumed as the initiating event. Firstly, the BWR has been simulated as it is, in order to generate data of a reference case. Following, four test cases have been calculated and the influence of the system on the ability to cool the core has been evaluated, by comparing it with the reference case.

The grace period of the solely retrofitted BWR can be extended by around 30 minutes. A great amount of primary steam is blown into the pressure suppression pool, due to a partial depressurization via the diverse blow-off valves. Thereby, the water inventory within the isolated primary circuit is reduced and the water level within the RPV sinks. Once a certain threshold value of the water level is reached, the reactor protection system activates the automatic, complete depressurization, to facilitate the injection of water. However, since it is anticipated that all active emergency injection systems are unavailable and external measures are not at hand, the core eventually uncovers and the decay heat cannot be removed sufficiently. The TCS cannot exploit its full potential.

To enlarge the operating period of the self-propelling heat removal system, in case no coolant injection is available, it is of uttermost importance to keep as much coolant within the isolated primary circuit as possible. Therefore, the partial depressurization has been considered as deactivated in the subsequent cases, to maximize the available coolant inventory. Consequently, the operating period of the Turbo Compressor System has increased and the grace period can be extended to 17 hours. Without further interventions and control measures, the self-propelling system tends to remove more heat than is produced. This in turn results in a depressurization of the primary circuit, which goes along with a strongly decreasing steam temperature. Accordingly, less heat is transferred to the sCO_2 and the amount of removed heat is reduced. Generally, the heat removal capacity of the Turbo Compressor System depends strongly on the temperature difference between the ambient air and the saturated steam. However, this effect is too weak to adapt the amount of removed heat to the decay heat. The system is not self-adapting. Therefore, the primary circuit pressure reduces, which causes the turbine entry temperature to decline even further. The operating conditions of the turbine depart from its design point, which has a negative effect on the efficiency of the turbine and the overall power balance of the Brayton cycle. At one point, this causes the system to stop as it is no longer self-sufficient. The system's performance depends strongly on the primary circuit pressure.

In order to keep the RPV pressure high and accordingly the driving temperature difference between the ambient air and the primary steam, the amount of removed heat has to be limited. Therefore, a simple control strategy for the Turbo Compressor System has been implemented in the subsequent case, to hold the operating conditions of the radial turbine closer to its design point. To reduce the amount of removed heat, two of the four cooling trains are successively shut-down. This way, the primary circuit pressure can be kept high enough to realize a temperature difference that ensures a positive power balance of the Turbo Compressor System for at least 72 hours. Therefore, the simulations confirmed the potential

of the self-propelling cooling system to increase the grace period significantly and to enable retrofitted BWRs of generation II to deal with certain design basis exceeding events independently over a longer period of time.
The simulation of a BWR that is additionally equipped with a Reactor Core Isolation Cooling System has shown that the combination of a self-propelling device that injects coolant into the isolated primary circuit of a BWR with the novel heat removal system is extremely beneficial. Hereby, the maximum heat removal capacity of the Turbo Compressor System could be reduced by 50 % compared to the other test cases. The coolant injection enables the BWR to realize the wetwell as a supplementary heat sink and can therefore deal with the peak in the decay heat at the beginning of the scenario, despite its smaller setup.

The following conclusions can be drawn from the performed analysis:
Key prerequisites for a successful operation of the self-propelling heat removal system are:

- sufficient coolant inventory
- high primary circuit pressure

Therefore, it is inevitable to adapt the depressurization system: Up to now it is common practice to depressurize the primary circuit of a BWR, if a station blackout occurs and / or the ultimate heat sink is lost. However, if the plant is retrofitted with the Turbo Compressor System, it is beneficial to prevent the partial depressurization and to restrict the amount of steam blown into the pressure suppression pool to the amount that is necessary to limit the primary circuit pressure. In addition, the threshold values regarding the RPV water level, which activate the automatic depressurization, should be reviewed. Unnecessary opening of the safety and relief valves has to be avoided, in order to ensure the long-term operation of such a system as it reduces the available coolant inventory and the primary circuit pressure.

Secondly, a comprehensive control strategy is necessary, in order to keep the primary circuit pressure high over time and to ensure a sufficient performance of the Brayton cycle. The amount of removed heat must be reduced over time and has to be adapted according to the decay heat. However, the residual heat varies, depending on the time since reactor startup and the point in time when the self-propelling heat removal system starts operating, in case the station blackout is not the initiating event that causes the reactor scram and occurs later in the course of events. Therefore, a flexible control mechanism has to be developed, ideally based on passive principles.

At this point in time the Brayton cycle has been designed for the boundary conditions at the beginning of the scenario, when the decay heat is at its height. The design point of the implemented turbomachinery has been chosen accordingly. Therefore, the turbine has the highest efficiency when the greatest expansion work is available. However, it might be advantageous to consider a later phase in the scenario as the design reference, in order to maximize the efficiency, when the potential expansion work is low, due to the decreased inlet temperature. This way, the operating range of the Turbo Compressor System could be further increased. Supplementally, the control strategy shall comprise a feature to optimize the number of revolutions of the turbomachinery according to the current inlet conditions. This can increase the efficiency of the turbine and / or the compressor compared to the results of the conducted analysis, where a constant number of revolutions has been assumed.

Further experiments should be conducted in the future, to provide a broader base of data for additional validation. Firstly, investigations regarding the pressure drop should be performed, for which all relevant parameters, including the wall roughness of the test section, are known. Secondly, experiments for the analysis of the behavior of radial turbines and compressors should be executed for all possible working conditions, to proof the validity of the model and to further ensure the accuracy of simulation results over the entire operating range. Thirdly, the specific behavior of the compact heat exchanger that is utilized for the Turbo Compressor System has to be understood in more detail, to draw definite conclusions about the conducted heat transfer and the actual pressure losses over the heat exchanger. Therefore, experiments should be conducted to obtain realistic information on these aspects.

In the conducted analysis, the compact heat exchanger is modeled as co-current flow, whereas in fact it is a cross-flow heat exchanger. This is due to the reason that ATHLET is presently not able to model cross flow without an unfeasible increase in computation time. Therefore, an additional heat exchanger model should be developed by the GRS, to account for the influence of the flow orientation on the heat transfer.

The adapted version of ATHLET provides a validated tool for the evaluation of the Turbo Compressor System and its interaction with existing safety systems of boiling water reactors. The conducted study has underlined that the Turbo Compressor System has the potential to serve as a diverse residual heat removal system and to extend the grace period during certain design extension conditions significantly. Its components are compact and can be retrofitted into existing boiling water reactors. The Turbo Compressor System works in accordance with the current safety concept and only minor adjustments regarding the operational, partial depressurization are necessary. The simulation has shown that a retrofitted BWR becomes capable to counter a combined station blackout and loss of ultimate heat sink scenario for at least 72 hours. The Turbo Compressor System is hereby independent from external resources, such as water or electricity. On the contrary, it even provides excess electricity, which can be used for various purposes throughout the plant. It is therefore advisable to further investigate the Turbo Compressor System as a potential retrofit option for residual heat removal.

8 References

[1] ADAMS, T.; ABDEL-KHALIK, S.; JETER, S.; QURESHI, Z.: An experimental investigation of single-phase forced convection in microchannels. *Int. J. Heat Mass Transfer* 41, 1997, p. 851–857.

[2] AUSTREGESILO, H.; BALS, C.; HORA, A.; LERCHL, G.; ROMSTEDT, P.; SCHÖFFEL, P.; CRON, D. VON DER; WEYERMANN, F.: ATHLET Mod 3.0 Cycle A - Models and Methods, GRS - P - 1 / Vol.4 Rev. 3, 2012.

[3] BASSAS, J.: Development and implementation of a Nuclear Power Plant steam turbine model in the system code ATHLET. Technische Universität München - GRS, 2011.

[4] BATET, L.; ALVAREZ-FERNANDEZ, J. M.; de les Valls, E. Mas; MARTINEZ-QUIROGA, V.; PEREZ, M.; REVENTOS, F.; SEDANO, L. A.: Modelling of a supercritical CO2 power cycle for nuclear fusion reactors using RELAP5–3D. *Fusion Engineering and Design* 4, 2014, p. 354–359.

[5] COLLIER, J.; THOME, J.: Convective boiling and condensation. Clarendon Press; Oxford University Press: Oxford, New York, 1994.

[6] DAVIS, C. B.; MARSHALL, T. D.; WEAVER, K. D.: Modeling The GFR With RELAP5-3D. *RELAP5 International Users Seminar.* Wyoming, 2005.

[7] Deutsche Edelstahlwerke GmbH: data sheet SS316. http://www.dew-stahl.com/fileadmin/files/dew-stahl.com/documents/Publikationen/Werkstoffdatenblaetter/RSH/1.4401_de.pdf, 28.08.2014.

[8] DIERCKX, P.: Curve and surface fitting with splines. Clarendon: Oxford, New York, 1993.

[9] DOSTAL, V.; DRISCOLL, M.; HEJZLAR, P.: A supercritical Carbon Dioxide Cycle for Next Generation Nuclear Reactors. MIT-ANP-TR-100, 2004.

[10] DROSG, M.: Dealing with Uncertainties. Springer: Berlin, Heidelberg, 2009.

[11] DUBBEL, H.; GROTE, K.: Taschenbuch für den Maschinenbau, 2005.

[12] DYREBY, J.; KLEIN, S.; NELLIS, G.; REINDL, D.: Development of Advanced Off-Design Models for Supercritical Carbon Dioxide Power Cycles. *International Congress on Advances in Nuclear Power Plants.* Anaheim, 2012.

[13] EDEN, K.; GEBHARD, HERMANN: Dokumentation in der Mess- und Prüftechnik. Vieweg+Teubner: Wiesbaden, 2011.

[14] EMENDÖRFER, D.; HÖCKER, K.: Theorie der Kernreaktoren. BI-Wiss.-Verl.: Mannheim, 1993.

[15] ENSREG: Compilation of recommendations and suggestions - Peer review of stress tests performed on European nuclear power plants, 2012.

[16] EUR - European Utility Requirements: Volume 2, 2001.

[17] FEHER, E. G.: The Supercritical Thermodynamic Power Cycle. *Energy Conversion* 8, 1968, p. 85–90.

[18] FENGHOUR, A.; WAKEHAM, W.; VESOVIC, V.: The Viscosity of Carbon Dioxide. *Journal of Physical and Chemical Reference Data* 1, 1998, p. 31–44.

[19] Frumholtz; J.: Transiente Analyse eines überkritischen CO2 Rekuperators: Karlsruhe, 2010.

[20] GEA Luftkühler GmbH: Luftgekühlter Wärmetauscher für CO2. Angebot, 06.09.2013.

[21] GOLDBERG, S. M.; ROSNER, R.: Nuclear Reactors: Generation to Generation. American Academy of Arts and Sciences: Cambridge, 2011.

[22] GROTE, W.: Ein Beitrag zur modellbasierten Regelung von Entnahmedampfturbinen. Ruhr-Universität: Bochum, 2009.

[23] HESSELGREAVES, J. E.: Compact heat exchangers. Pergamon: Amsterdam, New York, 2001.

[24] HEWITT, G. F.: Heat exchanger design handbook, 1998. Begell House: New York, 1998.

[25] IAEA: Safety related terms for advanced nuclear plants. IAEA-TECDOC-626: Vienna, 1991.

[26] IAEA: Safety Glossary - Terminology Used in Nuclear Safety and Radiation Protection: Vienna, 2007.

[27] Idaho National Laboratory: Relap5-3D Code Manual Volume 1, June 2005.

[28] Internationale Länderkommission Kerntechnik: Fundamental Safety Requirements for Nuclear Power Plants, 2008.

[29] KATO, Y.; NITAWAKI, T.; MUTO, Y.: Medium temperature carbon dioxide gas turbine reactor. *Nuclear Engineering and Design* 1-3, 2004, p. 195–207.

[30] KKB Brunsbüttel: Sicherheitsüberprüfung unter Berücksichtigung der Ereignisse in Fukushima - EU "Stresstests". Bericht 2011-0119. http://www.vattenfall.de/de/file/KKB_Stresstestbericht.pdf_19581321.pdf, 05.07.2012.

[31] KRASNOSHCHEKOV, E. A.; PROTOPOPOV, V. S.: Experimental Study of Heat Exchange in Carbon Dioxide in the Supercritical Range at High Temperature Drops. *High Temperature 4, p.* 375–382.

[32] KRB II Gundremmingen: Abschlussbericht zum Stresstest europäischer Kernkraftwerke unter Berücksichtigung der Ereignisse in Fukushima-I (Japan), 2011.

[33] LAVANTE, D. VON: Self-Propelling Cooling Systems: A Novel Passive Cooling System for Nuclear Power Plants. *Jahrestagung Kerntechnik.* Stuttgart, 2012.

[34] LAVANTE, D. VON: Personal Correspondence, July 2013.

[35] LAVANTE, D. VON; KUHN, D.; LAVANTE, E. VON: Self-Propelling Cooling Systems: Back-Fitting Passive Cooling Functions to Existing Nuclear Power Plants. *International Congress on Advances in Nuclear Power Plants.* Anaheim, 2012.

[36] LEMMON, E.; HUBER, M.; MCLINDEN, M.: NIST Reference Fluid Thermodynamic and Transport Properties - REFPROP, 2007.

[37] LERCHL, G.; AUSTREGESILO, H.; SCHÖFFEL, P.; CRON, D. VON DER; WEYERMANN, F.: ATHLET Mod 3.0 Cycle A - User's Manual, GRS - P - 1/ Vol.1 Rev. 6, 2012.

[38] LI, X.; SMITH, T.; KININMONT, D.; DEWSON, S.: Materials for Nuclear Diffusion-Bonded Compact Heat Exchangers. *International Congress on Advances in Nuclear Power Plants.* Tokyo, 2009.

[39] MARTINELLI, R.; NELSON, D.: Prediction of Pressure Drop During Forced Circulation Boiling of Water. *Trans. ASME* 6, 1948, p. 695–702.

[40] MAYINGER, F.; SCHEIDT, M.: Heat transfer in the supercritical region with vertical upflow. *Wärme- und Stoffübertragung,* 1984, p. 207–214.

[41] MYLAVARAPU, S.: Design, Fabrication, Performance Testing, and Modeling of Diffusion Bonded Compact Heat Exchangers in a High-Temperature Helium Test Facility. The Ohio State University, 2011.

[42] Nuclear Safety Standards Commission (KTA): KTA 3301 - Residual Heat Removal Systems for Light Water Reactors, 1984.

[43] PASCH, J.; CONBOY, T.; FLEMING, D.; ROCHAU, G.: Supercritical CO2 Recompression Brayton Cycle: Completed Assembly Description. Sandia Report - SAND2012-9546: Alburquerque, 2012.

[44] RAY, A.: Dynamic modelling of power plant turbines for controller design. *Appl. Math. Modelling* 4, 1980, p. 109–112.

[45] RINALDI, E.; PECNIK, R.; COLONNA, P.: Steady State CFD Investigation of a Radial Compressor Operating with Supercritical CO2. *Proceedings of ASME Turbo Expo 2013: Turbine Technical Conference and Exposition.* San Antonio, 2013.

[46] RSK-Stellungnahme: Ausfall der Primären Wärmesenke. 446. Sitzung, 05.04.2012.

[47] SCALABRIN, G.; MARCHI, P.; FINEZZO, F.; SPAN, R.: A Reference Multiparameter Thermal Conductivity Equation for Carbon Dioxide with an Optimized Functional Form. *Journal of Physical and Chemical Reference Data* 4, 2006, p. 1549.

[48] SCHÄFER, F.; TUSHEVA, P.; Kliem S.: Analysesimulator KKW-Biblis Block B, 2012.

[49] SIGLOCH, H.: Strömungsmaschinen. Hanser: München, 2009.

[50] SINGH, R.; MILLER, S.; ROWLANDS, A.; JACOBS, P.: Dynamic characteristics of a direct-heated supercritical carbon-dioxide Brayton cycle in a solar thermal power plant. *Energy,* 2013, p. 194–204.

[51] SON, C.; PARK, S.: An experimental study on heat transfer and pressure drop characteristics of carbon dioxide during gas cooling process in a horizontal tube. *International Journal of Refrigeration* 4, 2006, p. 539–546.

[52] SPAN, R.; WAGNER, W.: A New Equation of State for Carbon Dioxide Covering the Fluid Region from the Triple-Point Temperature to 1100 K at Pressures up to 800 MPa. *Journal of Physical and Chemical Reference Data* 6, 1996, p. 1509–1596.

[53] SPINDLER, K.: Wärmeübergang bei erzwungener Strömung von Kohlendioxid bei überkritischen Zuständen. AA.II.1.10. *DKV-Tagung.* Würzburg, 2005.

[54] STUK: European Stress Tests for Nuclear Power Plants - National Action Plan. Radiation and Nuclear Safety Authority, 2012.

[55] TAITEL, Y.; BORNEA, D.; DUKLER, A. E.: Modelling Flow Pattern Transitions for Steady Upward Gas-Liquid Flow in Vertical Tubes. *AIChE Journal* 3, 1980, p. 345–354.

[56] TENG, H.; CHENG, P.; ZHAO, T. S.: Instability of condensate film and capillary blocking in small-diameter-thermosyphon condensers. *Int. J. Heat Mass Transfer* 42, 1999, p. 3071–3083.

[57] The World Bank: World Development Indicators - online database. Electricity Production Sources and Access - Year 2011. http://wdi.worldbank.org/table/3.7, 28.08.2014.

[58] Tokyo Electric Power Company: Fukushima Nuclear Accident Analysis Report. http://www.tepco.co.jp/en/press/corp-com/release/betu12_e/images/120620e0104.pdf, 06.02.2015.

[59] VENKER, J.: A passive heat removal retrofit for BWRs. *Nuclear Engineering International* 711, 2013, p. 14–17.

[60] VENKER, J.; LAVANTE, D. VON; BUCK, M.; GITZEL, D.; STARFLINGER, J.: Concept of a Passive Cooling System to Retrofit Existing Boiling Water Reactors. *International Congress on Advances in Nuclear Power Plants.* Jeju Island, 2013.

[61] VENKER, J.; LAVANTE, D. VON; BUCK, M.; GITZEL, D.; STARFLINGER, J.: Konzept eines autarken Kühlsystems zur Nachwärmeabfuhr in Siedewasserreaktoren. *Jahrestagung Kerntechnik.* Berlin, 2013.

[62] VENKER, J.; LAVANTE, D. VON; BUCK, M.; GITZEL, D.; STARFLINGER, J.: Analysis of an Autarkic Heat Removal System: The Influence of Operator Intervention. *Jahrestagung Kerntechnik.* Frankfurt, 2014.

[63] VENKER, J.; LAVANTE, D. VON; BUCK, M.; GITZEL, D.; STARFLINGER, J.: Interaction between Retrofittable and Existing Emergency Cooling Systems in BWRs. *International Topical Meeting on Nuclear Thermal-Hydraulics, Operation and Safety - NUTHOS-10.* Okinawa, 2014.

[64] VENKER, J.; LAVANTE, D. VON; BUCK, M.; GITZEL, D.; STARFLINGER, J.: Transient Analysis of an Autarkic Heat Removal System. *International Congress on Advances in Nuclear Power Plants.* Charlotte, 2014.

[65] Verein Deutscher Ingenieure: VDI-Wärmeatlas. Springer: Berlin, 2006.

[66] VESOVIC, V.; WAKEHAM, W.; OLCHOWY, G.; SENGERS, J.; WATSON, J.; MILLAT, J.: The Transport Properties of Carbon Dioxide. *Journal of Physical and Chemical Reference Data* 3, 1990, p. 763–808.

[67] VILIM, R.: Development and Validation of a Radial Inflow Tubine Model for Simulation of the SNL S-CO2 Split-Flow Loop. Argonne National Laboratory - ANL-ARC-195: Oak Ridge, 2011.

[68] WALISCH, T.: Messung des Wärmeübergangs von überkritischem CO2 im Kreisrohr bei erzwungener sowie bei Mischkonvektion. Eidgenössische Technische Hochschule Zürich: Zürich, 1997.

[69] WILLIAMSON, B.; LYTER, J.; RONIGER, D.; ELLISON, P.: Revising BWR emergency procedures. *Nuclear Engineering International* 711, 2013, p. 18–19.

[70] WRIGHT, S.; CONBOY, T.; ROCHAU, G.: High-Temperature Split-Flow Recompression Brayton Cycle Initial Test Results. Sandia Report - SAND2012-6426: Alburquerque, 2012.

Appendix A – B-Spline Coefficients

Data of B-spline coefficients for enthalpy depending on temperature and pressure
Based on 2,500 data points
283.0 < T < 675.0 K
7400000.0 < p < 30000000.0 Pa

Temperature nodes

283.000000000000	283.000000000000	283.000000000000
283.000000000000	300.742184471151	307.000000000000
313.471117071109	317.590896583131	330.129747211179
364.285369471961	488.536141442175	675.000000000000
675.000000000000	675.000000000000	675.000000000000

Pressure nodes

7400000.00000000	7400000.00000000	7400000.00000000
7400000.00000000	8308808.10480993	9011527.34194426
10578864.7593296	14014544.7731855	17553470.2959975
30000000.0000000	30000000.0000000	30000000.0000000
30000000.0000000		

Coefficients for enthalpy

220558.504205522	220172.304036790	219188.099369454
218337.600214477	216661.033699772	214955.815917716
212576.140615245	212312.417571971	212428.454708407
260042.213702438	243941.436439250	241443.226584036
228711.358311320	231231.651160825	227684.392457651
223866.742464555	224055.397160042	223476.866990125
197766.240020181	230970.344813668	246560.716472781
258345.896470511	247112.927607952	245862.525081654
241043.969256876	238634.508155671	238787.744458685
406829.574561031	349963.448598533	294207.853246424
282780.846166054	279939.907323067	269877.959896046
261073.027274205	260275.455960023	258248.883685766
433214.536387415	408908.509396182	383527.520284445
318634.869926618	291153.181973778	290605.375461827
271378.193743598	270660.132067381	268669.495763377
437288.962544106	438499.714003000	441355.181786916
398579.810724666	320460.694607836	298997.760183985
292417.453523413	287976.699187851	285283.850555911
477773.514559469	472337.243584841	461065.939978619
456862.103616996	435045.704920549	375715.410397627
318558.756922321	321665.269200946	315649.704067933
553435.090553025	553667.367606121	554210.202080820

543544.577709103	533258.804660910	532408.259739146
485123.293568950	452896.110718962	441871.809936945
682580.626951102	679587.911508480	675054.067914609
677502.651396187	672887.450432028	651289.762593840
650058.234304005	646726.703953248	637452.562657510
798222.062560447	799111.242512143	799677.231883847
794777.146979587	791055.772835769	794477.903630155
775344.615381160	763458.965124715	759206.632066518
870509.378576169	869512.870110349	868252.541838697
867575.224208345	864846.464848599	857963.419612010
851857.791753400	846913.177067715	842441.690731495

Data of B-spline coefficients for the density depending on temperature and pressure
Based on 2,500 data points
283.0 < T < 675.0 K
7400000.0 < p < 30000000.0 Pa

Temperature nodes

283.000000000000	283.000000000000	283.000000000000
283.000000000000	297.545161192764	301.953229566744
310.327993082027	315.000000000000	317.584013752797
327.004455195182	338.825484121167	356.845636533786
404.315256748674	440.410413481602	494.225211255881
675.000000000000	675.000000000000	675.000000000000
675.000000000000		

Pressure nodes

7400000.00000000	7400000.00000000	7400000.00000000
7400000.00000000	8192347.68710889	8670996.04327657
8979835.28389740	10033868.8722952	13216161.3190866
14877068.6301838	17052588.6399775	19442620.1439100
21680088.5859280	30000000.0000000	30000000.0000000
30000000.0000000	30000000.0000000	

Coefficients for density

897.812469178997	899.096295551639	906.366666497552
910.036568399634	914.987909601379	927.466023220977
941.228560269579	955.296314207943	966.823184177147
978.088230330345	997.794225325224	1011.07654985276
1020.66868609880	635.193978714140	771.001520299712
902.501595322934	952.964106465428	893.104685194975
879.929037331695	925.728492918292	927.029483909210
944.095260531233	959.534533339474	979.601026666078

994.437343174928	1003.98593312672	1115.81912871793
972.257958066868	773.933670177775	730.023398647440
840.202573751627	886.373146685706	868.648449658839
908.189545720124	916.118579754882	927.622013942902
953.425301608218	969.032216468595	981.000179191209
437.534170959742	541.211660230698	793.956834497468
831.938718136081	753.677536558856	772.179468808087
833.281424722829	840.036673068249	868.282770396149
887.415980855993	917.270435207839	935.068821042187
947.924963411894	137.939088312241	222.816207930792
505.026995269447	572.232208764951	689.091532196778
751.293162243169	763.614312712780	820.800850093685
832.445357625460	856.704290345500	889.165828358585
911.735562708199	925.207116962169	224.216519598879
215.917290762792	283.335682770320	309.423276738976
507.872195582012	708.263704185330	715.613514744338
780.442717077632	801.501634792136	828.901904131041
866.861087287809	890.132733206589	905.298528494078
198.644641983831	224.739101719377	215.906224626654
274.629779237879	301.472391030536	592.040490244661
686.060241697915	720.924880895936	768.950223907886
799.307416445153	844.480878402880	867.060650290855
884.228476546744	176.421638425079	184.313863252225
208.554806489273	234.012919084815	263.090177315202
346.222645708308	596.542846261971	672.006399289977
717.324280271219	745.671701108305	803.994331016768
830.644076785227	851.287791855849	156.690839062038
164.788268860043	177.243953611243	193.825459338820
218.359969191006	275.111962414465	375.472552811370
520.889193956439	608.214225435226	670.324062050980
743.808873524330	775.272386835727	799.026058096440
129.984460051048	135.497337114007	145.310948826192
157.715179070614	170.918911415590	207.937663836753
260.901173158134	327.613777781652	400.412083809091
476.344152548261	599.193183939808	651.921678258573
685.924281831081	111.776220699466	116.385319472503
123.627333140779	132.904225655485	144.452329973667
172.442303328310	211.757585347760	262.089867802661
304.916558380206	352.738465676602	444.083715337595
510.456918919456	550.634837143030	94.8264846350802
98.4544596010249	104.396506009342	111.837035968443
120.411799689140	142.129375677941	171.144267485729
206.318946000723	238.786760261236	274.211242788757
340.691422570874	391.880554349276	428.518414116945
72.7602036058656	75.4003905801115	79.5646175508164

84.7672508136247	90.9796582635900	106.021668440460
125.613002679873	149.024261730257	168.939818846085
190.739508567543	232.330710258139	265.967013363396
291.522989395875	64.0726550784927	66.3725484108062
70.1034395598382	74.7313683566436	80.0496535430720
93.3419407942100	110.558402858361	130.892260394824
149.261214432782	169.077608207993	206.154011844335
235.178382932400	257.195566000056	58.1488677235604
60.2242909808849	63.5432313016160	67.6681755428801
72.4912634207873	84.3472571503429	99.6793050290533
117.821991013849	133.723725487309	150.958602764515
183.448871065642	209.220392106984	228.847199725479

Appendix B – Process Signal

A process signal is calculated by other models included in the subroutines of ATHLET.
For example the sum of the gained expansion work of the turbines, according to equation 3.22, and the necessary compression work of the compressors, according to equation 3.32, is computed in the subroutine for the calculation of the quantities of the turbines

```
      PTURBS = SUM(PTURB)
```

Another subroutine gets the current value of process signals, so that it can be provided as input data for other controllers

```
      ELSEIF(IDS.EQ.43) THEN
C-----   Turbine Power
         A     = PTURBS
!       write(*,*)'gdsig:',TF,PTURBS
         IATIME= 1
```

The process signal, for example called PTURBSUM, is defined in the process signal block that follows the control word GCSM. The input is therefore extended by

```
@
S---- PTURBSUM
@ YNAME       VARTYP    OBJNAM      MODNAM      SPV0
  PTURBSUM    PTURBS    TURBINE1    -           0.25
```

The type of the process signal is the overall power output of the turbines and compressors in Watt. Due to the code extension it can now be calculated and it is triggered by the word PTURBS. To calculate the power output of the entire turbomachinery, the process signal can be applied to any turbine or compressor in the system, for example TURBINE1. The position of the corresponding turbine junction within the turbine pipe is selected as the length coordinate SPV0.

PTRUBSUM can no serve as an input variable for a control signal for AIRFANP that switches in case the power output of the turbomachinery falls below the power necessary to drive the air fans, which corresponds to 1,000,000 W.

```
S---- AIRFANP
@ YNAME    CONTYP   X1NAME     X2NAME   X3NAME   X4NAME
  AIRFANP  SWITCH   PTURBSUM   -        -        -
@ IOPT   GAIN   A1          A2         A3     A4
  0      1.0    1000000.0   800000.0   0.0    0.0
@ Y0    EPSCON    IPEXO
  1.0   -0.00001  0
```

Appendix C – Uncertainty Analysis

Performance of the Turbine

The total uncertainty of the turbine's efficiency is affected by statistical and systematic uncertainties. It can be obtained by equation C.1, as both combined uncertainty components are independent of each other.

$$\Delta\eta_T = \sqrt{\Delta\eta_{T,stat}{}^2 + \Delta\eta_{T,sys}{}^2} \tag{C.1}$$

The statistical uncertainty of the efficiency of the turbine is characterized by the multiple uncertainties of the temperature and pressure measurements, which are assumed to be independent of each other. Therefore, the combined uncertainty can be calculated, according to the law of error propagation, by adding the individual uncertainties squared [10].

$$\Delta\eta_{T,stat} = \sqrt{\left(\frac{\partial\eta_T}{\partial T_2}\Delta T_2\right)^2 + \left(\frac{\partial\eta_T}{\partial T_3}\Delta T_3\right)^2 + \left(\frac{\partial\eta_T}{\partial p_2}\Delta p_2\right)^2 + \left(\frac{\partial\eta_T}{\partial p_3}\Delta p_3\right)^2} \tag{C.2}$$

The influence of each individual uncertainty component can be determined by the partial derivative of the efficiency with respect to the temperatures and pressures, as shown in equation C.3 to C.6.

$$\frac{\partial\eta_T}{\partial T_2} = \frac{c_{p2}}{h_2 - h_{3,\mathrm{is}}} - \frac{(h_2 - h_3)\, c_{p2}}{\left(h_2 - h_{3,\mathrm{is}}\right)^2} \tag{C.3}$$

$$\frac{\partial\eta_T}{\partial T_3} = -\frac{c_{p3}}{h_2 - h_{3,\mathrm{is}}} \tag{C.4}$$

$$\frac{\partial\eta_T}{\partial p_2} = \frac{\frac{\partial h_2}{\partial p_2}}{h_2 - h_{3,\mathrm{is}}} - \frac{(h_2 - h_3)\,\frac{\partial h_2}{\partial p_2}}{\left(h_2 - h_{3,\mathrm{is}}\right)^2} \tag{C.5}$$

$$\frac{\partial\eta_T}{\partial p_3} = \frac{(h_2 - h_3)\,\frac{\partial h_{3,\mathrm{is}}}{\partial p_3}}{\left(h_2 - h_{3,\mathrm{is}}\right)^2} - \frac{\frac{\partial h_3}{\partial p_3}}{h_2 - h_{3,\mathrm{is}}} \tag{C.6}$$

The systematic error caused by the uncertainties of the database of the fluid properties is conservatively calculated as the maximum error. It is determined by adding the absolute values of the product of the partial derivatives C.8, C.9 and C.10 with the known deviation [13].

$$\Delta\eta_{T,sys} = \left|\frac{\partial\eta_T}{\partial h_2}\Delta h_2\right| + \left|\frac{\partial\eta_T}{\partial h_3}\Delta h_3\right| + \left|\frac{\partial\eta_T}{\partial h_{3,\text{is}}}\Delta h_{3,\text{is}}\right| \quad \text{(C.7)}$$

$$\frac{\partial\eta_T}{\partial h_2} = \frac{1}{h_2 - h_{3,\text{is}}} - \frac{(h_2 - h_3)}{\left(h_2 - h_{3,\text{is}}\right)^2} \quad \text{(C.8)}$$

$$\frac{\partial\eta_T}{\partial h_3} = -\frac{1}{h_2 - h_{3,\text{is}}} \quad \text{(C.9)}$$

$$\frac{\partial\eta_T}{\partial h_{3,\text{is}}} = \frac{(h_2 - h_3)}{\left(h_2 - h_{3,\text{is}}\right)^2} \quad \text{(C.10)}$$

The results of the uncertainty analysis are summarized in Table 0-1. The statistical error is mainly determined by the uncertainty of the outflow temperature, but the overall deviation depends mostly on the systematic uncertainty, caused by the accuracy of the NIST database.

Table 0-1: Results of the Uncertainty Analysis – Efficiency of the Turbine

	I	II	III
$\frac{\partial\eta_T}{\partial T_2}\Delta T_2$	0.009	0.006	0.006
$\frac{\partial\eta_T}{\partial T_3}\Delta T_3$	0.093	0.059	0.046
$\frac{\partial\eta_T}{\partial p_2}\Delta p_2$	-0.001	-0.001	-0.001
$\frac{\partial\eta_T}{\partial p_3}\Delta p_3$	0.001	0.001	0.001
$\Delta\eta_{t,stat}$	0.09	0.06	0.05
$\frac{\partial\eta_T}{\partial h_2}\Delta h_2$	0.022	0.015	0.015
$\frac{\partial\eta_T}{\partial h_3}\Delta h_3$	0.215	0.148	0.119
$\frac{\partial\eta_T}{\partial h_{3,\text{is}}}\Delta h_{3,\text{is}}$	0.193	0.133	0.104
$\Delta\eta_{t,sys}$	0.43	0.30	0.24
$\Delta\eta_t$	0.44	0.30	0.24

Performance of the Compressor

The procedure described for the error calculation of the turbine's efficiency is also valid for the determination of the total uncertainty of the efficiency of the compressor, as in equation C.11

$$\Delta\eta_C = \sqrt{{\Delta\eta_{C,stat}}^2 + {\Delta\eta_{C,sys}}^2} \tag{C.11}$$

The statistical uncertainty is thereby caused by the uncertainty of the pressure and temperature measurements and can be combined to $\Delta\eta_{C,stat}$

$$\Delta\eta_{C,stat} = \sqrt{\left(\frac{\partial\eta_C}{\partial T_4}\Delta T_4\right)^2 + \left(\frac{\partial\eta_C}{\partial T_1}\Delta T_1\right)^2 + \left(\frac{\partial\eta_C}{\partial p_4}\Delta p_4\right)^2 + \left(\frac{\partial\eta_C}{\partial p_1}\Delta p_1\right)^2} \tag{C.12}$$

With the partial derivatives

$$\frac{\partial\eta_C}{\partial T_4} = \frac{c_{p4}}{h_4 - h_1} - \frac{c_{p4}(h_4 - h_{1,\mathrm{is}})}{(h_4 - h_1)^2} \tag{C.13}$$

$$\frac{\partial\eta_C}{\partial T_1} = -\frac{c_{p1}\left(h_4 - h_{1,\mathrm{is}}\right)}{(h_4 - h_1)^2} \tag{C.14}$$

$$\frac{\partial\eta_C}{\partial p_4} = \frac{\frac{\partial h_4}{\partial p_4}}{h_4 - h_1} - \frac{\frac{\partial h_4}{\partial p_4}(h_4 - h_{1,\mathrm{is}})}{(h_4 - h_1)^2} \tag{C.15}$$

$$\frac{\partial\eta_C}{\partial p_1} = \frac{\frac{\partial h_{1,\mathrm{is}}}{\partial p_1}(h_4 - h_{1,\mathrm{is}})}{(h_4 - h_1)^2} - \frac{\frac{\partial h_1}{\partial p_1}}{h_4 - h_1} \tag{C.16}$$

The systematic uncertainty, due to the accuracy of the data base regarding the enthalpy of sCO_2 is considered as the maximum error

$$\Delta\eta_{C,sys} = \left|\frac{\partial\eta_C}{\partial h_4}\Delta h_4\right| + \left|\frac{\partial\eta_C}{\partial h_1}\Delta h_1\right| + \left|\frac{\partial\eta_C}{\partial h_{1,\mathrm{is}}}\Delta h_{1,\mathrm{is}}\right| \tag{C.17}$$

With the partial derivatives

$$\frac{\partial\eta_C}{\partial h_4} = \frac{1}{h_4 - h_1} - \frac{h_4 - h_{1,\mathrm{is}}}{(h_4 - h_1)^2} \tag{C.18}$$

$$\frac{\partial\eta_C}{\partial h_1} = \frac{h_4 - h_{1,\mathrm{is}}}{(h_4 - h_1)^2} \tag{C.19}$$

$$\frac{\partial \eta_C}{\partial h_{1,\mathrm{is}}} = -\frac{1}{h_4 - h_1} \tag{C.20}$$

The results of the uncertainty analysis are summarized in Table 0-2. The systematic uncertainty due to the accuracy of the fluid properties is in the range of 20%. However the overall uncertainty is mainly influenced by the statistical error that exceeds 100% for all three cases. This is primarily due to the accuracy of the experimental data for the inflow conditions. Since the operating point is in the direct proximity of the critical point, already small deviations in the temperature and the pressure, have a very strong influence on the enthalpy, where the temperature fluctuation is most determining.

Table 0-2: Results of the Uncertainty Analysis – Efficiency of the Compressor

	I	II	III
$\frac{\partial \eta_C}{\partial T_4}\Delta T_4$	-6.327	-0.929	-0.530
$\frac{\partial \eta_C}{\partial T_1}\Delta T_1$	0.104	0.333	0.365
$\frac{\partial \eta_C}{\partial p_4}\Delta p_4$	2.684	0.944	0.947
$\frac{\partial \eta_C}{\partial p_1}\Delta p_1$	-0.099	-0.048	-0.020
$\Delta\eta_{c,stat}$	6.87	1.37	1.15
$\frac{\partial \eta_C}{\partial h_4}\Delta h_4$	-0.069	-0.057	-0.032
$\frac{\partial \eta_C}{\partial h_1}\Delta h_1$	-0.021	-0.101	-0.127
$\frac{\partial \eta_C}{\partial h_{1,\mathrm{is}}}\Delta h_{1,\mathrm{is}}$	0.090	0.158	0.159
$\Delta\eta_{c,sys}$	0.12	0.20	0.21
$\Delta\eta_c$	6.87	1.38	1.16

Appendix D – ATHLET Input

Thermo-Fluiddynamic Objects

Firstly, the priority chain of the connection of the cooling cycle to the primary circuit is listed under the control word TOPOLOGY. It links the main steam line (MSL001) with the feedwater line (FWL001), where the steam is condensed in the heat exchanger (CHANNEL1).

```
----- TCS
@
@  IPRI0   ISYS0
    1         1
@  SBO0   ANAMO       SEO0     IARTO
     0.0      MSL001        2.315     1
     0.0      S1-VL          1.0        1
     0.0      PARA-VL      0.0       1
     0.0      S1-VL1         1.0        1
     0.0      PCHE-IN1     0.0        1
     0.0      CHANNEL1   0.7        1
     0.0      PCHE-OUT    0.0        1
     0.0      S1-LL           4.5        1

----- CONNECT
@
@   IPRIO   ISYSO
     1          2
@  SBO0   ANAMO     SEO0     IARTO
     0.0      FWL001      0.0         1
     0.0      S1-LLSJP    0.085     1
     4.5      S1-LL          0.0         1
```

Secondly, the involved thermo-fluiddynamic objects are described under the control word OBJECT.

```
K---- S1-VL          vapor line (pipe)
@
@  ITYPO   FPARO   ICMPO
   21      1.0     0
@
----- NETWORK
@  SN0(i)  NI0(i)
   0.0     1
   1.0
@
----- GEOMETRY
@  SG0      Z0       D0      A0      V0      DEP0
   0.0      16.71    0.63    0.0     0.0     0.0
   1.0      17.71    0.63    0.0     0.0     0.0
@
----- DRIFT
@  S01    JFLO0   JDRIFT
   0.0    2       1
@
----- INITCOND
@  SI0    P0          T0      G0    Q0     ICK00
   0.0    70.85D+5    287.0   0.0   0.0    3
   1.0    70.85D+5    287.0   0.0   0.0    3
```

A valve (VL-VALVE1) is implemented in the steam line (S1-VL1), which is controlled by a time-dependent signal. It is open and only closes if the Turbo Compressor System, or a single train of it, stops.

```
K---- S1-VL1          vapor line (pipe)
@
@  ITYPO   FPARO   ICMPO
   21      1.0     0
@
----- NETWORK
@  SN0(i)  NI0(i)
   0.0     1
   1.0
@
----- JUNTYPES
@  ST0    JTYP0   ATYP0
   1.0    3       'VL-VALVE1'
@
----- GEOMETRY
@  SG0      Z0       D0      A0      V0      DEP0
   0.0      17.71    0.63    0.0     0.0     0.0
   1.0      18.71    0.63    0.0     0.0     0.0
@
```

```
----- DRIFT
@  S01    JFLO0  JDRIFT
  0.0      2       1
@
----- INITCOND
@  SI0   P0          T0     G0   Q0     ICK00
   0.0   70.85D+5   287.0   0.0  0.0     3
   1.0   70.85D+5   287.0   0.0  0.0     3
```

The object PARA-VL connects the vapor line (S1-VL) to four steam lines (S1-VL1/2/3/4), which belong to the four separated cooling trains.

```
K---- PARA-VL
@  ITYPO   FPARO   ICMPO
    1       1.0      0
@
----- GEOMETRY
@  SG0     Z0      D0      A0      V0      DEP0
   0.0     18.71   0.63    0.0     0.0     0.0
   1.0     18.71   0.63    0.0     0.0     0.0
@
----- DRIFT
@  S01    JFLO0  JDRIFT
   0.0     2      1
@
----- INITCOND
@  SI0   P0          T0     G0   Q0     ICK00
   0.0   70.85D+5   287.0   0.0  0.0     3
   1.0   70.85D+5   287.0   0.0  0.0     3
@
----- BRANCHING
  S1-VL1    3    0.32
  S1-VL2    3    0.32
  S1-VL3    3    0.32
  S1-VL4    3    0.32

K---- PCHE-IN1
@
@  ITYPO   FPARO   ICMPO
   1        1.0      0
@
----- GEOMETRY
@  SG0     Z0       D0    A0    V0    DEP0
   0.0     18.71    0.26  0.0   0.0   0.0
   0.05    18.705   0.26  0.0   0.0   0.0
@
----- INITCOND
@  SI0   P0          T0     G0   Q0     ICK00
   0.0   70.85D+5   287.0   0.0  0.0     3
```

```
K---- CHANNEL1
@
@  ITYPO   FPARO   ICMPO
     21         75000     0
@
----- NETWORK
@  SN0(i)  NI0(i)
  0.000   10
  0.75
@
----- GEOMETRY
@  SG0       Z0          D0            A0            V0         DEP0
     0.00      18.705    0.001222    1.57D-06    0.0         0.0
     0.75      18.005    0.001222    1.57D-06    0.0         0.0
@
----- FRICTION
@  ITPMO   ALAMO   ROUO
    2            0.03          1.D-06
@  SF0     SDFJ0   ZFFJ0   ZFBJ0
@
----- DRIFT
@  S01     JFLO0   JDRIFT
    0.0       2           1
@
----- INITCOND
@  SI0      P0              T0      G0      Q0      ICK00
    0.0       70.85D+5    80.0    0.0      0.0       0
```

The object PCHE-OUT connects the four separated heat exchangers exits (CHANNEL1/2/3/4) to one pipe (S1-LL).

```
K---- PCHE-OUT
@
@  ITYPO   FPARO   ICMPO
    1            1.0          0
@
----- GEOMETRY
@  SG0       Z0          D0       A0     V0     DEP0
    0.0          18.055    0.434    0.0     0.0     0.0
    0.97        17.085    0.434    0.0     0.0     0.0
@
----- INITCOND
@  SI0      P0              T0      G0      Q0      ICK00
    0.0       70.85D+5    80.0    0.0      0.0       0
@
----- BRANCHING
  CHANNEL1    3    0.32
  CHANNEL2    3    0.32
  CHANNEL3    3    0.32
  CHANNEL4    3    0.32
```

```
K---- S1-LL
@
@  ITYPO   FPARO   ICMPO
    21       1.0       0
@
----- NETWORK
@  SN0(i)  NI0(i)
    0.0      2
   4.5
@
----- GEOMETRY
@  SG0    Z0        D0       A0     V0    DEP0
     0.0    17.085   0.434    0.0     0.0    0.0
     4.5    12.585   0.434    0.0     0.0    0.0
@
----- DRIFT
@  S01    JFLO0   JDRIFT
     0.0    2         1
@
----- INITCOND
@  SI0      P0              T0      G0      Q0     ICK00
    0.0      70.85D+5    80.0    0.0     0.0       0
```

The object S1-LLSJP contains the magnetic valve (RUECK-VALVE), which is time-dependent and opens at the beginning of the station blackout.

```
K---- S1-LLSJP           liquid line (pipe)
@
@  ITYPO   FPARO   ICMPO
     22       1.0       0
@
----- JUNTYPES
@     ST0      JTYP0   ATYP0
       0.085    3          'RUECK-VALVE'
----- GEOMETRY
@   SG0       Z0        D0       A0     V0     DEP0
      0.000     12.585   0.434    0.0     0.0     0.0
      0.085     12.5      0.434    0.0     0.0     0.0
----- DRIFT
@  S01    JFLO0   JDRIFT
     0.0    2         1
----- INITCOND
@  SI0      P0              T0      G0      Q0     ICK00
    0.0      70.85D+5    80.0    0.0     0.0       0
```

Accordingly, a priority chain of the cooling cycle lists the main components, the printed circuit heat exchanger (PCHE1), the turbine (TURBINE1), the air-cooled heat exchanger (LGWT1) and the compressor (KOMPRESS1).

```
----- BRAYTON
@
@ IPRI0   ISYS0
   1        4
@ SBO0   ANAMO     SEO0     IARTO
   0.0      IN1              0.1      1
   0.0      PIPEZU1          1.0      1
   0.0      PCHE1            0.7      1
   0.0      TURBINE1         0.5      1
   0.0      PIPE1            0.5      1
   0.0      LGWT1           15.0      1
   0.0      KOMPRESS1        0.5      1
   0.0      OUT1             0.1      1
   0.0      OUTA1            0.1      1

----- OUTLET
@
@ IPRI0   ISYS0
   1      4
@ SBO0   ANAMO    SEO0    IARTO
   0.0      OUTA1     0.1       1
   0.1      OUTB1     0.0       1

----- CYCLE
@ IPRI0   ISYS0
   1      4
@ SBO0   ANAMO    SEO0    IARTO
   0.0      OUT1        0.1      1
   0.0      CYCLE1     15.0      1
   0.0      PIPEZU1     1.0      1
```

The thermo-fluiddynamic objects of the Turbo Compressor System are described in the following.

Each printed circuit heat exchanger consists of 75,000 channels, indicated by FPARO

```
K---- PCHE1
@
@  ITYPO   FPARO   ICMPO
    21       75000    0
@
----- NETWORK
@   SN0(i)  NI0(i)
     0.0      5
     0.7
@
----- GEOMETRY
@  SG0     Z0      D0           A0             V0       DEP0
    0.0     0.0     0.000764    6.14D-07     0.0      0.0
    0.7     0.0     0.000764    6.14D-07     0.0      0.0
@
----- FRICTION
@  ITPMO   ALAMO   ROUO
    2          0.03        1.D-06
@
----- INITCOND
@  SI0    P0     T0       G0            Q0      ICK00
    0.0    0.0     0.0      6.3333D-4   0.0      0
    0.7    0.0     0.0      6.3333D-4   0.0      0

K---- PIPEZU1
@
@  ITYPO   FPARO   ICMPO
    21       1.0        0
@
----- NETWORK
@  SN0(i)  NI0(i)
    0.0      1
    1.0
@
----- GEOMETRY
@  SG0      Z0      D0      A0    V0      DEP0
    0.0      0.0      0.28    0.0    0.0      0.0
    1.0      0.0      0.28    0.0    0.0      0.0
@
----- INITCOND
@  SI0      P0      T0     G0     Q0      ICK00
    0.0      0.0     0.0     47.5   0.0      0
    1.0      0.0     0.0     47.5   0.0      0
```

The turbine is placed within a turbine pipe (ICMPO=9) it is called with the turbine stage junction CO2TURB

```
K---- TURBINE1
@
@  ITYPO   FPARO   ICMPO
     21      1.0      9
@
----- NETWORK
@  SN0(i)  NI0(i)
    0.0      2
    0.5
@
----- JUNTYPES
@  ST0    JTYP0   ATYP0
    0.25   7       CO2TURB
@
----- GEOMETRY
@  SG0      Z0     D0     A0    V0    DEP0
     0.0     0.0    0.28   0.0   0.0   0.0
     0.5     0.0    0.5    0.0   0.0   0.0
@
----- INITCOND
@  SI0   P0    T0     G0          Q0     ICK00
     0.0  0.0   0.0    6.3333D-4   0.0    0
     0.5  0.0   0.0    6.3333D-4   0.0    0

K---- PIPE1
@
@  ITYPO   FPARO   ICMPO
     21      1.0      0
@
----- NETWORK
@  SN0(i)  NI0(i)
     0.0     2
     0.5
@
----- GEOMETRY
@  SG0    Z0    D0   A0    V0    DEP0
     0.0   0.0   0.5  0.0   0.0   0.0
     0.5   0.0   0.5  0.0   0.0   0.0
@
----- INITCOND
@  SI0   P0    T0    G0    Q0    ICK00
    0.0   0.0   0.0   47.5  0.0    0
    0.5   0.0   0.0   47.5  0.0    0
```

The air-cooled heat exchanger is also subdivided into four parts. Each part, like the LGWT1, consists of 255 cooling channels.

```
K---- LGWT1
@
@  ITYPO   FPARO   ICMPO
    21        255.0      0
@
----- NETWORK
@  SN0(i)  NI0(i)
   0.0       15
  15.0
@
----- GEOMETRY
@  SG0      Z0       D0        A0     V0       DEP0
    0.0       0.0      0.025     0.0     0.0       0.0
  15.0       0.0      0.025     0.0     0.0       0.0
@
----- FRICTION
@  ITPMO   ALAMO   ROUO
   2            1.            0.009
@
----- INITCOND
@  SI0       P0      T0      G0          Q0       ICK00
    0.0       0.0     0.0    0.186275   0.0       0
   15.0      0.0     0.0    0.186275   0.0       0
```

Similar to the turbine, the compressor is indicated with the turbine junction stage CO2KOMP, which is listed after the definitions of the thermo-fluiddynamic objects

```
K---- KOMPRESS1
@
@  ITYPO   FPARO   ICMPO
  21      1.0    9
@
----- NETWORK
@  SN0(i)  NI0(i)
   0.0       2
   0.5
@
----- JUNTYPES
@  ST0    JTYP0   ATYP0
   0.25    7          CO2KOMP
@
----- GEOMETRY
@  SG0      Z0      D0     A0    V0     DEP0
   0.0       0.0     0.5     0.0    0.0    0.0
   0.5       0.0     0.28   0.0    0.0    0.0
```

```
----- INITCOND
@  SI0    P0    T0    G0    Q0    ICK00
   0.0    0.0   0.0   47.5  0.0   3
   0.5    0.0   0.0   47.5  0.0   3
@

K---- CYCLE1
@
@  ITYPO   FPARO   ICMPO
   21      1.0     0
@
----- NETWORK
@  SN0(i)  NI0(i)
    0.0     5
   15.0
@
----- GEOMETRY
@  SG0     Z0     D0     A0    V0    DEP0
    0.0    0.0    0.28   0.0   0.0   0.0
   15.0    0.0    0.28   0.0   0.0   0.0
@
----- INITCOND
@  SI0     P0           T0     G0    Q0    ICK00
  0.00     18050000.0   80.0   0.0   0.0   0
  15.0     18050000.0   80.0   0.0   0.0   0
```

To achieve design point conditions of the turbomachinery during the steady state calculation which is required by ATHLET, the design point mass flow is provided at the beginning of the simulation, with the time-dependent signals S2-FILL in IN1 and S2-SINK in OUTB1. However, the prescribed mass flow is reduced to zero before the Turbo Compressor System is activated and does not influence its behavior.

```
K---- IN1
@
@  ITYPO   FPARO   ICMPO
    11        1.0     0
@
----- NETWORK
@  SN0(i)  NI0(i)
     0.0      1
     0.1
@
----- JUNTYPES
@  ST0    JTYP0   ATYP0
    0.00    6         'S2-FILL'
@
----- GEOMETRY
@  SG0    Z0      D0      A0     V0      DEP0
    0.0      0.0     0.28     0.0     0.0      0.0
    0.1      0.0     0.28     0.0     0.0      0.0
----- INITCOND
@  SI0      P0            T0       G0    Q0      ICK00
  0.0       18050000.0   80.0      47.5   0.0      0

K---- OUT1
@  ITYPO   FPARO   ICMPO
    21        1.0        0
@
----- NETWORK
@  SN0(i)  NI0(i)
    0.0      2
    0.1
@
----- GEOMETRY
@  SG0       Z0      D0      A0     V0    DEP0
    0.0        0.0     0.28    0.0    0.0    0.0
    0.1        0.0     0.28    0.0    0.0    0.0
@
----- INITCOND
@  SI0    P0    T0    G0    Q0     ICK00
    0.0    0.0   0.0   47.5  0.0      0
    0.1    0.0   0.0   47.5  0.0      0
```

```
K---- OUTA1
@
@  ITYPO   FPARO   ICMPO
    21       1.0       5
@
----- GEOMETRY
@  SG0      Z0      D0      A0     V0    DEP0
   0.0       0.0     0.28    0.0    0.0    0.0
   0.1       0.0     0.28    0.0    0.0    0.0
@
----- INITCOND
@  SI0    P0   T0    G0     Q0     ICK00
   0.0     0.0   0.0   47.5  0.0     0
   0.1     0.0   0.0   47.5  0.0     0

K---- OUTB1
@
@  ITYPO   FPARO   ICMPO
    22       1.0       0
@
----- JUNTYPES
@  ST0    JTYP0  ATYP0
   0.10    6       S2-SINK
@
----- GEOMETRY
@  SG0      Z0      D0      A0     V0    DEP0
   0.0       0.0     0.28    0.0    0.0    0.0
   0.1       0.0     0.28    0.0    0.0    0.0
----- INITCOND
@  SI0    P0   T0    G0     Q0     ICK00
   0.0     0.0   0.0  -47.5  0.0     0
@
```

Turbine Data

The control word TURBINE is input for the simulation of the turbomachinery. The general data of the simulated shaft is defined by the TURBOSET. It includes the design point shaft speed (TUSPD0). However, the shaft speed is determined by the time-dependent signal TUSPD, which is constant in the conducted simulations.
In addition, the turbine and compressor design point data is listed under CO2TURB and CO2KOMP. ATHLET requires information about the inlet and exit pressure (P0IN and P0EX), the massflow (G0), the efficiency (ETA0), as well as the inlet enthalpy, which is utilized to determine the sCO2 density at the inlet.

```
C---- TURBINE
K---- TURBOSET
@
@  TUSPD0    THETA   BE        STUSPD    SGENP         SLABW
   60000.0   5.0     1.0D-03   'TUSPD'   'GENERATOR'  'SLABW'
@
K---- CO2TURB
@ P0IN          P0EX         G0     H0IN       ETA0   POW0
  18000000.0    9000000.0    47.5   706710.0   0.85   1800000.0
@
K---- CO2KOMP
@ P0IN         P0EX          G0     H0IN       ETA0   POW0
  8940000.0    18060000.0    47.5   367460.0   0.8    -2000000.0
```

Heat Conduction Objects

Several heat conduction objects are involved in the modelling of the Turbo Compressor System, listed under the control word HEATCOND.

The compact heat exchanger is modeled as 75,000 copies of one heat conduction object (HCO), which connects one vapor / water channel, to one sCO_2 channel. The geometry of the HCO has been approximated as a plate (IGEO0=0), with a thickness equal to the average distance between the two channels (DS10) of 0.00056 m. The width of the plate (DI0) is 0.0019 m. The heat transfer coefficients are calculated by means of correlations (HTCCALC), and the heat exchanger material is austenitic steel.

```
K---- PCHE_1
@
@  AOLH          SBOLH   SEOLH    AORH       SBORH   SEORH
   'CHANNEL1'   0.0       0.7       'PCHE1'     0.0       0.7
@  NIHC0   N10    N20    N30    IGEO0   ICOMP0  ACOMP0   ICHF0   IDUM
@
    1        1       0       0       0        0          'DUMMY'  2        0
@
----- GEOMETRY
@  FPARH   TL0
    75000.    0.
    COPY_TFO R
@
@  SG0    Z0     DI0      DS10     GAP10   DS20    GAP20   DS30
    0.0     0.0    0.0019   0.00056   0.0       0.0       0.0       0.0
@
----- HTCDEF
@  AIAL1 (1...4)
   'HTCCALC' 'HTCCALC' 'DUMMY' 'DUMMY'
@  SH0    HTCL0(1...4)                       QTHRU0
   0.00    4.0D+04   11217.0   0.0    0.0    0.0
@
----- MATPROP
@  AMATL0(1...3)
@
  'AUST-STEEL' 'DUMMY' 'DUMMY'
@
```

Since air-cooling cannot be simulated by ATHLET, the air-cooled heat exchanger is modeled by connecting the LGWT1 to time-dependent temperature signals (HEATAB1 and HEATAB21). These are selected, in order to determine a sCO2 compressor inlet temperature of 42 °C.

```
K---- LGWT1_1
@
@  AOLH        SBOLH   SEOLH    AORH       SBORH   SEORH
   'HEATAB1'   -15.0   -0.01    'LGWT1'    0.0     7.0
@
@  NIHC0  N10   N20   N30   IGEO0  ICOMP0  ACOMP0   ICHF0  IDUM
   1      1     0     0     0      0       'DUMMY'  2      0
@
----- GEOMETRY
@  FPARH  TL0
   255.    0.
   COPY_TFO R
@
@  SG0   Z0    DI0   DS10     GAP10  DS20   GAP20  DS30
   0.00  0.0   0.7   0.00165  0.0    0.0    0.0    0.0
@
----- HTCDEF
@  AIAL1 (1...4)
   'HTCCALC' 'HTCCALC' 'DUMMY' 'DUMMY'
@  SH0   HTCL0(1...4)                  QTHRU0
   0.00  4.0D+04  100.0  0.0  0.0      0.0
@
----- MATPROP
@  AMATL0(1...3)
   'AUST-STEEL' 'DUMMY' 'DUMMY'

K---- LGWT1_2
@
@  AOLH        SBOLH   SEOLH    AORH       SBORH   SEORH
   'HEATAB21'  -15.0   -0.01    'LGWT1'    7.0     15.0
@
@  NIHC0  N10   N20   N30   IGEO0  ICOMP0  ACOMP0   ICHF0  IDUM
   1      1     0     0     0      0       'DUMMY'  2      0
@
----- GEOMETRY
@  FPARH  TL0
   255.   0.
COPY_TFO R
@
@  SG0   Z0    DI0   DS10     GAP10  DS20   GAP20  DS30
   0.00  0.0   0.7   0.00165  0.0    0.0    0.0    0.0
@
----- HTCDEF
@  AIAL1 (1...4)
   'HTCCALC' 'HTCCALC' 'DUMMY' 'DUMMY'
@  SH0   HTCL0(1...4)               QTHRU0
```

```
@
  0.00    4.0D+04    100.0   0.0     0.0     0.0
@
----- MATPROP
@  AMATL0(1...3)
  'AUST-STEEL' 'DUMMY' 'DUMMY'
```

Since the in ATHLET implemented turbine model does not allow to simulate the starting process of the turbomachinery, the Turbo Compressor System has to be operating from the beginning of the simulation, before the station blackout is anticipated. Therefore, an additional heat source has to be provided to achieve acceptable turbine inflow conditions. This is realized with PCHE1AN, where a time-dependent temperature signal (HEATIN) is connected to the sCO2 channel (PCHE1) of the printed circuit heat exchanger. The heat transfer coefficient is also a time-dependent signal, which reduces to zero when the station blackout occurs.

```
K---- PCHE1AN
@
@  AOLH        SBOLH   SEOLH    AORH        SBORH   SEORH
    'HEATIN'    -1.0        -0.3        'PCHE1'      0.0          0.7
@
@  NIHC0   N10     N20     N30     IGEO0   ICOMP0  ACOMP0   ICHF0   IDUM
     1          1        0        0        2           0            'DUMMY'  2          0
@
----- GEOMETRY
@  FPARH   TL0
     75000.     0.
     COPY_TFO R
@
@  SG0     Z0      DI0     DS10      GAP10   DS20    GAP20   DS30
     0.00     0.0     0.003   0.00081   0.0         0.0       0.0         0.0
@
----- HTCDEF
@  AIAL1 (1...4)
    'HTCCALC' 'ANLAUFEN' 'DUMMY' 'DUMMY'
@  SH0     HTCL0(1...4)                      QTHRU0
@
  0.00    4.0D+04    8.E+02   0.0     0.0     0.0
----- MATPROP
@
  'AUST-STEEL' 'DUMMY' 'DUMMY'
```